A FLOATING LINER FACILITY AND STUDIES OF FRICTION AT A RECIPROCATING PISTON-CYLINDER WALL INTERFACE

Md Rezaul Islam

B.Sc., M.Sc.

Thesis submitted to the University of Nottingham for the degree of Doctor of Philosophy

March 2016

Table of Contents

Key

Nomenclature

$^{\circ}$ATDC	Degree After Top Dead Centre
$^{\circ}$C	Degree Celsius
a	Acceleration, ms^{-2}
A	Area, m^2
B	Bore Diameter, mm
bara	Bar Atmospheric
barg	Bar Gauge
f	Co-Efficient of Friction
F_b	Boundary Friction Force
F_f	Friction Force, Newton
F_H	Hydrodynamic Friction Force
F_N	Normal Load, Newton
F_p	Preload, Newton
F_r	Connecting Rod Force , Newton
F_s	Seal Force, Newton
F_t	Thrust Force, Newton
h	Oil Film Thickness
I	Mass Moment of Inertia, kgm^2
I/O	Input Output
l	Connecting Rod Length, mm
L	Characteristics Length, mm
m	Mass, kg
N	Rotational Speed, rpm
N	Newton

p	Cylinder Pressure
P	Oil Film Pressure
R_a	Arithmetic Average Surface Roughness
R_p	Maximum Peak Height, μm
R_v	Maximum Valley Depth, μm
s	Stroke
S	Duty Parameter
T	Torque, Nm
T	Temperature
T	Ring Tension, Newton
U	Velocity, ms^{-1}
v	Velocity, ms^{-1}
V	Volt

Subscripts

max	Maximum
c	Crank
M	Motor
p	Piston

Symbols

θ	Crank angle, Degree
μ	Viscosity, mPas
σ	Standard Deviation
τ	Shear Force, Newton
σ	Shear Strength
α	Angular Acceleration, $rads^{-2}$

Abbreviations

BDC	Top Dead Centre
bmep	Brake Mean Effective Pressure
CAFE	Corporate Average Fuel Economy
CCS	Cold Crank Simulator
CO_2	Carbon Dioxide
CVD	Chemical Vapour Deposition
DAQ	Data Acquisition
DC	Direct Current
DLC	Diamond-Like Carbon
EU	European Union
FLR	Floating Liner Rig
fmep	Friction Mean Effective Pressure
HSL	Helical Slide Honing
HTHS	High Temperature High Shear
ICE	Internal Combustion Engine
kPa	Kilo Pascal
KV	Kinematic Viscosity
LST	Laser Surface Texturing
MoDTC	Molybdenum Dithiocarbamate
NI	National Instruments
PCJ	Piston Cooling Jet
PH	Plateau Honing
PIC	Programmable Interface Controller
PPR	Pulses Per Revolution
PTFE	Polytetrafluorethylene
PVD	Physical Vapour Deposition
SAE	Society for Automotive Engineers

TDC	Top Dead Centre
TS	Thermal Spraying
TTL	Transistor Transistor Logic
USA	United States Of America
ZDDP	Zinc Dialkyldithiophosphates

Abstract

The piston-cylinder liner interface comprises more than half of the total engine rubbing friction. With current demand being for internal combustion engines with better fuel economy, lower exhaust emissions and higher performance, reducing this form of friction is the subject of much study. The research reported in this thesis is concerned with the development of an existing floating liner rig to measure the friction in this region. The performance features of the modified setup have also been assessed. Parametric studies have been undertaken with the modified setup to identify the potential means of friction reduction.

Modifications undertaken in the sealing method and driveline assembly has facilitated friction measurement at higher gas loading of up to 80 barg. The modified sealing assembly with a sealing ring overcame the problem of arbitrary force interruption through irregular liner and seal contacts. Addition of five times higher inertia flywheel aided the motor to support the rig with adequate torque during high gas loading operations. Calibrations have been performed at each different build of piston-liner combination to reduce build to build variability in measurement.

Experimental studies have been undertaken to assess the friction characteristics for different factors such as operating pressure, temperature and speed, lubricant oil formulation, piston-liner clearance, piston material etc. Tests have been undertaken at a range of operating conditions; peak pressure of 0 to 80 barg, speed of 1000 to 2000 rpm and average mid-liner temperature of 40 to 90 $^{\circ}$C. Peak cylinder pressure has been observed to be dominating the friction followed by temperature and speed. Friction spikes were observed near the top dead centre for pressurised operations; where normal load on the rings are highest in a cycle. Higher speed generally results in a higher total frictional loss. However at higher temperature and peak pressure, contrasting effect of speed on total friction

has been reported. The study further identified that piston motion play important roles in determining mixed/boundary friction along with the local gas pressure, velocity and oil film temperature.

Friction reductions have been obtained by using a lower viscosity oil and higher piston-liner clearance. Maximum friction reduction of 18% has been reported in this study by using SAE 0W-30 oil in place of SAE 5W-30. Diametric clearance of 80 μm obtained a maximum reduction of 12% compared to a lower clearance of 20 μm. The use of steel piston has shown potential in reducing friction over aluminium piston but the design and weight of piston played a dominant role in the frictional loss.

Acknowledgements

First of all, my thanks go to Professor Paul Shayler for giving me the opportunity to pursue research under his supervision. I sincerely appreciate his continuous support, patience and guidance throughout my PhD.

I am also grateful to all my colleagues at Engine Research Group for creating such a great and friendly work environment. My special thanks go to Dr. Robert Dodd to show me the way into this research work and to support me throughout the past four years.

I would also like to thank the former technicians of Engine Research Group: John McGhee, Paul johns, John Clarke, Geoff and Steve Hohner who provided me with great support in the lab during the early days of my work. My sincere gratitude goes to the current technicians: John Lane, Nigel Sykes and Paul Bramman to provide adequate support and occasional laughter through humorous statements.

I would like to acknowledge the financial and technical support from Ford Motors UK, Innovate UK and Lubricants UK in perusing the research project.

I am deeply indebted to my parents M Zohurul Islam and Rowshan Ara, and my siblings Sadia and Saif for their encouragement to undertake the PhD Study and continuous moral support and blessings. To my family and friends around the world who always wished good for me.

Chapter 1 Introduction

Rubbing friction is a dissipative process in which mechanical work is converted to heat. It is an important cause of inefficiency of reciprocating internal combustion engines (ICE). The Sankey diagram illustrated in Figure 1.1 for the energy flow in an ICE, from the heat released by combustion to the various heat sinks and brake work output, shows that rubbing friction is significant. Friction leads to the increase in fuel consumption and high wear of the moving parts. In passenger cars an average 28% of fuel energy is lost as rubbing friction for an average speed of 60 km/h, considering both urban and low traffic conditions [1]. The sum of rubbing friction and ancillary work accounts for a significant fraction of indicated work which varies from 10 percent at full load to 100 percent at idling [2]. Frictional losses not only penalise fuel economy, these also influence the size of coolant systems as these are dissipated as heat.

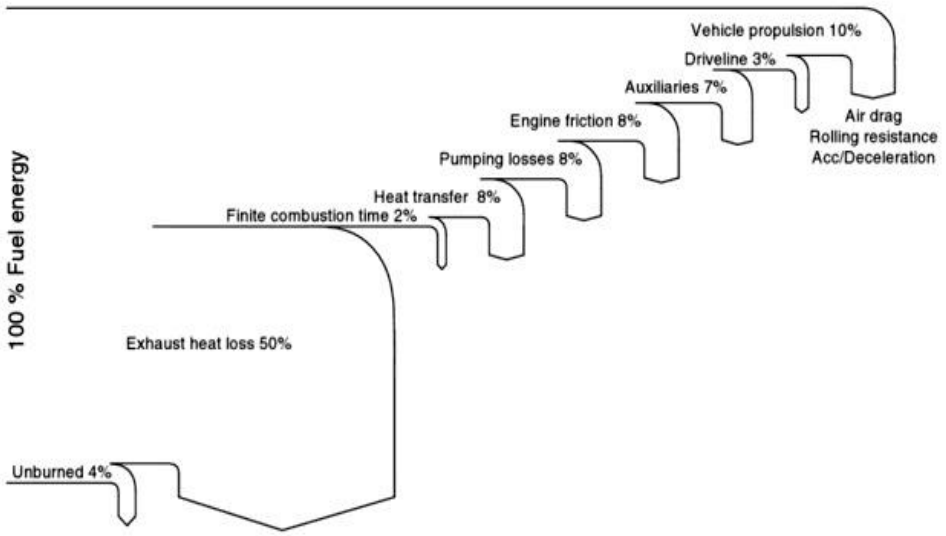

Figure 1.1: Sankey diagram for a conventional car gasoline engine [3].

Frictional dissipation occurs at various sites throughout an engine where there is relative motion between surfaces in close proximity. These sites include:

- The interfaces between pistons and cylinder walls
- the main and big end bearings
- rubbing seals of the crankshaft
- the bearings and interfaces between cams and cam followers of the valve train
- gears or pulleys and belts, which drives the camshaft and engine accessories.

Of these, friction losses at the interface between the pistons and cylinder wall account for largest proportion, typically 50-75%, of total friction in reciprocating internal combustion engines [4]. For this reason, understanding and reducing friction at the piston-cylinder wall interface is particularly important. This is the area of research undertaken and reported in this thesis.

The loss associated with friction and lubrication in engines continues to attract the efforts of many international centres and groups not least because of the effect on fuel economy and wear. Many questions of practical and academic interest remain to be resolved. This is particularly true of friction losses produced by the reciprocating motion of a piston in a cylinder. These friction losses are difficult to isolate from other contributions to losses in a firing engine and parametric studies of design entailing engine rebuilds are fraught with problems. Consequently many experimental studies are carried out using bench-top facilities such as a Cameron-Plint test machine [5], or resort to motored tear-down procedures [2]. The measurement of friction force opposing piston motion at piston-cylinder wall interface is most commonly addressed by one of two measurement methods which will be described in detail in later chapters. The first infers the friction force by applying Newton's second law of motion, net force= mass x acceleration, to the piston. The second infers the friction force using a so called floating liner,

which is more common, but far from routine and the body of published results remains as small. One limitation of the construction of a floating liner rig is the difficulty of changing the liner to investigate design features, not least because such changes and engine rebuilds introduce experimental noise which is difficult to eliminate.

The investigations reported in this thesis are concerned with the design, development, commissioning and use of a non-firing, motored floating liner test facility to investigate piston-liner friction. The developments have been carried out on the existing test facility [6] to achieve simulated firing engine conditions and to measure the piston-liner friction with high confidence. The effects of operating factors such as speed, cylinder pressure and temperature, piston and liner micro and macro design features, and lubricant design on friction were of particular interest.

1.1 Background

Reducing fuel consumption and reducing CO_2 emissions are major challenges for the automotive industry. High forecourt fuel costs, EU agreement on fleet CO_2 targets and Corporate Average Fuel Economy (CAFE) targets in the USA and public concern over the environmental impact of vehicles all exert pressure on the industry to manufacture more efficient cars [7]. The adverse effects of climate change has forced the world to think about the reduction of greenhouse gas emissions, especially CO_2. Light duty vehicles are one of the major contributors to CO_2 emissions and responsible for 15% of total CO_2 emission in whole EU [8]. In the USA, passenger vehicles contribute 20% of CO_2 emissions [9]. The world big economic powers have recognised their responsibility towards a sustainable and living friendly environment and consequently demanded a significant improvement in emissions from the passenger vehicles like other fields. To advance towards it, targets have been continually set by the EU legislators to cut the CO_2 emissions of new manufactured cars in steps from 2009. The law

permitted the average CO_2 emissions to a maximum of 130 g/km by 2015 and 95 g/km by 2021 [10]. The provisional CO_2 emission data of cars sold in 2014 has already shown a significant reduction of around 12% (123.4 g/km) from 2010 emissions [11]. In USA similar kind of restrictions were imposed on automotive manufacturers by the CAFE program to increase the fuel economy at minimum to 27.5 mpg for cars and 22.2 mpg for light duty trucks [12]. From customer's point of view, the fuel economy is more desirable in cutting the fuel costs as well as dealing with increasing vehicle taxes [13].

Several approaches are undertaken by the regulatory bodies to improve the fuel consumption of automotive vehicles and are acted upon by the manufacturers. Some of the concepts include using alternative fuels like biofuels or fuel cells, alternative drivelines like hybrids, improved aerodynamics and reduced weights, reduced rolling resistance, downsizing of engines and new technologies to reduce the parasitic losses in engine [14].

At present fossil fuels seem likely as the main source of energy for automotive engines over the next 40 years [15]. Although some reduction in CO_2 emission is being achieved by, for example raising biofuel contents of forecourt fuels, improving engine efficiency remains a high priority. Several areas of engine development have been identified as having the potential to contribute to this, including friction reduction. The applications of new technologies for friction reduction in cars, could achieve a friction losses reduction of 18% in 5-10 years and of 61% in 15-25 years [1]. Some of the potential technologies to reduce friction in engines include the use of advanced lubricants with low shear and low viscosity characteristics and novel additives, advanced coatings and micro surface texturing on engine components. This would be worth economic savings of 174,000 million Euros and 576,000 million Euros respectively along with 290 million and 960 million tonnes reduction in CO_2 emissions.

As piston-liner assembly friction has been identified as the largest contributor to engine friction, the research in this area is of great interest. The potential factors which can reduce the piston-liner friction are:

- piston ring pack design,
- skirt design,
- geometric effect such as piston-liner clearance,
- surface coatings, surface roughness,
- surface micro texturing and
- new low viscosity and low shear lubricants and additives [1].

The next three sections are concerned with the relative impact of piston-cylinder wall friction on total engine parasitic losses, significance of different measurement mechanisms in the study of friction reduction and finally the approach taken in this research to measure friction and apply methods in piston-liner friction reduction.

1.2 Engine friction components and piston-liner contribution

The different areas of the engine where frictional losses take place are friction between piston rings, piston skirt and cylinder liner; friction in the big end, small end bearing, crankshaft and camshaft bearings; friction in valve mechanism; friction in the gears or pulleys and belts, which drives the camshaft and engine accessories. The piston-liner assembly, crankshaft and valve train components are the major contributors to the engine total friction while the piston assembly is singularly the largest contributor.

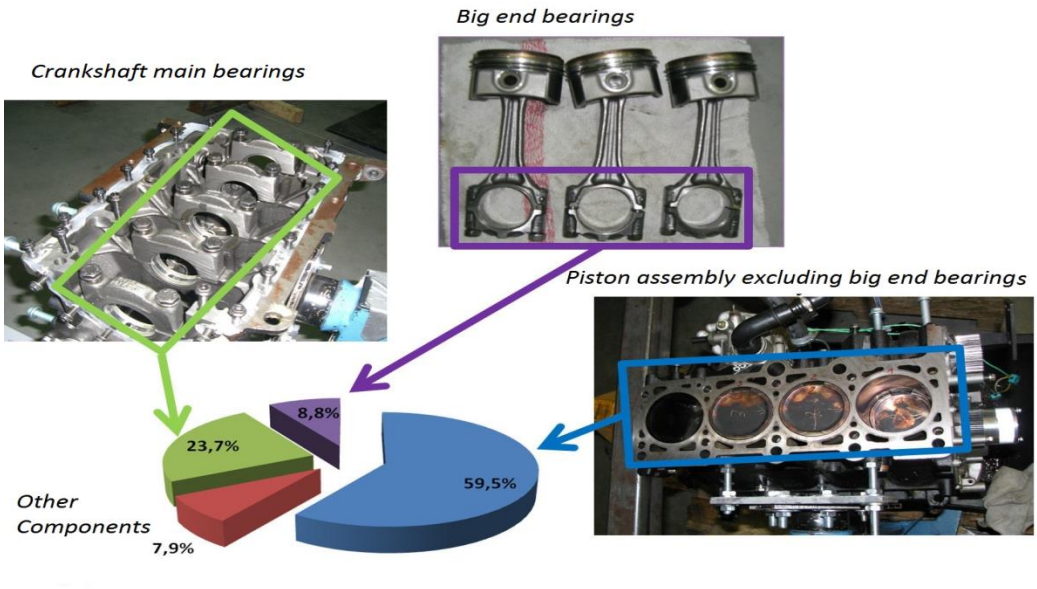

Figure 1.2: Example for distribution of friction losses by various engine components [7]

An example [7] of the contributions of the main component assemblies is illustrated in Figure 1.2, from which it can be seen that the that piston assembly excluding the big end bearings contributes 60% to engine friction while the main bearings which support the crankshaft are responsible for 24% of that. Of the whole engine 20-44% frictional losses occur in all the bearings and seals [7]. Thus frictional losses associated with piston-liner assembly and crankshaft assembly are of high interest as reduction of these losses would lead to great economic savings.

The various engine components operate in different modes of lubrication depending on the operating conditions such as speed, load and temperature. Lubrication of the rubbing surfaces is divided into three regimes- boundary, mixed and fluid film lubrication (elasto-hydrodynamic and hydrodynamic). These are often explained (considered in detail in Chapter 2) by reference to the Stribeck diagram, which shows how the friction coefficient varies as the lubrication regime changes. When operating in the boundary lubrication regime, the friction coefficient is very high, in order of 0.1 [16-18]. Here the lubrication oil film

thickness is lower than the average surface roughness. In hydrodynamic lubrication regime, the oil film is thick enough to separate the two surfaces in relative motion. In between these regions, mixed lubrication occurs with intermittent contacts between surfaces are taken place. The transition between these regimes largely depends on engine operating speeds, loads and lubricant viscosity [2]. Boundary conditions are achieved only at low engine speeds during engine start up and shutdown and at high loads. It causes the wear between surfaces and in extreme scenario may cause seizure between the surfaces and thus it is mostly undesirable. With the increasing speeds and decreasing loads the surface asperities start to separate by oil film and thus mixed lubrication occurs with intermittent surface contacts. The transition between mixed and boundary lubrication is not only determined by operating conditions but also by surface micro properties and lubricant design.

Main and big end bearings of the crankshaft assembly generally operate in the hydrodynamic lubrication regime. These bearings support high loads under normal operating conditions, which arise from piston/connecting rod inertia and cylinder gas pressure. During steady state operation the surfaces of journal and bearing are fully lubricated and journal eccentricity arising from the load is designed to achieve minimum oil film thicknesses of about 2 μm [2, 7]. Any lower film thicknesses can cause metal to metal contacts leading to excessive boundary/mixed friction and wear and eventually to a catastrophic failure.

The critical friction contributors of the valve train assembly are the camshaft journal bearings and the rocker arm/cam interface. According to Staron et al. [19], the cam / tappet interface is the major contributors to the losses due to the high load operation in small contact areas. The lubrication regime is boundary dominated at low engine speeds; however, it moves to an elasto-hydrodynamic regime at high speeds [20]. At lower engine speeds the friction arises from spring

forces, whereas at higher speeds the dominating force is inertia of moving components.

Lubrication of the piston-liner interface is hydrodynamic throughout most of the piston stroke. The surfaces in relative motion are separated by the oil film and there is no contact between surface asperities [21]. Near each end of the stroke, boundary contacts between rubbing surfaces occur leading to mixed and boundary lubrication. The main sources of friction forces in the piston assembly are the piston rings/cylinder wall and skirt/wall interfaces [2]. The modes of lubrication and friction in the ring and skirt section vary depending on the operating conditions and design. Ring friction forces depend on the normal loads and are varied across the cycle. Under no load or during intake and exhaust strokes the rings operate in boundary/mixed regime near the top and bottom dead centres [22]. Particularly at the top dead centre the top ring experiences boundary friction because of oil starvation [23]. The case is more severe under firing condition where the normal load on the top ring is highest at top dead centre due to high cylinder pressure. Piston skirt and lands carry the side thrust and generally operate in hydrodynamic region [24]. Friction forces in this section are resulted from the inertia force of reciprocating masses (piston, connecting rod). The transition from mixed/ boundary to hydrodynamic lubrication in the piston rings is different and the behaviour is dictated by several parameters. Some of the important parameters are normal load due to ring tensions and cylinder gas load, operating speed, oil film temperature/viscosity, ring profiles and surfaces micro features [25, 26].

1.3 Piston-liner assembly friction measurement

The difference between brake output power and the net indicated power of an engine is the sum of friction power losses and the power taken in driving ancillaries. Net indicated power is determined from the measurement of cylinder

pressure throughout the cycle. The need for the cylinder head to be modified to fit pressure transducers makes this an expensive and non-trivial measurement to make.

Friction is sometimes estimated by measuring the work required to motor the engine. Although the total engine friction work is a valuable measurement, more valuable is the ability to establish a breakdown of the total by progressively dismantling the engine and measuring the change in motoring work required, as termed as motored engine breakdown test. In these tests high operating temperatures similar to fired engine are obtained through the supply of heated oil or water around the system or running the engine initially in firing condition. Though motored tests can estimate friction loss for a similar firing engine condition still there are some uncertainties in measurements as additional heat loss through cylinder wall and blow by gases (not part of friction force) are achieved which are measured in friction mean effective pressure (fmep) calculation. Moreover, sudden pressure rise during combustion of firing engine are not achieved in motored condition which alters the temperature and peak pressure in cylinder; thus altering the friction force measurement.

Other approximate methods of measuring friction are Willans line and Morse test [2]. These are now rarely used for more than an indication of engine health. In the former, a plot of fuel consumption versus brake load recorded at constant speed is extrapolated back to zero fuel consumption to obtain the total frictional losses in terms of fmep. In a Morse test, individual cylinders in a multiple cylinder engine are cut out from firing to determine the reduction in brake torque. The engine friction losses are then inferred from the total indicative power and brake power.

All the methods described above can only determine the friction losses on a single engine build, but would not allow doing the parametric studies of engine friction

which requires component change and probable rebuild of the system. Currently, piston friction is directly measured by using a floating liner system where cylinder liner is supported by some floating arrangement to directly measure the piston-liner interface friction. These systems have been developed over the years to obtain the similar condition of a real engine and isolating piston friction from other mechanical losses in the engine.

In this study piston-liner assembly friction was measured at varied operating conditions under simulated engine specifications using a floating liner rig. This setup is able to measure the friction force at various positions of a stroke at different running speeds, oil temperatures and cylinder peak pressures. Furthermore, the compression ratio can be adjusted by varying the piston-cylinder head/seal clearances. The most important feature of this rig is the ability to study the effect of various piston- cylinder assembly macro and micro design features without altering the whole setup.

1.4 Thesis Aims and Objectives

The aims of the research investigation reported in the thesis were to develop a floating liner rig facility to measure friction force in the piston-liner assembly and investigate the effect of engine operating conditions and component design features on measured friction. The rig existed prior to the start of the project but was not fully commissioned and required further development. The design features of interest included both micro and macro features. These aims have been pursued through the following objectives:

- The development of existing test facilities and test procedures to achieve the desired range of test conditions, repeatability and quality of data.
- Identify a suitable method to process the measured raw data into interpretable friction forces and corresponding cycle fmep.

- Investigate the mode of lubrication/friction regimes across a cycle under varied operating conditions such as engine speeds, oil temperatures and cylinder pressures.
- Interpret the data as a four stroke engine operation by combining the measured data at uncompressed and pressurised conditions.
- Examine the influence of macro design parameters such as piston-liner clearances and piston materials and designs on engine friction.
- Investigate the effect of lubrication oil characteristics on friction in piston-liner interactions.
- The analysis and interpretation of results should reveal the mechanism of any effects on friction levels and lubrication regime.

1.5 Thesis layout

The thesis consists of seven chapters. After the introduction (Chapter 1), the following chapters are laid out as below:

- Chapter 2 covers a review of the literature related to piston-liner friction sources, the lubrication behaviour and its impact on different lubrication or friction regimes, different micro and macro design features affecting the piston-liner friction and finally different methods used to measure friction in this particular assembly. Emphasis was particularly given on the review of different floating liner rig designs that can undertake direct measurement of piston-liner friction.
- Overview of the newly constructed floating liner test facility and the novel features of its design are given in Chapter 3.
- In Chapter 4, the operation and behaviour of the floating liner facility in the piston-liner friction measurement are discussed. Moreover, the major development stages were also illustrated in this chapter.

- Chapter 5 is focused on the processing of raw data to crank resolved and cycle averaged friction forces along with the interpretation of the test results. The test repeatability was also discussed in this chapter to gain confidence on friction force measurement with this setup.
- In Chapter 6, the results of parametric studies on piston-liner friction are discussed. The studies entail the operational conditions such as peak pressure, rotational speed and liner or oil temperature, lubricant viscosities, and macro design factors like piston-liner diametrical clearances and piston materials.
- Chapter 7 contains the discussion of the works contained in the thesis and the key conclusions. Potential future works are also presented in this chapter.

1.6 Contribution to knowledge

The contribution from the author revolves around the development of the novel floating liner rig design, parametric studies of friction in the piston-liner interfaces and processing and interpretation of the friction data. Previous studies with floating liner design has shown that cylinder head sealing separated from the engine structure can still pose some uncertainty in friction force measurement by the application of pressure force on the liner. The development of a sealing assembly with clearance from the liner along with the use of a piston compression ring in the seal has managed to separate the direct application of gas pressure on the liner and also managed to achieve similar firing engine gas loading. The proposition of calibrations also proved to be effective in eliminating the uncertainty in friction measurement. The parametric studies undertaken have added some new dimensions in understanding piston-liner friction. The study shows piston and ring motion can play an important role along with local operating conditions in determining the friction. The previous studies with steel piston have shown reduction in friction compared to aluminium piston. The study

reported in this thesis has acknowledged the benefit of steel piston with no gas loading operation; however there was a coupled effect of shorter piston skirt size and higher piston weight towards the increase in friction during pressurised operation.

Chapter 2 Literature review

2.1 General background on piston-liner friction and lubrication

The piston assembly is usually taken to include the big end and small end bearings and this would be appropriate in an engine tear down test for friction as the big end bearing contribution is removed when the piston and connecting rod is removed. However, the study reported in this thesis deals more specifically with the friction between the piston and piston rings and the cylinder liner. The contributions of these components are influenced by a number of factors including ring tension, gas pressure inside the cylinder and inertia forces of reciprocating masses. Ring tension is defined as the tangential force required to close the ring gap [27]. Tension of the rings depends on ring design and materials which may be different for compression and oil control rings and vary from engine to engine based on purpose [28, 29]. Engine load dictates gas pressure whereas engine speed and reciprocating masses are responsible for inertia forces.

Ring tension and gas pressure behind the compression rings push them against the cylinder wall by radial forces, hence contributing to the friction during sliding motion [2]. Gas pressure along with inertia forces further contribute to the side thrust which is supported by both piston rings and skirt. Major portions of side thrust are transmitted to the liner via the piston skirt [30]. Moreover, side thrust varies along the cycle depending on the pressure and speed and also changes the direction depending on the stroke direction [31].This side Thrust (F_t) can be calculated by the following equation 2.1 using the force balances in Figure 2.1.

$$\mathbf{F_t = F_r \sin\emptyset = (-ma + \frac{\pi B^2}{4} p + F_f)\tan\emptyset} \qquad (2.1)$$

Where, m is the mass of reciprocating assembly, a is acceleration, p is gas pressure relative to crank case pressure and B is the bore size.

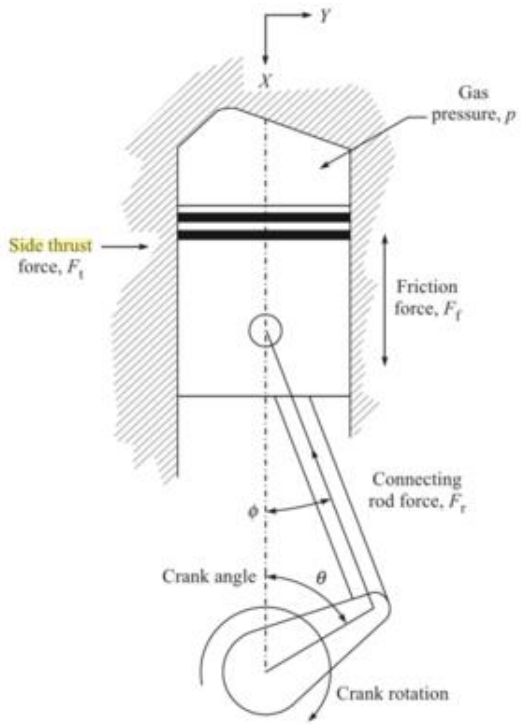

Figure 2.1: Force balances in piston-liner assembly [31]

Side thrust acts at the opposite side of crank throw and thus towards the left in Figure 2.1 during the expansion (down) stroke and to the right during the compression (up) stroke [31]. Pressure is generally higher during expansion stroke of a firing cylinder and thus higher thrust force is exerted on the left side, hence called major thrust side [2, 31]. The right side is called minor thrust side as less pressure force is exerted on the piston during compression stroke.

Friction in the piston-liner assembly can be dominated by ring pack [2, 32]. Contribution from piston skirt can be as high as 42% at higher speed in gasoline engines and 11% in diesel engines at lower speeds [33]. Rosenberg ascribed that friction in the assembly is largely influenced by the following design parameters: ring tension, ring profile, ring gap, width of the rings, ring land width and clearances, liner temperature, skirt design and skirt-liner clearance [34]

The ring friction is dependent on the ring load, surface properties and the lubrication conditions [29]. The lubricant condition is determined by the viscosity

of the oil, and piston sliding velocity [29]. Takiguchi et al. [35] noted that though number of rings in the ring pack influences the frictional behaviour, the frictional loss is determined by total tension of the rings. The study by Millington et al. [36] suggests each compression ring contributes to about 0.07 bar towards fmep.

The frictional losses between the piston skirt and cylinder liner depend on piston design, diametric clearance, tilting action of the piston, piston skirt design, surface roughness and lubricant condition [37]. Other than side thrust friction forces in skirt-liner interfaces also arise from secondary motion of piston by lateral movement (slap) and rotation about the piston gudgeon pin which causes the piston to tilt near dead centres [38].

2.1.1 Friction Characterisation

The parameters used to characterise friction in an engine, include the co-efficient of friction (f) and friction mean effective pressure (fmep). Friction forces in an engine vary with location and time during engine cycle and these dependences can be captured in expressions by local friction coefficients. Friction mean effective pressure, on the other hand, represents the work dissipated per cycle per unit engine displacement. In the case of fmep, crank or time resolved information is lost but provides a measure of engine friction which is independent of engine size [2].

As fmep is the ratio between work and volume, the unit is same as pressure and often obtained as bar or kPa [2, 39]. fmep obtained from one engine can be compared with other engines of different sizes to assess engine design efficiency.

Co-efficient of friction (f), defined as the ratio of the instantaneous friction force to the normal load, characterises frictional behaviour of the interface between two rubbing surfaces. Two sliding surfaces under similar operating conditions (normal pressure, relative velocity, temperature) demonstrate similar coefficient of friction

[40]. Thus this value can be used to assess the frictional performance of the sliding surfaces.

2.1.2 Lubricated Friction

In the piston-liner assembly the piston rings and skirt are separated from the liner by a film of lubricating oil which has a thickness which varies along the piston path. Lubricant conditions between the surfaces are strongly time dependent which varies with engine speed, gas load, temperature and counter surface effects, consequently determining the friction and wear behaviour [29].

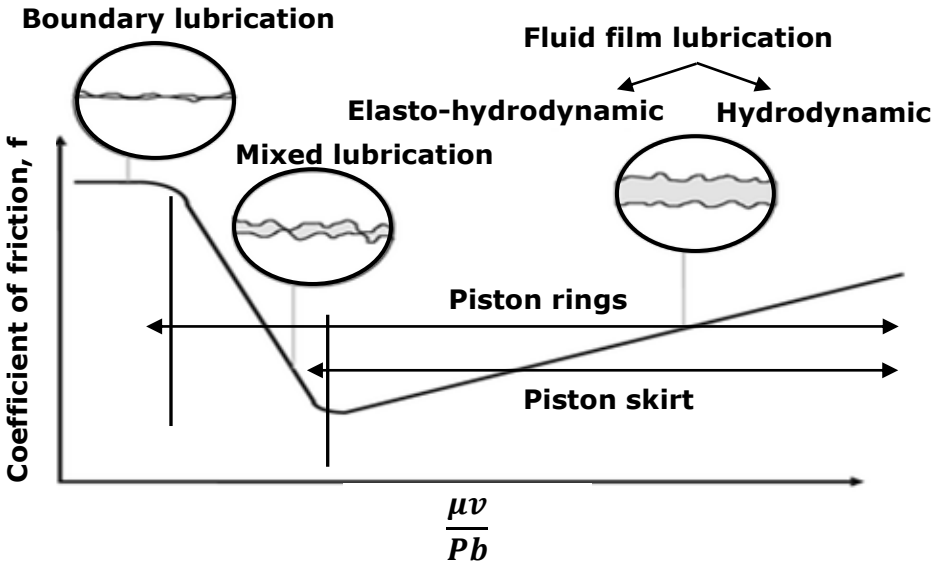

Figure 2.2: Stribeck curve showing different lubrication regimes [41]

The variation in lubricating conditions can be illustrated by a Stribeck diagram presented in Figure 2.2. The figure was edited from the original version [41] to demonstrate the lubricating regimes of piston skirt and rings. In a typical Stribeck diagram [2, 24, 40], friction coefficient (f) is presented as a function of a dimensionless number called duty parameter $\frac{\mu N}{P}$ where μ is viscosity, N is speed and p is the load. However, this was originally devised for a journal bearing system thus needed a modified version to demonstrate the transient conditions of piston assembly. Ting [42] modified the dimensionless parameter to Sommerfeld

number $\frac{\mu v}{Pb}$ for ring friction analysis where speed N was replaced by instantaneous velocity (v) and ring width (b) was considered to convert the pressure load into normal load.

The lubricant regimes are also sometimes distinguished by a lubricant film parameter (h/σ) which is the ratio of mean film thicknesses to standard deviation of surface heights. This increases non-linearly with increasing Sommerfeld number [40]. For a lower Sommerfeld number, the friction coefficient is comparatively higher at about 0.1 or more [40]. This lubricating condition is termed as boundary lubrication where the surface asperities come into contact to each other. An oxidised boundary film of oil molecules cover the surfaces which are about 1-3 nm and saves the surfaces from high wear [24, 34, 40]. The reported h/σ values in this condition are lower than 1 [40]. In extreme case of boundary lubrication, boundary film can be broken. Friction coefficient can consequently increase to 1 or more, consequently causing high wear and eventually seizure occurs.

The lubrication regime shifts from boundary to mixed lubrication with the increase in Sommerfeld number. Friction coefficient decreases in this regime with increasing Sommerfeld number and eventually drops to a critical value. This regime is also termed as quasi-hydrodynamic or thin film lubrication where some intermittent contacts exist between the surfaces [24, 40]. In this regime the film thicknesses increase to 0.025-2.5 μm and can also be characterised by h/σ values of 1-5 [40]. As the surface asperities are separated more with increasing oil film thickness, unit load can become very large in the contact areas and can cause elastic deformation [34]. Thus elasto-hydrodynamic lubrication can occur near the critical friction coefficient.

Hydrodynamic or thick film lubrication occurs beyond mixed lubrication regime where the surfaces are completely separated by thick film of oil [34, 40]. Film

thicknesses in this condition are more than 0.25 μm and ideally stay between 5-500 μm [40]. In this regime, both the friction coefficient and h/σ increases linearly with increasing Sommerfeld number.

In the piston-liner assembly, the piston skirt motion is generally considered to be operating in the elasto-hydrodynamic lubrication regime except at high loading conditions near TDC where the piston slap can cause asperity contacts [43, 44]. Piston rings predominantly operate in hydrodynamic regimes except near the dead centres [24, 45].

As the piston approaches TDC and BDC near the end of the strokes, the instantaneous velocities become close to zero. Thus lubrication regimes move towards the left of the Stribeck diagram, resulting in higher frictional coefficient. At higher load the film thickness decreases significantly between the top ring and liner interfaces and eventually reaches below 1 μm near TDC [2]. With the increase in speed and viscosity and decrease in load, film thickness increases and can reach as high as 8 μm. Experiments by Ting [42] obtained a maximum and minimum friction coefficient of 0.16 and 0.02 respectively for ring packs whereas Rosenberg [34] obtained a value of 0.2 and 0.001 respectively for whole assembly. The investigation by Ting [42] couldn't distinguish between boundary and mixed lubrication which affirms that piston rings operate in boundary region for a short amount of time.

2.1.3 Hydrodynamic friction

In hydrodynamic lubrication the friction force/resistive motion arises from the shearing of the lubricant and its viscosity which produces a shear stress at the surface [40]. The occurrence of thick film lubrication relies on two conditions [46]:

- Surfaces should slide relative to each other at a sufficient velocity to enable formation of lubricating film.

- Surfaces should have a relative inclination angle or step or move towards each other.

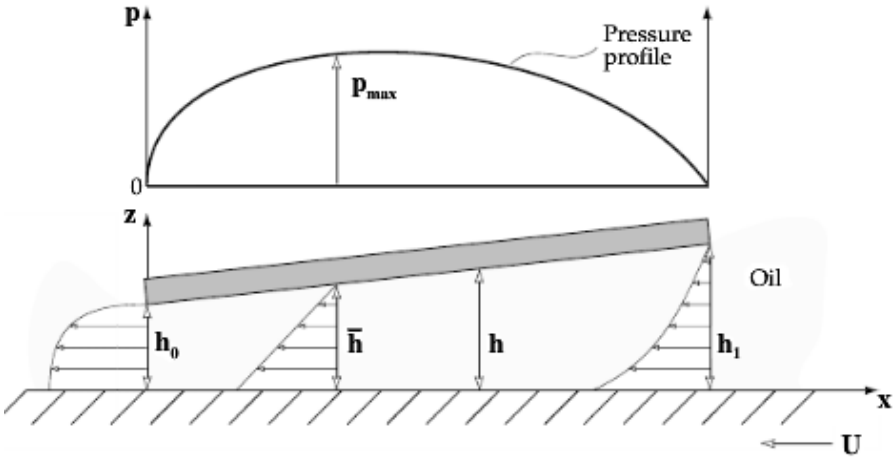

Figure 2.3: Principles of hydrodynamic film formation by wedge effect [46]

The mechanism of film formation can be explained by wedge and squeeze effects [46]. Wedge effect occurs when a surface slide along another inclined surface as shown in Figure 2.3 where U is relative sliding velocity and h represent oil film thickness with an optimum thickness of $\bar{h}$ at maximum pressure P_{max} . When the bottom surface moves towards the converging wedge, lubricating oil is dragged along it. In consequence a pressure field is generated which aids in separation of surfaces. Pressure force increases at the beginning of the wedge causing restriction in entry flow and the velocity profile to bend inwards. On the other hand, pressure gradient is negative at the exit and causes velocity profile to bend outwards.

Squeeze effect occurs when the surfaces approaches each other i.e. the gap between the surfaces is reduced [46]. This effect is important when oil film thickness is reduced to a certain level that film thickness is closer to the height of surface asperities. Thus oil film is squeezed in the narrow gap of surface asperities

generating a film pressure and squeeze velocity. This pressure generation cannot be maintained constantly as the squeeze film is always in unsteady state [18]

The wedge effect in piston assembly can be achieved by tilting action of piston relative to the bore and change in eccentricity of piston axis [47]. The curved or tapered surface of piston ring further promotes wedge effect [48]. However, squeeze effect is generally observed near TDC and BDC for both ring and skirt due to secondary motion [47].

The friction force during hydrodynamic lubrication (F_H) can be calculated by integrating the shear stress τ for a contacting surface area of A of sliding surfaces accordingly to equation 2.3 [49].

$$\mathbf{F_H} = \int \boldsymbol{\tau} \mathbf{dA} \qquad (2.3)$$

$$\boldsymbol{\tau} = \frac{\mathbf{h}}{\mathbf{2}} \frac{\partial \mathbf{P}}{\partial \mathbf{x}} - \boldsymbol{\mu} \frac{\mathbf{u}}{\mathbf{h}} \qquad (2.4)$$

The shear force can be calculated by using the equation 2.4 which assumes the lubricating oil is incompressible [49]. This equation shows the viscous shear stress depends on film thickness (h), pressure gradient ($\frac{\partial P}{\partial x}$) of the oil film, lubricant viscosity (μ) and relative surface speed (u). Thus surface properties do not influence the hydrodynamic friction force.

In piston-liner assembly ring-liner interfaces can be considered as an infinitely long bearing as the circumference of each ring is way greater than its dimension in the direction of travel [46]. Moreover the rings are subjected to variable loading condition in a cycle thus making the force approximation extremely complex [2]. The forces acting on a typical compression ring-cylinder liner interface, lubricated by viscous oil film are shown in Figure 2.4.

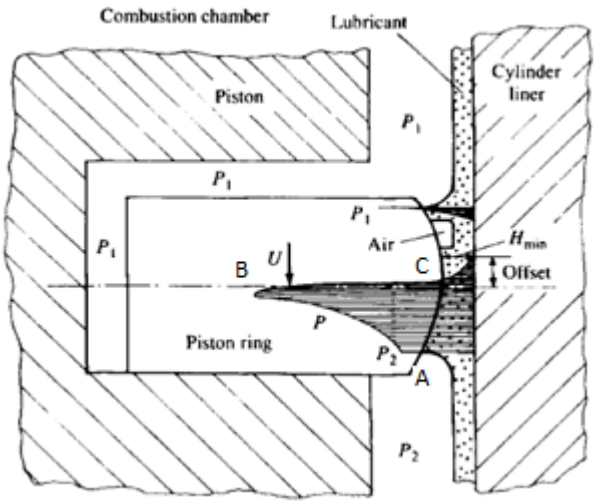

Figure 2.4: Schematic of lubricated conjunction between piston ring and cylinder liner [2]

In Figure 2.4, the cylinder pressure P_1 acts on the top and back of the piston ring whereas the inter ring gas pressure P_2 acts on the oil film and back side of the ring. With the variation in cylinder pressure and ring face geometry the forces on the ring vary abruptly in a cycle [2]. Late in the expansion stroke pressure reversals can occur which may cause the ring to move to the upper surface of the groove or to flutter in between.

Ring tension forces the ring against the liner and the barrel shape presents a converging profile, giving rise to pressure distribution A-B as the ring moves downward [45]. When ring direction is reversed the pressure decreases as shown by the surface C-B. Hydrodynamic pressure of the generated film along with asperity contact pressure balances the load on the ring [45]. The film pressure generated on the ring-liner interface can be predicted by solving Reynold's equation in equation 2.5.

$$\frac{\partial}{\partial x}\left(h^3 \frac{\partial P}{\partial x}\right) = 6u\mu \frac{\partial h}{\partial x} + 12\mu \frac{\partial h}{\partial t} \qquad (2.5)$$

This assumes the film thickness is very small compared to ring height and width [2]. The equation shows the film pressure depends on oil film thickness and the variation in thickness with time and stroke position directly influence the generated pressure, consequently the force balance.

2.1.4 Boundary friction

In boundary lubrication, a film of molecular level (typically <3nm for a monomolecular film) separates the sliding surfaces which helps in minimising any adhesive or chemical wear [40]. Important physical properties of the film which dictate the boundary friction are melting point, shear strength and hardness. Two important mechanism of surface film formation are physiosorption and chemisorption [50]. Physiosorption is the mechanism by which lubricant molecules are absorbed physically, forming a boundary film without the need of special additives. This film is adequate to protect the surfaces during lower load and temperature, but can be sheared off easily under higher loading. In Chemisorption, chemical reactions between oil additives and metal surfaces form a boundary film in this method which is much stronger than physically absorbed film.

The force required to overcome boundary friction (F_b) can be approximated by using equation 2.6 and corresponding friction coefficient (f) from equation 2.7 [24].

$$\mathbf{F_b} = \boldsymbol{A_o}\,\boldsymbol{\sigma_o} \qquad (2.6)$$

$$\mathbf{f} = \frac{\boldsymbol{\sigma_o}}{\boldsymbol{\sigma_m}} \qquad (2.7)$$

Where A_o is the real area of contact and σ_o and σ_m are shear strength of absorbed oil layer and softer sliding surface respectively.

The real area of contact depends on applied load, asperities and yield strength of softer material whereas the shear strength of absorbed layer depend on chemical

properties of lubrication oil [24]. Thus the boundary friction depends on properties of the lubricant, and surface roughness, plasticity, elasticity, shear strength and hardness. As the boundary friction depends on various interdependent variables, it is very hard to obtain a physical calculation rather various empirical and statistical correlations were made to get an approximation [49] .

2.2 Factors affecting piston-liner friction

The different micro and macro design factors affecting piston-liner friction are cylinder liner and piston ring surface finishing, piston ring profile, piston skirt profile and surface finishing, liner and piston axis concentricity etc. Moreover, lubricant formulation plays an important role in determining piston assembly friction.

2.2.1 Cylinder liner surface finishing

Cylinder liner surface finishing has great influence on the piston assembly friction as piston rings and skirt slide over the liner. Surface roughness and honing patterns are the two most important surface finishing parameters. Surface roughness is generally characterised by arithmetic average surface roughness, Ra [40] .

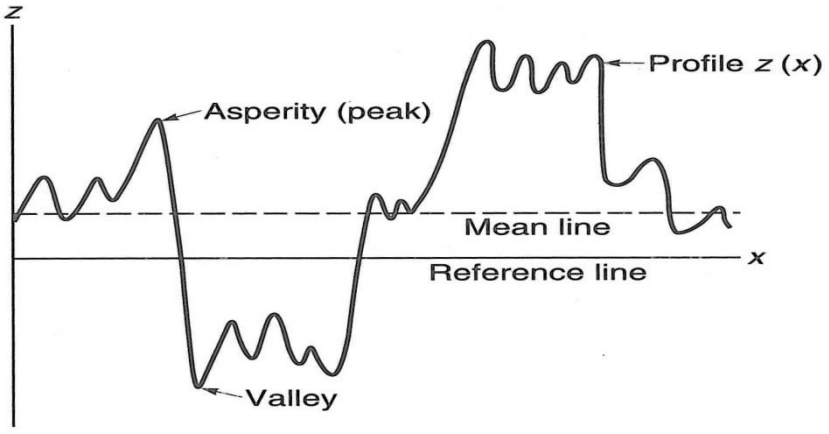

Figure 2.5: Schematic of a surface profile [40]

The Ra for the surface profile in Figure 2.5 can be defined by the flowing equation 2.8.

$$\boldsymbol{Ra} = \frac{\mathbf{1}}{\boldsymbol{L_x}} \int_{\mathbf{0}}^{\boldsymbol{L_x}} |\boldsymbol{z} - \boldsymbol{m}|\, \boldsymbol{dx} \qquad (2.8)$$

Where mean value, $m = \frac{1}{L_x} \int_0^{L_x} z\, dx$ and L_x is the profile sampling length.

Thus average roughness parameter, Ra measures the surface deviation from mean line and thus higher surface roughness or deviation is referred by higher Ra value.

Surface roughness is also characterised by maximum peak height, Rp and maximum valley depth, Rv [40].

Honing patterns are machined in the liner to finish the internal surface allowing enhanced lubrication and reduced asperity contacts during piston reciprocating motion [51] .A plateau honing finish is generally used in engine manufacturing. In this deep valleys are formed with the peaks removed to form plateaus of increased surface area [52]. The resulting surface topography is a cross hatch plateau-like surface, with honing grooves containing valleys with depths that are greater than the surface roughness as shown in Figure 2.6.

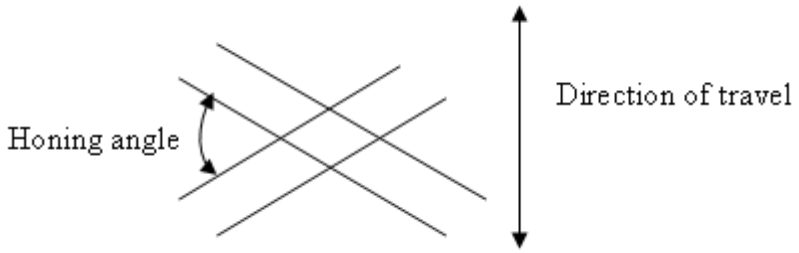

Figure 2.6: Schematic of honing pattern

A plateau-honed cylinder liner surface profile, which has a fairly flat surface base with deep valleys, is appropriate for piston assembly lubrication [51]. The valleys act as oil reservoirs and facilitate lubrication during engine critical moments like start up or when oil supply pressure is low.

Surface roughness has an important influence on friction. Rough surfaces tend to produce higher frictional values than smooth surface [53]. Durga et al. [54] investigated the effect of surface roughness on friction coefficient for a cast iron cylinder liner. They reported a 50% lower friction co-efficient around mid-stroke region with a smoother surface of Ra=0.07 μm compared to Ra=0.3 μm with SAE 5W-30oil at lower speeds of 100 and 450 rpm. They also found that application of plasma sprayed coating on fairly coarse surface (Ra=0.3 μm) obtained a lower friction values than honed cast iron liners under similar test conditions.

Galligan et al. [55] also studied the surface finish effect and found that highly polished liner gives lower friction values than standard surface finish. However, after a certain running time the friction values are levelled as the peaks are worn off by piston rings.

Honing finish is also very important other than surface roughness to control lubrication and friction. Smooth surface finish without any valleys does not have oil retention capability [51]. Thus plateau honing (PH) can reduce piston-liner friction compared to conventional finish with better lubrication facility. Reducing the peaks from liner surfaces reduces Rp values and consequently can reduce friction spikes near TDC [53]. However, reducing Ra to obtain smoother surface is also necessary to obtain lower friction [56]. Thus lower Ra is also desirable in a plateau honing finish.

Helical slide honing (HSL) is reported by Mezghani et al. [52] to be more effective than plateau honing as a friction reduction measure. They recorded a 36% increase in friction reduction using HSL compared to PH, which they attributed to a reduction in contact areas. The cross hatch angle produced from HSL was higher (130°) compared to PH of 50° honing angle. However, decreasing cross hatch angle can decrease friction due to increase in pressure driven flow blockage and consequently increasing film thicknesses, as predicted by Jocsak et al. [57]. Jocsak et al. also reported a higher oil transport to combustion chamber with

lower honing angle which is undesirable. Although the HSL method finishes the liner surface with higher honing angle than PH method, still HSL method is more suitable to obtain lower friction due to lower Ra and Rp values in the finishing surfaces [52]. Thus an optimised honing pattern with reduced surface roughness is necessary to obtain lower friction.

Surface roughness and honing patterns are not the only parameters in dictating the sliding friction. Recent research has shown that micro and nano scale surface topography are also influencing in piston-liner friction and have opened possible opportunities in reducing friction. Micro dimples can be produced on contacting surfaces by fine-particle peening treatment which can reduce the friction in lubricated condition by up to 50% [58]. One of the most promising investigations is modifying contacting surfaces in a controlled way by using laser surface texturing (LST). Kovalchenko et al. [59] investigated effect of LST on sliding friction by creating micro dimples of 4-7 μm depths on steel surfaces with diameters of 58-140 μm at average distances of 200 μm. They reported lower friction coefficient with textured surface than a regular honed surface. Furthermore they observed pronounced effect of LST at higher speed and load conditions and recommended removal of bulges from the edges of the dimples to achieve a positive impact of LST.

The laser textured surfaces promote increase in oil film thicknesses during ring reciprocating motion on the liner [60]. The dimples produce a wedge flow effect and thus promote higher hydrodynamic friction contribution and lower mixed/boundary friction and wear.

2.2.2 Effect of ring profile and surface finishing

The radial load of the piston rings on the cylinder liner causes the friction which varies with variation of ring face profile along with variation in cylinder pressure.

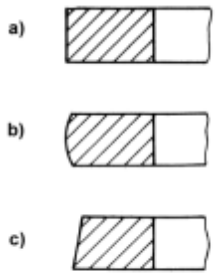

Figure 2.7: Different compression Rings: a) rectangular, b) barrel and c) tapered face

Plain compression ring with a rectangular cross section (Figure 2.7a) though meet the sealing demands required for an ordinary running condition but it exerts more force on the piston compared to a barrel shaped profile (Figure 2.7b) [29]. Barrel shaped ring profile with lower radius of curvature can further reduce the friction [61]. The ring with a tapered face profile (Figure 2.7c) can help relieving the ring force against the liner wall as it also enables the gas pressure to act on the face side [29]. Ring tension increases the radial load on the liner, thus reduction of tension can obtain reduced friction. Quillen et al. [62] reported a 20-30% reduction of friction with a low tension oil control ring. They further observed 15-25% friction reduction with a skewed barrel shaped top ring.

Piston ring finishing is also important as liner finishing in determining piston assembly friction. Wakabayashi et al. [63] investigated the transition of ring surface finish with running time and observed increase in friction with increasing surface roughness, Ra and vice versa. They reported a decreasing frictional loss contribution from the top two rings after 20 hrs of running time due to decrease in Ra. However, an increasing friction was observed for the oil control ring due to increase in Ra. Due to higher ring tension of oil control ring higher overall friction contribution from ring pack was observed, which shows ring tension as well as surface roughness determines the ring-liner friction. Wakuri et al. observed a reduced friction with run in rings compared to new rings due to decrease in

surface roughness. Other studies observed similar behaviour where engine friction reduced during running stage and in effect it reduced the fuel consumption [64-66].

Laser surface texturing is also applied on piston rings to obtain a reduced friction. Ryk et al [67] reported a reduction of 25% in piston assembly friction with LST applied along the width of piston ring compared to a regular barrel shaped ring.

2.2.3 Effect of low friction coating on piston-liner friction

Advanced surface coating methods have been used to lower friction in sliding components. Over the last 20-30 years new techniques such as physical vapour deposition (PVD), chemical vapour deposition (CVD) and thermal spraying (TS) have been used to industrially deposit coatings on engine components [1]. These methods can be used to produce coatings range from a few micrometres to several millimetres thick. For piston-liner assemblies a very thin coating can be successfully deposited on the surfaces without any need of redesign and remanufacturing of the components.

As hydrodynamic and elasto- hydrodynamic contacts have very few asperity contacts, surface coatings are less effective than for dry or boundary lubricated contacts [1]. In the boundary lubrication regime these coatings acts as a route to achieve friction reduction on the surfaces. The friction of the components are reported to be decreased by more than 80% for dry lubrication and by 10–50% for boundary lubrication by using these advanced surface coatings [68, 69].

Hard, thin, diamond-like carbon (DLC) deposition has potential to obtain friction reduction in piston assembly by reducing friction in both dry and boundary lubricated sliding condition [70]. Podgornik et al. [71] reported a minimum 30% reduction in friction in lubricated contacts by using DLC coatings on steel surfaces.

Different surface treatments like anodic oxidizing, electroplating with nickel or chromium, and Si-C dispersed Ni–P plating, can be applied on ring grooves to

obtain reduced boundary friction [72]. Skirt friction due to piston slap can be reduced by applying thin coating based on polytetrafluorethylene (PTFE), MoS_2 or graphite [73]. Ferrous sulphate film also offers possibilities to reduce skirt friction [72].

Hard chromium coatings have long been applied on piston ring to reduce friction and wear [29]. Several other techniques like gas- or ion-nitriding, Si_3N_4 dispersed Ni–P plating and Cr-N arc-ion plating are also applied successful on the rings to obtain lower friction [72].

2.3.4 Lubricant formulation

Lubricant formulation and presence of additives on it play a key role in limiting friction in hydrodynamic lubrication. Low viscosity assures that shear takes place within the lubricant with low friction and solid contacts are avoided. Moreover, it helps to form a chemical layer on the surfaces to limit wear [50].

Large energy savings could be achieved if lubricant viscosity could be reduced without changing the other functions of lubricant. The variation in lubricant viscosity during engine operation occurs due to a dependence of viscosity upon temperature, pressure and shear rate [40]. Using lubricant with lower viscosity could possibly reduce the frictional work at similar working temperature. Taylor et al. [74] found that change of oil viscosity grade from SAE 15W-40 to 1SAE 0W-30resulted in a 25% reduction in piston assembly friction.

The formation of boundary films is strongly dependent on lubricant oil formulation. Anti-wear additives like zinc dialkyldithiophosphates (ZDDP) and friction modifiers like molybdenum dithiocarbamate (MoDTC) and calcium additives are used in the oil to form wear-resistant layers and thus reducing boundary friction [75-77]. Zhang et al. [78] observed that MoDTC and ZDDP decompose to form MoS_2 and MoO_3 films on metal surfaces at high temperatures, resulting in a lower boundary friction coefficient.

Modern day oils can attain lower friction coefficient of as low as 0.04 in boundary lubricated conditions but sulphur, chlorine, and phosphorus based additives can cause poisoning of catalyst and some other exhaust treatment devices of engines [1]. Research has been carried out to formulate oil with new additive packs replacing ZDDP, which contains little or zero non sulphated ash, phosphorus and sulphur (SAPS) and can be employed in future engine oils [79]. Another research paper shows that organic friction modifier additives in oils can reduce hydrodynamic friction by promoting slip [80]. The use of liquid crystal mesogenic fluids also has potential to reduce hydrodynamic friction but their behaviour is not yet fully understood [81].

Different nano materials such as WS_2, MoS_2, and H_3BO_3 have been considered as a potential replacement of conventional oils and significant friction reduction has been reported by using those materials with optimised concentration and particle sizes [82]. Water based lubricants with certain polymeric or protein additives have also been investigated and they attained co-efficients of friction as low as 0.0006-0.4 [1].

2.3.5 Other design parameters

Crank offset has potential to obtain lower piston assembly friction by reducing the thrust force on the liner during expansion stroke [83]. Different skirt profile designs have also been investigated to attain better lubrication and reduced friction [84]. The use of Low friction pads on skirt has been proved to be beneficial by reducing friction due to piston slap [85]. Further, the design of rotating liners in engine has been imparted and a friction reduction of 23-31% has been reported with this novel design [86].

2.3 Piston Friction Measurement

Friction losses in the piston liner assembly can be measured through motored breakdown test. The major deficiency of this method is that engine operating pressure is lower than a firing engine and consequently the measured frictional loss is lower [2]. Leong et al. [85] undertook a motored breakdown test to study the effect of oil viscosity on piston assembly friction. Effect of liner surface micro finishing and piston skirt design were also studied in the investigation. In this study brake torque was initially measured for full assembly with both crankshaft and piston assembly in place. The piston assembly including piston, connecting rod and big end bearing were later removed to measure the crankshaft assembly contribution and from the difference of two measured torque, piston assembly contribution was obtained. This study further assumed that contribution from crank assembly was the same for both sets of tests. Similar study was undertaken by Silveira et al. [87] to investigate relative friction contribution from different components and further modifying piston design to improve on frictional inefficiency. The studies could only be undertaken under small loads and similar loads could not be maintained under broken down motored conditions. Thus there lies a big uncertainty on determining the friction contribution from the piston assembly in this method. Furthermore, the measured friction could only be obtained as an average cycle result, thus variation of friction force in a cycle could not be measured.

Special test rigs have been designed by several researchers to study friction force variation in a cycle. Ting [42] developed a reciprocating test rig to measure piston ring friction coefficient under simulated engine conditions. The rig was run by a slider-crank mechanism which could simulate engine speed and the compression ring and the liner were prepared with similar engine specifications to ensure realistic surface metallurgical conditions. The normal loads on the stationary ring

were varied in a controlled way by a novel ring/transducer holder and lubricating conditions were achieved by controlling the oil feed. Thus the rig was able to measure friction forces at different operating conditions.

Bolander et al. [88] developed similar test rig where cylinder liner was reciprocating in a stationary ring under loaded condition. The varied loads were applied in this rig through dead weights and running speed was varied from 15 to 300 rpm. Thus piston ring-liner friction under varied operating condition could be studied with this rig. Johansson and co-workers [26] used a reciprocating tribometer at Volvo technology, Sweden to mimic conditions of liner-ring interface at TDC. In this method a segment of liner was taken instead of full liner to measure the friction forces under simulated condition.

These above mentioned piston friction rigs are limited by their operating conditions and moreover they are not true representatives of real engine friction behaviour as friction and lubrication conditions in the rings and skirts are interdependent in the piston assembly [89]. Crank angle resolved friction for the whole piston assembly over the cycle can be obtained by either resolving forces on, or acceleration of, the piston or by the floating liner method. Former approach is an indirect friction measurement method which needs very little engine modifications but is highly error prone. The later one needs some modifications in liner support to separate it from engine structure and measure the force on the liner due to friction force through load sensors.

2.3.1 Instantaneous friction force measurement techniques

The approach described by Uras and Patterson [90] entails measuring the load on the connecting rod using a strain gauge sensor, gas pressure on the piston and acceleration of the piston as a function of crank angle . The friction force is obtained by rearranging equation 2.1 as shown in equation 2.9.

$$\mathbf{F_f = F_r cos\emptyset + ma - \frac{\pi B^2}{4} p} \qquad (2.9)$$

In their setup a grasshopper linkage system was used to transmit the strain gauge output. The crank position and rotational speed were acquired through an optical pickup and these data were used to obtain instantaneous piston acceleration. This measurement method could measure piston assembly friction in both firing and motoring conditions without any engine modification. However it is prone to measurement errors particularly at higher loads and speeds when the friction force is much lower than gas pressure force and inertia forces for 10% of the cycle. The gas and inertia forces can be of 100000 to 30000 N compared to 50-300N of friction force near TDC at high load [89]. Thus an error of 0.1% in total force measurement due to inaccurate pressure, acceleration and strain measurement can lead to 15% error in piston assembly friction.

Yun and Kim [91] tried to improve the method by adopting some error eliminating techniques. They identified that a phase delay in the acquired signals can cause error in calculation. Relative time delays between signal acquisitions were obtained to eliminate this error. Moreover, the pressure force depends on the cylinder pressure as well as crankcase pressure acting at the bottom of the piston. Thus crankcase pressure was also measured along the cycle rather than assuming it to be atmospheric.

Yun et al. [91] used an accelerometer to measure instantaneous speed as calculation of acceleration from rotational speed can be error prone due to speed fluctuations. Measurement frequency response functions (FRF) were also obtained to identify the accurate measurement range. Furthermore, the measured signals were passed through a low pass filtering at 300 Hz to reduce signal noise. This filtering proved to transform the peak force near TDC to a rounded one, thus introducing further errors in measurement. Despite the improvement techniques, this method was identified to be limited only in low speed and low load conditions.

The problems with this measurement technique were also observed by Priest et al. [89, 92]. They recorded a friction force acting in the wrong direction late in the compression stroke. The reason behind this behaviour was identified as drift in calibration of cylinder pressure transducer with surrounding temperature. Though the error was reduced by undertaking the measurement at high lubricating oil temperature yet it was concluded that this measurement method is satisfactory only at low temperature and speed conditions.

2.3.2 Floating liner rigs

In the floating liner approach, force transducers are installed in between the engine structure and the liner which moves under the action of the friction force on it. The design must ensure the test rig is stiff laterally with relative flexibility in axial direction, thus reducing the effect of side forces on the friction measurements. Modifications of gas pressure sealing are also necessary to allow less leakage without interference of pressure on measured friction force.

Earliest work with a floating liner principle was reported by Tischbein in 1940 [93]. In the test setup a horizontal cylinder liner was suspended by a wire and was allowed to move longitudinally without any resistance. The piston reciprocating motion was achieved by a slide-crank mechanism and displacement of the liner due to frictional force was recorded by photographic device. In the piston assembly the ring was pressed against the liner wall by a special expanding device to simulate gas load on the ring. Further the temperature was regulated by a heating coil wrapped around the liner and lubricating condition between the ring and liner was achieved by regulated oil drops through five radial holes in the liner. Thus variation in ring-liner friction co-efficient with temperature, pressure, speed, quantity and quantity of oil were studied using this simulated engine.

Further medications were undertaken by Tischbein [93] as inaccurate measurements of friction and acceleration were obtained by the easily moving

liner. In the modified rig, the liner was supported by four stiff rings and deflection of one spring was recorded. With the stiffer setup the deflection was kept within thousandth of mm and natural frequency was placed in a higher value to avoid resonance during low frequency piston motion.

Similar approach was taken by Forbes and Taylor [94] in concurrent time to record displacement photographically. They made the first attempt to build a fully representative floating liner rig to measure piston assembly friction in a low compression (5:1) spark ignition engine. The vertical liner sleeve in their setup was elastically mounted and was clamped by two annular steel diaphragms. A labyrinth seal was used to achieve gas sealing yet not constraining piston motion. This setup was able to measure friction force in both motored and firing condition up to speed of 2000 rpm. Leary et al. [95] and Livengood et al. [96] continued this work along with optimisation of basic design. Rogowski [97] managed to improve the accuracy of this approach by changing the photographic force measurement to an electromagnetic one.

Furuhama and Takiguchi [23] were first to manage friction force measurement in a floating liner rig directly through piezoelectric load cell. Their design was based on a single cylinder diesel engine where the liner was further isolated from cylinder head as gas force on the liner through the head was much larger compared to friction force. The high mass and stiffness of the liner caused very little movement of 1-2 μm in vertical direction, which was the primary reason to use a piezoelectric type pickup. In the setup the gas sealing was primarily achieved by installing an O-ring between the head and liner. But the gas force on the ring induced an extraneous force signals thus had to be modified.

The sealing in Furuhama's setup was modified by fixing the O ring in the groove made at the inner face of liner. This modification resulted in similar gas force effect acting on the bottom of the O-ring, consequently to the liner. Further trials

were undertaken by adjusting the clearance between the head and liner. A small clearance resulted in similar force transfer from seal to liner and a bigger clearance though reduce this effect but ended up achieving a poor gas sealing. Moreover, the force measurement was affected by liner lateral movement due to side thrust and had to be suppressed. Furuhama et al. [23] optimised the design to eliminate the effect of gas force and liner lateral movement on friction force measurement. Their final design presented in Figure 2.8 became the base for subsequent floating liner setups [84, 98-101] .

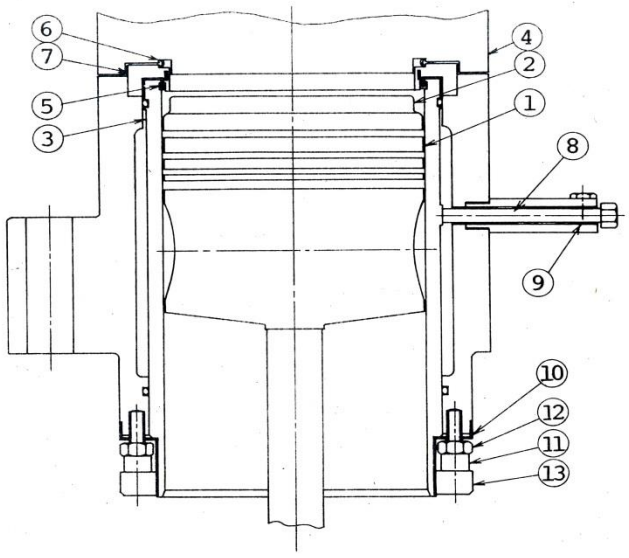

1. Piston
2. Relieved top land
3. Cylinder liner
4. Cylinder head
5. Gas seal O-ring
6. Seal ring
7. O-ring holder
8. Lateral stopper (bar)
9. Elastomer
10. Lateral stopper (ring)
11. Piezo pickup
12. Clamping bolt
13. Clamp screw

Figure 2.8: Floating liner design by Furuhama et al. [23]

In the optimised design, Futurama et al. used a lateral stopper bar to support the lateral movements. Intermittent force impulses were also observed due to piston secondary motion in the form of piston slap and were supressed by an elastomer damper fixed with the stopper bar. Another annular plate was installed at the lower end of liner to further reduce the effect of slap on friction force

measurement. Ideally the position of pickup should be near the lateral stopper to reduce the effect of block deformation under gas load. But instead it was fixed near the annular plate to minimise effect of liner vibration on friction results.

Gas sealing in the setup was redesigned with an O-ring holder to isolate the head from liner yet achieving the seal. An O-ring installed in between the liner and head was positioned by ring holder to accommodate half of it in the liner and the rest in the head. Thus a positive gas sealing was achieved with a balanced gas forces. A metal ring between the ring holder and head was used as a gasket and further facilitated the sealing. In addition, some part of piston crown had to be taken off to accommodate the modified cylinder head. This setup was able to measure friction forces in both motored and fired condition up to a maximum speed of 1400 rpm. But beyond this speed annular plate introduced some extra forces/ impulses which made it difficult to perform under high speed operations.

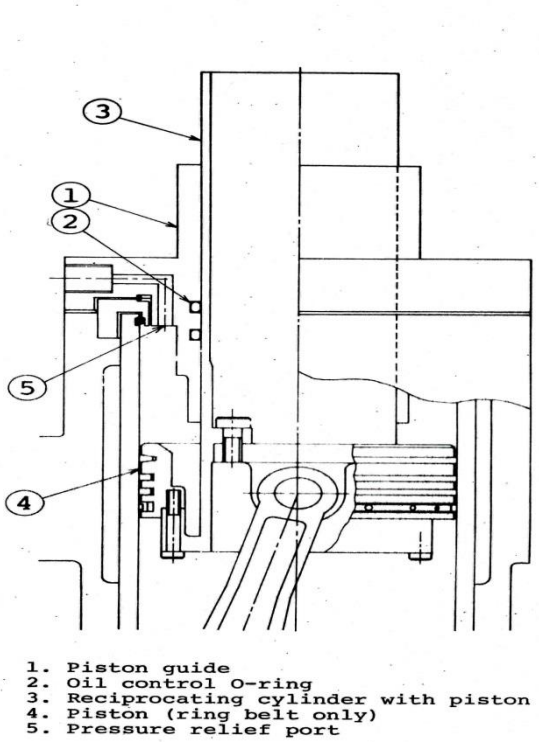

Figure 2.9: Schematic of piston ring friction rig designed by Furuhama et al. [23]

Furuhama et al. [23] also investigated the ring-liner and skirt-liner friction separately through modification of above mentioned test setup. In the modified setup presented in Figure 2.9, cylinder head was replaced by a guiding channel. A guide was fixed to the piston and was allowed to slide on the guiding channel without any lateral movement. The piston was modified to avoid any body-liner contact, thus isolating ring force in measurement. Skirt was taken off from the modified piston and piston-liner diametrical clearance was increased to 1 mm to avoid any further lands contacts.

Measurement of skirt friction was undertaken by Furuhama et al. [23] with ring packs removed from the piston. The results of separate measurement showed that friction contribution from the ring packs was much higher than that of the skirt. There were some doubts on the skirt force measurement as oil on the piston-liner interface was thicker than that of actual engine. Thus additional hydrodynamic force could be generated in the measurement process.

The measurement of separate ring and skirt frictions could only be undertaken under motored condition. Maximum pressure achieved for the ring packs measurement was 30 bar whereas for total piston assembly 45 and 70 bar were achieved under motored and fired conditions respectively. Though pressure under motored condition were less than fired one, still it was observed that friction force was proportional to pressure for rest part of the stroke. Thus it was concluded that motoring test with floating liner rig can be a good estimation of friction force and can further be adapted to the conditions of firing engine.

The rig designed by Furuhama et al. [23] in Musashi Institute of Technology, Japan has been used and updated by their colleagues over years [84, 99, 100, 102-105]. Kikuchi et al. [99] replaced the axial load cell with three components load cells to further study the secondary motions. In the updated setup eight load cells were installed in the thrust direction along the length of the liner. An

accelerometer was further installed to measure the inertial vibrations of liner and was incorporated on the original force measurement to obtain a noise compensated friction trace. Kim et al. [84, 105] incorporated a sapphire window in the single cylinder engine to study oil film distributions. They added fluorescent dye in the lubrication oil during the analysis and used a high speed camera to acquire the reflection of light from the film. Cho et al. [21] from KAIST and Liao et al. [106] from MIT used the Furuhama technique [23] to measure piston ring force under non-pressurised conditions. Wakabayashi et al. [63] imparted provision of exchangeable liner sleeve to measure piston assembly and ring friction.

Similar design to Musashi was implemented and modified by several other researchers. Most of the modification were emphasised on the gas sealing and reduction of liner vibrations due to piston secondary motion. Wakuri et al. [22, 107] used a hydrostatic bearing to support the side forces without effecting force measurement. The effect of gas forces on the liner was further reduced by replacing the metal gasket in the seal assembly with a high heat resistant thin rubber sheet. Taylor et al. [108] investigated piston assembly friction using this setup.

The method adapted by Wakuri et al. [107] consumed a lot of space to accommodate the hydrostatic bearing support, thus making the installation complicated in a multi cylinder engine. Yun et al. [98] tried to resolve the problems of Musashi rig without using the space consuming hydrostatic bearing. In the setup lateral stopper was installed within the sealing assembly and further the viton O –ring was covered by thin annular copper plate to save from combustion heat. With the modified setup the interruptions of force measurements by gas forces, side thrust and slap were greatly reduced.

Koch et al. [109] undertook another approach to minimise gas force effect on friction measurement. In their development approach, a special cylinder gasket was fitted between top of liner and head to reduce the gas force exerted on the liner. Maximum 5% of total forces were estimated to be shared by gas force through static calibration. Flexibility in different liner micro and macro designs is another important feature of this setup.

A novel design of floating liner rig was patented by Ha [101] from Hyundai Motor Company, South Korea in which he aimed to avoid intrusion of the normal piston path by the cylinder head. In his assembly removal of top part of piston crown was avoided and a pressure balancing chamber was designed outside the liner. In the new gas pressure compensation design a discharge hole was drilled through the top of the liner to communicate with the outer chamber. Three O-rings were used to seal the chamber and further coolant path was installed around the rings to increase the thermal durability. A schematic of different pressure balancing method applied in some of the above described setups are shown in Figure 2.10.

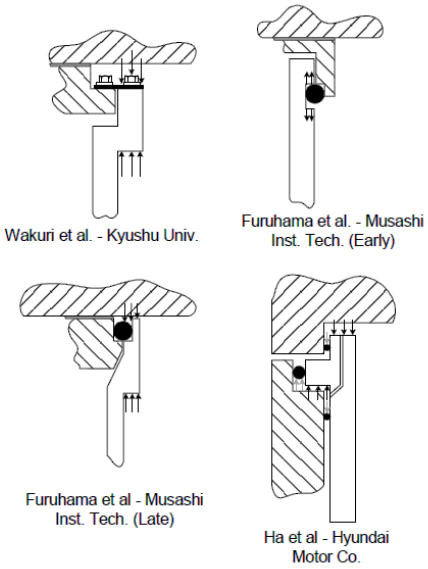

Figure 2.10: Schematic of different gas sealing systems (centre of cylinders are right to the pictures) [6]

An uncertainty of less than 0.3% in pressure compensation was reported by Ha. In his setup, lateral support was placed around the top part of liner. A protrusion around the outer circumference of upper portion of liner and an indentation in the cylinder block corresponding to liner protrusion helped in accommodating the lateral support. The support was stiffened in lateral direction to avoid distortion of friction force signals by side thrust and slap. Moreover, axial stiffness of lower support accommodating the load cells was increased to minimise the axial deflection. Stiffness in axial direction also increased the natural frequency of the system and thus avoided resonance by lower frequency piston reciprocating motion. Axial stiffness of upper support was avoided in this setup to transfer the friction loading to upper support. This was achieved by installing a multi-layer cantilever which reduced the bending stiffness of the lateral support with the same compressive stiffness. Ha and co-workers [25] used this rig to study the effect of operating conditions and some macro design features (piston-liner clearance and ring tension) on piston assembly friction force.

Another different design of motored floating liner rig was reported by O'Rourke et al. [110] where the liner was clamped by radial supports. The clamps were cantilevered from the load cells and were able to measure friction forces at every 0.5° of crank angle. The setup had the provision of simplified and quicker piston-liner exchange. The tested liners were manufactured with stock engine specifications. In this setup the liner temperature was varied by flowing heated oil through a band heater surrounding the liner. Multi axis force measurements were performed with this assembly in the speed range of 500 to 6500 rpm. Moreover, gas sealing with pressure force balance was achieved by sealing the gap between the liner and cylinder head by an O-ring.

Similar liner clamping principle was employed by Gore et al. [111] in Loughborough University, UK. In their setup three preloaded load cells were installed at 120° to each other for even measurements. They introduced some

modification in the sealing device by replacing the cylinder head with a labyrinth seal at both inner and outer faces of the liner as shown in Figure 2.11. This allowed complete decoupling of seal from liner, consequently not constraining the liner displacement. Although the labyrinth seal ensured frictionless contact at the top of the liner, high air leakage past the gaps was obtained.

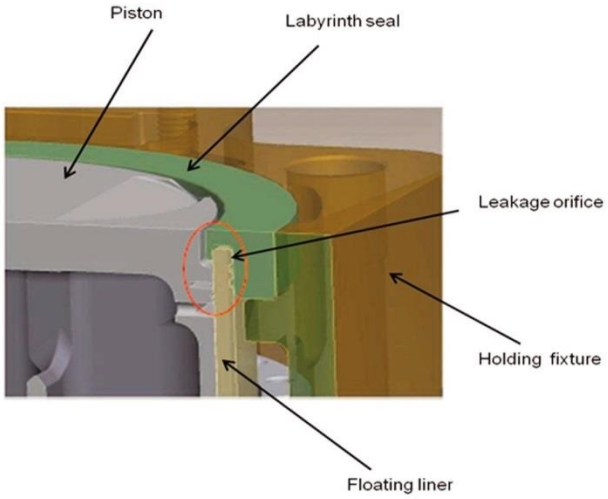

Figure 2.11: Sealing arrangement employed by Gore et al. [111]

Kunkel et al. [112] identified the major deficiencies of conventional floating liner devices and tried to improve on them. Reproducibility of friction results was an important issue which occurred due to frequent sealing device replacements and using four load sensors. He observed that two load cells decreased the rigidity and measurement range but improved reproducibility. Influences of gas and side forces were eliminated through some calibrations and then force correction. The interference by pressure force on the liner was measured by pressure variation under steady speed. Measured force signals were also filtered by band stop filters after examining system natural frequency. Further side force interferences were eliminated by taking account of the interference from vibration at different speeds.

Achieving a high peak pressure similar to a fired engine without imparting gas forces on the liner was a biggest challenge faced by most of the researchers. Kim et al. [113] used a supercharger to boost the cylinder pressure at all speeds. A recent report [114] by AVL powertrain, UK shows a higher peak pressure achievement by using a motored engine boosting method. In their system, nitrogen was heated in a closed circuit at 5 bar and supplied in the cylinder chamber during motored operation. Thus peak pressures of 120 bar in gasoline engine and 200 bar in diesel engine were obtained. Moreover, the very high temperature of 350°C of nitrogen in the intake manifold attained higher piston temperature of 260-310 °C, a realistic engine condition.

2.4 Discussion

The complex friction and lubrication behaviour in piston ring-cylinder liner and piston skirt-liner interface is very hard to predict; making it indispensable to undertake actual measurement process. The different components experience variation in lubrication modes around a piston reciprocating cycle and consequently a varied friction force is experienced in the assembly. The transition from boundary and mixed to hydrodynamic lubrication occurs depending on various factors which include the operational conditions, surface topography, macro features like skirt and ring design and lubricant formulation.

Piston rings particularly the top ring is the biggest contributor to the friction losses in this assembly. Higher friction forces between the ring and liner interfaces near the dead centres (in boundary/mixed lubrication) compared to the majority of the stroke (in hydrodynamic lubrication) can lead to high wear and consequently lower engine life. Surface finishing of liner and piston rings along with the ring design is given particular importance to achieve proper lubrication and hence lower frictional losses by advancing the transition of lubrication regime. The crater produced in liner surface by plateau honing or laser texturing can promote better

oil film formation near the dead centres by acting as oil reservoirs. Barrel or tapered shape of piston rings can also help in oil film formation by the wedge mechanism. Interaction of surface and lubricant is highly influencial in dictating the friction in boundary lubrication regime through the formation of boundary film. Thus lubricant formulation plays an important role in this case.

Different bench rigs and indirect measurement techniques have been introduced in the piston-liner friction measurement. None can reach the higher accuracy with closer engine condition as the floating liner can. The direct measurement of the piston assembly friction (excluding small and big end bearings) have been undertaken by isolating the liner and cylinder head from the engine structure. The cylinder head sealing in the floating liner has been modified over years to isolate the gas pressure force from the liner yet achieve high cylinder pressure closer to firing engine. An O-ring seal or metal gasket in between cylinder head has been used to balance the pressure force on the liner. Still some uncertainties were present in those methods. A labyrinth seal method [111] has also been developed to overcome the problems with cylinder head sealing but faced problems with gas sealing. High radial stiffness in the lateral support and axial stiffness of liner bottom end support have been implemented to suppress the effect of side thrust and inertia force respectively on friction force measurement. The impulsive noises by piston slap have been suppressed by using elastomeric damper with liner bottom or top end support. Exchangeable liner design has been imparted in many designs [63, 110] but were limited by the peak cylinder pressure.

Chapter 3 Floating liner test facilities

3.1 Introduction

In this chapter, an overview of the floating liner test facility and component designs is presented. A schematic cross section of the facility is given in Figure 3.1 and photograph of the assembled rig is shown in Figure 3.2. The design of the test facility was developed with the intentions of investigating a range of components based on a fixed bore of 86 mm and stroke of 94.6 mm. Of particular importance was the ability to change the liner design. A series of developments were undertaken on the previous setup [6] to attain this current arrangement. Major developments include the modification of the sealing assembly to avoid extraneous force interference on the friction force measurement and modification of driveline assembly to support high gas loading operations.

A 15 kW electric motor was used to drive the single cylinder motored rig. Cylinder liners were modified for the rig and were prepared with different surface topographical specifications for parametric studies within the test programme. The rig can simulate engine conditions by adjusting the operating parameters such as cylinder pressure, liner temperature and rotational speed. The engine peak pressure conditions can be achieved by injecting a controlled flow of compressed air in the cylinder through an air injection system. The electric motor, through a driveline, supplies adequate torque to run at required speeds and loads.

In the setup, temperature of the liner can be adjusted and controlled by supplying heated oil to the piston and consequently heating the liner. A lubrication oil circuit, consisting of heating reservoir and adequate pumps and pipe fittings maintains the oil circulation in a closed loop. This oil can be changed to different grades and viscosities to study the effect of lubrication oil formulation and

viscosity on piston-liner friction. Moreover, the micro and macro features can be studied by interchanging different liners and pistons.

Some of the macro features which could be investigated by using this facility are piston-liner diametric clearances, piston ring profiles, and piston shapes, sizes and material. Different liner-piston combinations can be used to test with desired diametric clearances and piston designs. Liners with different surface topographical features like roughness, honing angle can also be investigated to study micro features of piston-liner assembly.

This rig is capable of acquiring crank resolved friction data through load cells at very high speed operation of up to 3000 rpm. Several thermocouples and piezoelectric pressure sensors are also instrumented in the rig to measure temperatures and pressures respectively. These data are acquired and processed continuously during rig operation by LabVIEW software installed in a computer. Moreover, control of some operating conditions such as cylinder pressure and speeds are also undertaken by the software.

3.2 Mechanical design and general assembly

The floating liner rig was designed to measure the resistive force on the liner due to piston-liner rubbing friction. The bottom part of the liner is fixed on the diaphragm by clamping the outside flange with two half-moon mild steel clamps and the flexibility of diaphragm allows the liner movement in the axial direction. However, the top of the liner is held in position by a rigid diaphragm around the liner such that there is, little or no movement in the lateral direction. This allows the axial friction force in the piston-liner assembly to be isolated and directly measured by load cells that are positioned underneath the liner.

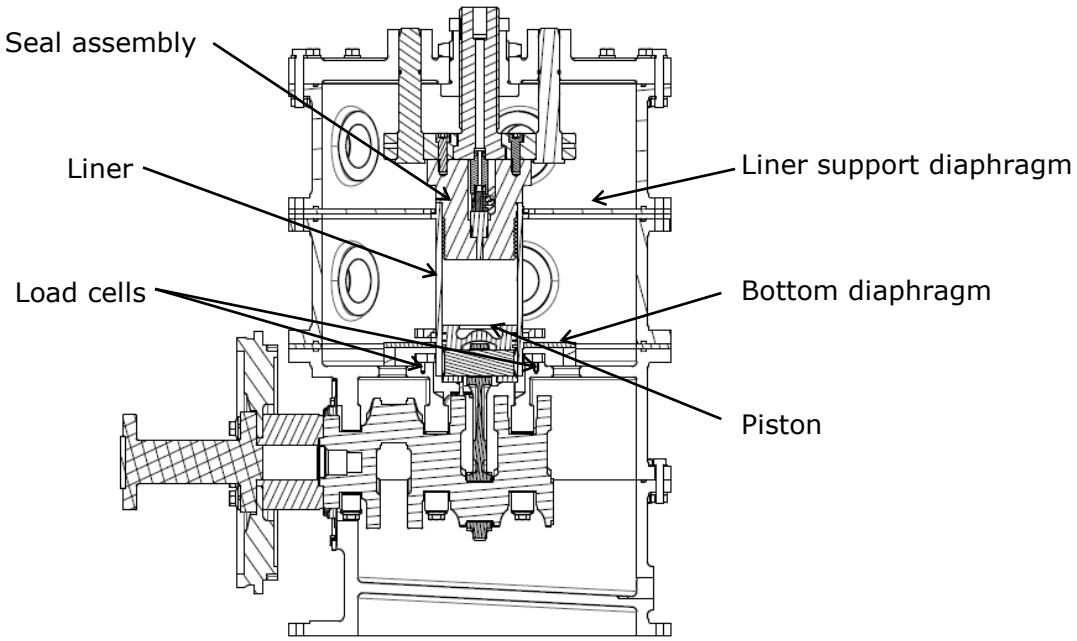

Figure 3.1: Schematic view of Floating Liner Rig

The whole assembly is fixed inside a stack of four cylindrical casting blocks. The bottom block is used as an oil sump whereas the next one is used to mount the crank assembly. The crankshaft used in the setup was modified from a 4 cylinder 2.2 L diesel engine crank referred to as 'Engine A', retaining three main bearing supports and two crank throws. The dynamic balance was achieved with a counter weight balance around the unused crank throw. The liner along with two diaphragms at the top and bottom of it are fixed between the second and third castings. The piston is fixed at one end of connecting rod with a gudgeon pin and reciprocates along the liner surface. The other end of the connecting rod is connected with the crank throw with a big end bearing. Thus the rotary motion of the crank is converted to reciprocating motion of piston with the help of the connecting rod. The piston cooling jet is placed underneath the liner at the anti-thrust side to allow the oil jet to impinge directly at the bottom of the piston without touching at its bottom dead centre position.

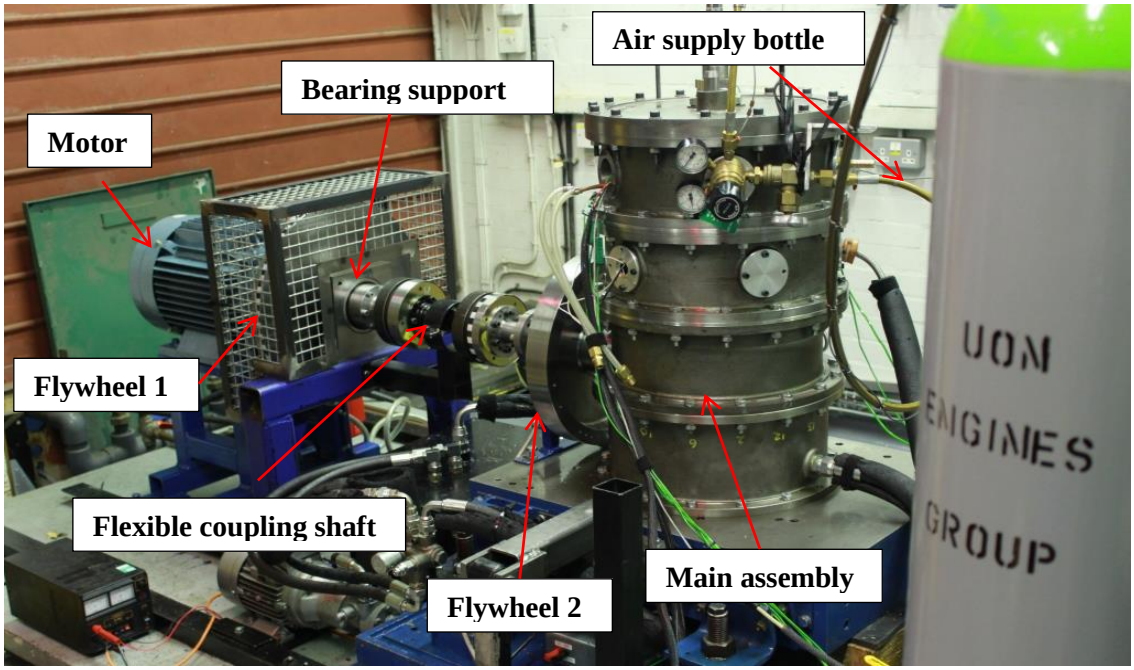

Figure 3.2: Floating Liner Rig installed on the test bed

Two compression rings at top two piston ring grooves and an oil control ring at the bottom groove were used to seal the gap between the piston and liner. The rig was not equipped with conventional valves, gear or gasket sealing to allow relatively quick and numerous piston and liner combination changes and rig rebuilds. These were replaced with a non-contacting sealing plug assembly which is mounted at the top cover of the rig. The clearance between piston and plug could be adjusted to achieve the desired compression ratio. The diametric clearance between the plug and liner was kept at 200 μm and the gap was sealed with a top piston compression ring.

The lubricating oil was fed into the piston through the piston cooling jet and around the liner in a jacket. This was heated and cooled so as to control the temperature of the cylinder liner. The liner features drillings on both the thrust and anti-thrust sides to allow thermocouples to be installed to measure the liner temperature at top and bottom ring reversals, and at the mid-stroke.

The whole rig is fixed on a seismic mass consisting of a concrete rectangular block of 75.5x56x14 cm size which is mounted on four flexible rubber mounts on its side. The crank is connected with the driveline assembly consisting of a spacer between crank and a flywheel, an extension shaft for encoder mount, flexible couplings shaft, bearing support, another flywheel and a motor. The shaft encoder provides two digital output pulses, one at every rotation and another at every 0.5° crank angle. This allows the system to measure the speed and resolved friction force at 0.5° crank angle resolution.

3.3 Basic hardware configurations

The basic components of the floating liner rig mounting arrangements are cylindrical liner, piston, piston rings, connecting rod, and piston cooling jet, sealing plug assembly, crank assembly, flexible diaphragm, rigid top diaphragm and liner cooling jacket. The cylindrical liner is the floating component of the system which experiences friction forces at the inside surface because of reciprocating piston assembly. The sealing plug equipped with a top piston ring, so the seal's only contact with the liner is by the ring and it also ensures rise in cylinder pressure by sealing the air gap at the top of piston. In this section the configurations of liners, piston-assembly (piston, piston rings, connecting rod and piston cooling jet) and sealing plug are outlined.

3.3.1 Cylinder liner

The cylindrical cast iron liners have an adapted configuration to fit into the rig. The inner surfaces of the liners have variable texture specifications such as variable average roughness parameter (Ra) and honing patterns. The Figure 3.3 shows the picture of one test liner.

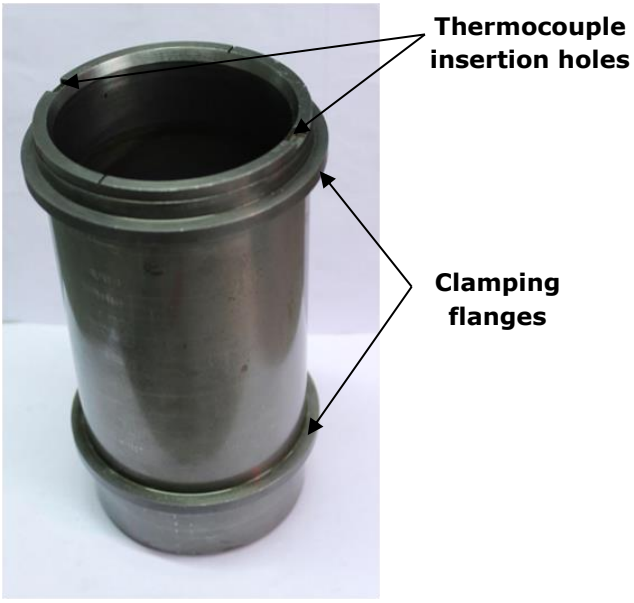

Figure 3.3: Photo of tested liner P2.

The liners have an average inner diameter or bore size of 86 mm, outside diameter of 100 mm and height of 201 mm. The flanges of 6 mm height and 6 mm width, at the top and bottom of the liner, are used to secure the liners with top and bottom diaphragms respectively. The flanges are apart by a distance of 137 mm. Top and bottom dead centres of the piston are positioned at 43 and 137.6 mm respectively from the top of the liners. Three holes, each of 1mm diameter are bored out on both thrust and anti-thrust side of the liners at different depths for the thermocouples insertion. The thermocouples are inserted 43, 90 and 140 mm deep into the liner to measure the temperature at top, middle and bottom of the stroke respectively.

3.3.2 Piston assembly

Pistons of two different materials, steel and aluminium, were used in this study. Pistons used for the test study are shown in Figure 3.4. The aluminium pistons have standard 'Engine A' configurations. The bespoke steel pistons were produced to meet the same duty; though the designs differ substantially in features such as skirt depth. The nominal diameters of both the pistons ranged from 85.92 to

85.98 mm, giving piston-liner diametric cold (room temperature 15°C) clearances of 20 to 80 µm.

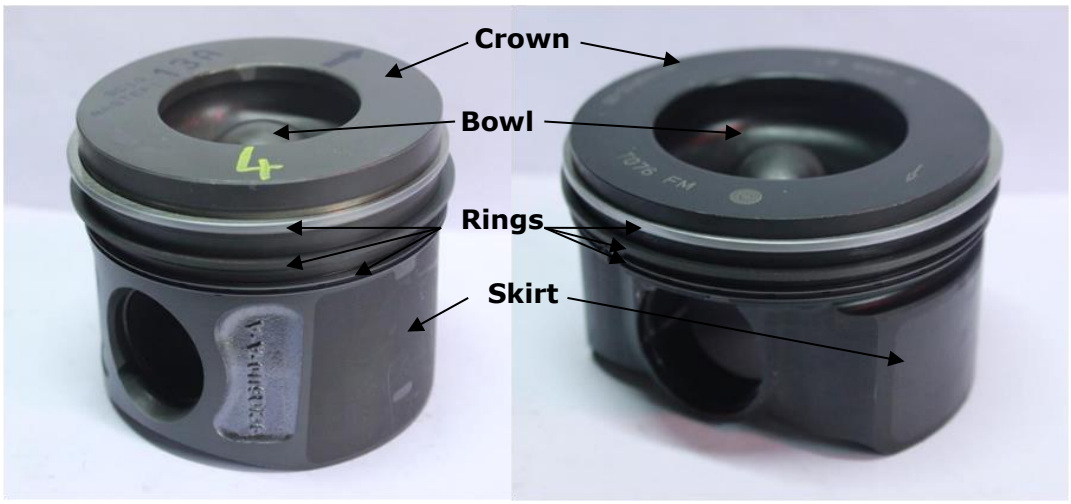

Figure 3.4: Aluminium (left) and steel (right) pistons with piston rings

Both the aluminium and steel pistons have an average diameter of 85.94 mm. The total height of the aluminium piston is around 74.5 mm while the steel pistons have a height of 56 mm. Moreover some materials were taken off from the skirt regions in steel pistons, parallel to gudgeon pin cross section planes. Despite the shorter height and less volume of material, steel pistons weigh more than aluminium pistons, around 600 g compared to 500 g for aluminium piston. Both pistons have similar bowl design having a volume of 25 ml. The difference in height between the pistons was a result of differences in the side faces and skirts. The same sets of rings were used in both pistons in this study. All the three ring grooves in the pistons have depths of around 4 mm and widths of around 2 mm. Both pistons have similar internal oil gallery to allow the oil flow around the ring grooves inside the piston. The schematic of a basic piston shape is shown in Figure 3.5.

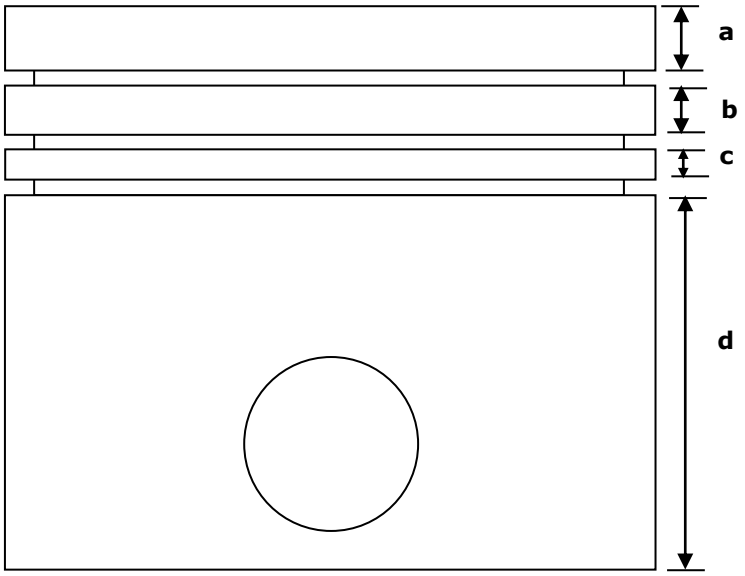

Figure 3.5: Schematic of a basic piston shape

The dimensions a, b and c of the lands above and between the ring grooves, and the dimension d of the piston skirt are different for two pistons. For aluminium piston a=8.5, b=6.5 and c=4 mm while for steel pistons they are 4, 3.5 and 2 mm. Furthermore the skirt length d is 49.5 mm for aluminium whereas 34 mm for steel pistons. Thus lesser areas of the steel pistons are in contact with the liner during the piston motion. Because of the shorter height of steel pistons, the connecting rod length is higher than that for aluminium pistons to reach the same TDC and BDC positions. For steel pistons the connecting rod length is 166.5 mm. For aluminium it is 160 mm. Though the lengths of connecting rods are different, their shape and the size of the big and small end bearings are the same.

The connecting rod is connected to the crank shaft by the big end bearing. The crank assembly for the setup had a crank throw of 47.3 mm to give a stroke of 94.6 mm. Lubrication oil is supplied at a minimum pressure of 2 bars to the main journal bearing supports and big end bearing through the internal casting gallery.

A piston cooling jet is fixed in the crank case casing below the piston at the anti-thrust side. The 1.5 mm internal diameter nozzle of jet is positioned to direct the oil to the inlet hole of piston gallery which then comes out of the outlet at the thrust side. The jet is designed to work at a minimum oil pressure of 1 bar and supplied with oil from the main oil gallery circuit.

3.3.3 Top sealing plug

The sealing plug assembly is used in the setup to seal the air at the top of piston. In the assembly a plug of diameter of 85.8 mm at the bottom and 100mm at the top, is fixed with a thick diamond shaped holder. The holder has two 30mm diameter pins attached to it as shown in Figure 3.8. These pins are used as guiding pins for the seal assembly. The holder also connects the plug with an externally threaded column for the supply of air and fixation of the assembly with the top casting plate.

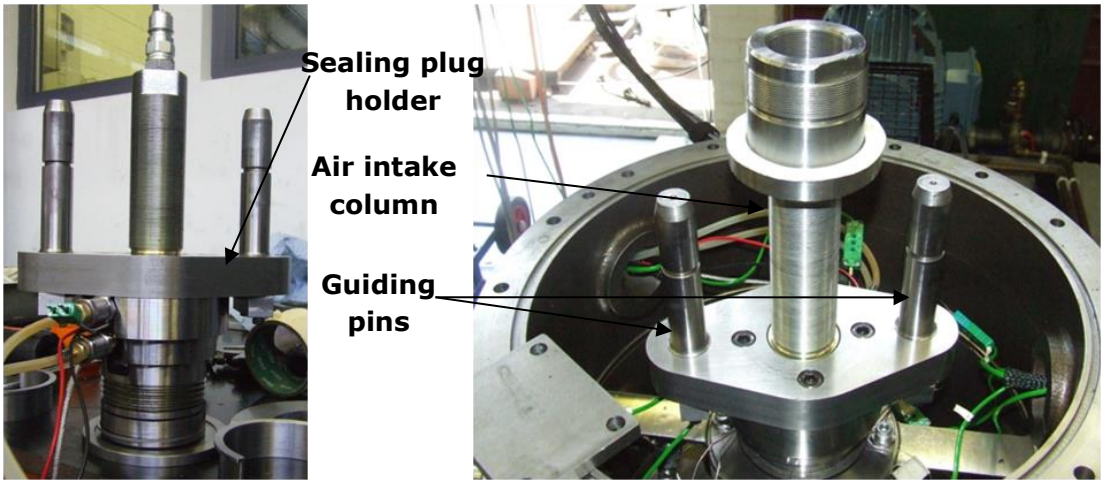

Figure 3.8 : The sealing plug assembly

The sealing plug has a total height of 115 mm with a hole of 43mm diameter bored out at its centre down to 90 mm from the top as shown in Figure 3.9. This

space is used to accommodate a collar of 42mm outer diameter, 35mm height and 36 mm inner diameter. This collar holds the injector with a cooling coil wrapping around it. Continuous flow of water through the coil helps in maintaining the temperature of the injector along with the plug at around 40°C. Another 25 mm deep hole with a diameter of 5 mm is bored out at the bottom to fit the injector nozzle.

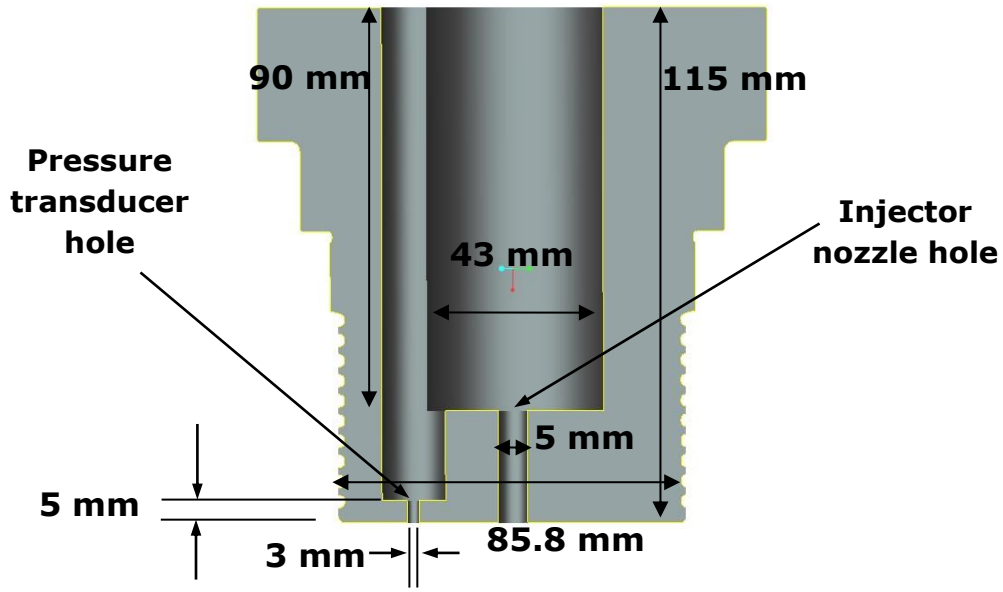

Figure 3.9 : Cross section of sealing plug

In the seal assembly a regular ''Bosch'' GDI fuel injector is installed to inject controlled flow of air at the cylinder. Two silicon rubber O-rings are used to seal the gap between the injector nozzle and the hole. An extension column with 8 mm inner diameter bridges the gap between the injector and the air supply column. An extra hole is bored out to fit a pressure transducer. This hole has 3x0.75mm thread for its bottom 5 mm and is unthreaded for the rest of the 13mm plug height as shown in Figure 3.10. The front of the plug is slotted to take out the cooling coil and injector and pressure transducer wires.

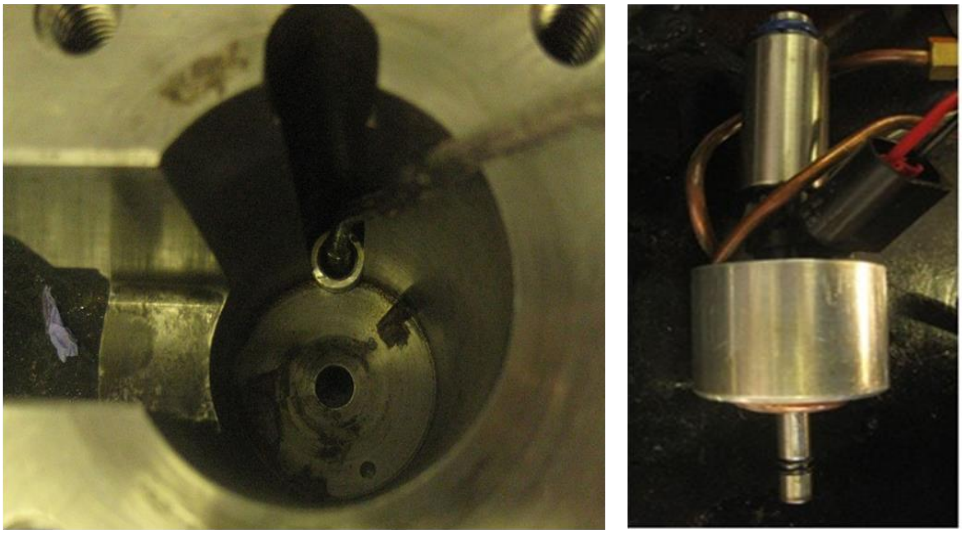

Figure 3.10 Top view of sealing plug with pressure transducer fitting (left) and injector assembly (right)

The sealing assembly is fixed with the top casting plate with the help of locking nuts. The externally threaded column helps in adjusting the vertical position of the seal assembly thus allowing adjustment of the compression ratio.

3.4 Floating liner and load cell mounting

The cylinder liner is prevented from moving laterally in the rig by two diaphragm supports at the top and bottom flanges on the liner. A gap of 12mm between the top flange and top of the liner accommodates the clamping arrangement with the top diaphragm. The assembly is shown in Figure 3.11. Two half-moon clamps are placed at the bottom of the top flange to fix the top of the liner with the top diaphragm. On the other hand, the bottom flange helps to clamp the liner with bottom diaphragm which is fixed at crankcase casting. The top diaphragm was designed to stop the lateral movement without interrupting any friction force measurement. However, a very small portion of axial force is transferred from the liner to the top diaphragm while the bottom diaphragm takes major portion of the vertical load from the liner; the effect is eliminated by conducting in-situ load cell calibrations.

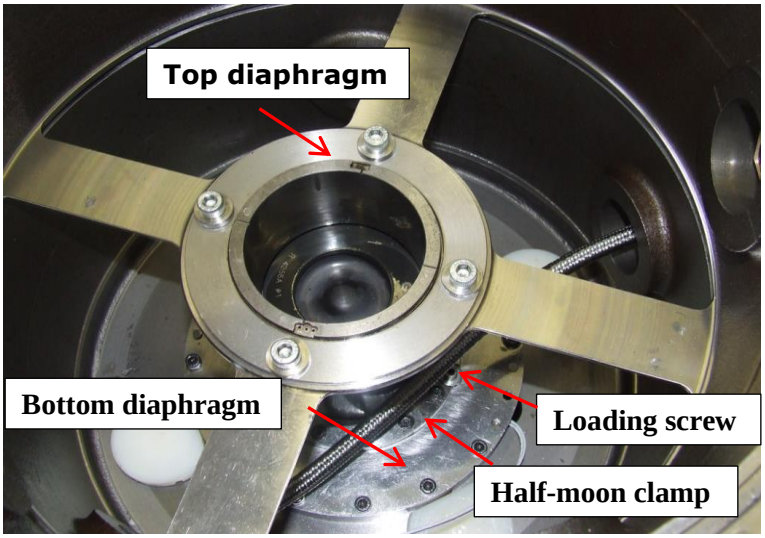

Figure 3.11: Liner clamped with top and bottom diaphragm

A bottom diaphragm supports the liner and transfers the load to the load cells that are mounted underneath the diaphragm to measure the force exerted on the liner as shown in Figure 3.12. The bottom diaphragm is a sandwiched metal structure, designed to introduce stiffness and damping out vibration. The assembly has an inner diameter of 100 mm to accommodate the liner, an outer diameter of 220 mm and thickness of 6 mm at the outer periphery.

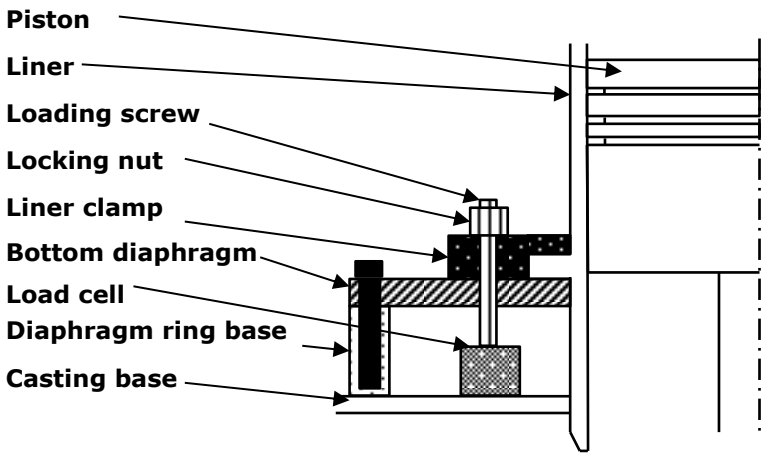

Figure 3.12 : Schematic of liner clamping with bottom diaphragm assembly

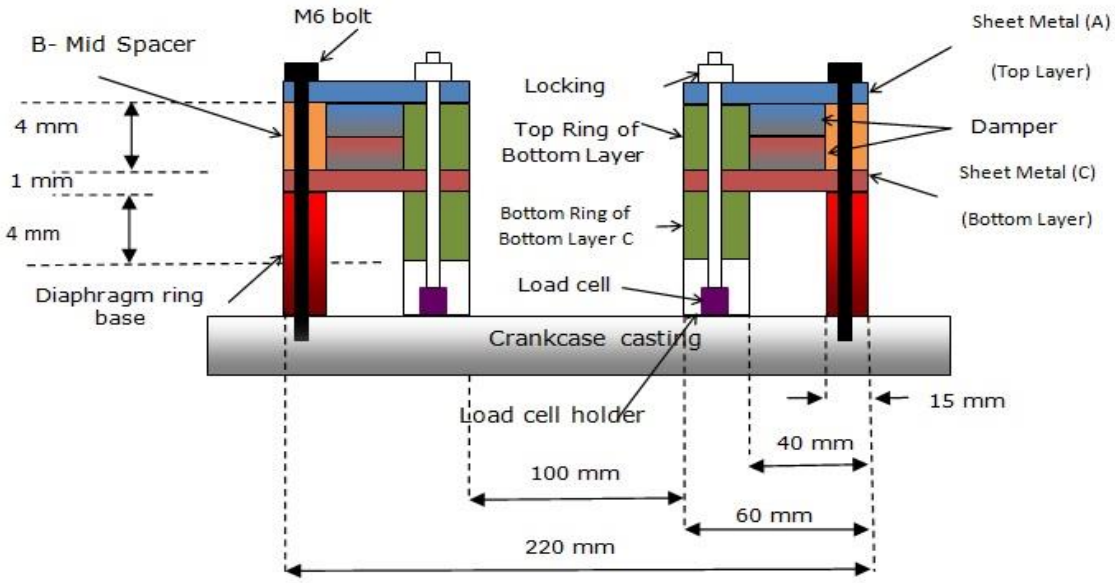

Figure 3.13 : Schematic of bottom diaphragm and load cell assembly (not drawn with scale).

In the bottom diaphragm, two metal sheets of 1 mm thicknesses mild steel are separated by a 4 mm thick and 15 mm wide spacer at the outer periphery and 4 mm thick and 20 mm wide ring at the inside periphery as shown in Figure 3.13. The outer periphery of sheet metals and the mid spacers have 16x 6 mm through holes with a PCD of 102mm. To fix the bottom diaphragm with the ring base on the casting M6x40mm bolts are used (Figure 3.14). Both the top and bottom sheet metals have 2.5 mm dampers fixed with thermoplastic glues at their inner surfaces and they form a 4 mm sandwiched layer when compressed together as shown in the Figure 3.13. The dampers are ‘’Paulstra’’ aluminium anti vibration sheets which are commercially formed by bonding highly damping elastomers to aluminium sheets. The dampers were chosen for their desired temperature operating range of -30 to 80°C and good noise and vibration reduction capacities.

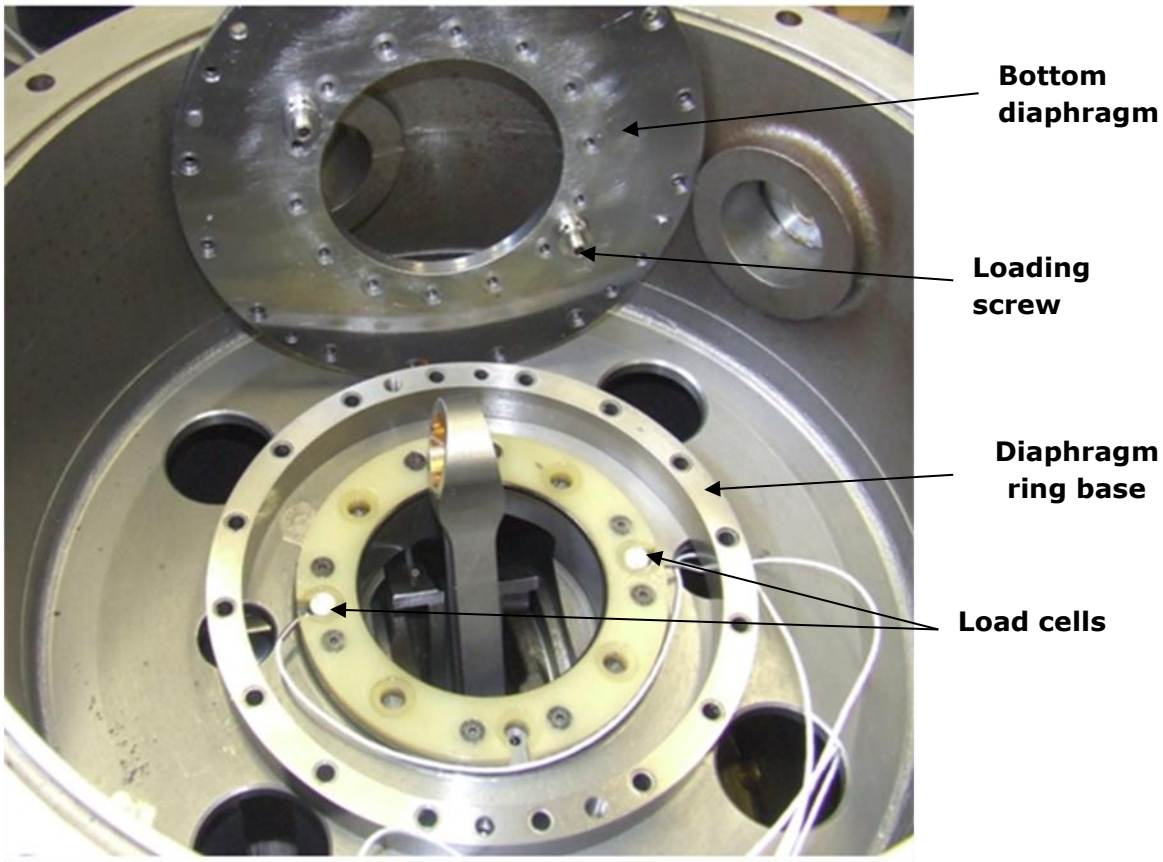

Figure 3.14 : Bottom diaphragm and load cell assembly.

The inner periphery of the diaphragm has 14x5 mm equally spaced holes of 60 mm PCD, where the liner flange is clamped to the diaphragm by two half-moon clamps. Two 6mm holes opposite to each other are also drilled for insertion of two loading screws as shown in Figure 3.14. The two load cells are placed underneath the diaphragms where the loading screws are used to transfer the load on the diaphragm from liner, to the load cells. In this setup preloads are applied to the load cells with the help of loading screws and locked in place by locking nuts. This is undertaken as the load cells are only responsive to compressive loading, the preloads help in measuring force in both downstroke (downward force at the liner) and upstroke (upward force) of piston motion .

3.5 Rig Drive and Lubrication system

The rig is driven by a 15kW 415V three phase ABB M2QA 160 L4A cast iron electric motor. This is fixed to rail supports embedded in the concrete floor as seen in Figure 3.2. The motor has a nominal torque of 98 N m at a speed of 1500 rpm with a maximum torque capacity and speed of 235 N m and 3000 rpm respectively. Two flywheels, with inertia of 1.07 and 0.42 kg m^2 were designed and installed in the driveline to support the motor during high peak pressures (over 80 barg) operation. The high inertia of the flywheels ensures sufficient torque supply to the rig, as at a high pressure of 80 barg at 1000 rpm the maximum torque requirement could rise as high as 600 N m and the motor was not capable enough to supply this torque. The first flywheel, coupled at the motor shaft on one side, has a mass of 41 kg and is supported by a 70x125x31 mm SKF 2214 E-2RS1TN9 self-aligning ball bearing on the other side. The other flywheel installed on the rig side of the driveline has a mass of 17.3 kg and diameter of 185 mm.

The reasons behind using two flywheels and a separation between them: a) the height of the centre of the crankshaft from the casting block of 200 mm was not sufficient to accommodate a 230 mm radius flywheel over the rig side, and b) A single larger flywheel on the motor side resulted in excessive energy transfer through the shaft and eventually caused shaft failure at some certain speeds (at 400 and 750 rpm the rig experiences resonance), during pressurised testing.

A flexible rubber coupling shaft of 470 mm supplied by Centa transfers the driving torque from the motor to the rig. This shaft has two rubber couplings; each of 160 mm diameter and 75 mm thicknesses, which protect the driveline from torsional vibration. Finally, a 112.5 mm long solid extension shaft with a diameter of 50 mm connects flywheel 2 with the propeller shaft. This shaft also serves the purpose of supporting the shaft encoder as shown in Figure 3.15. A disc was fixed

at the end of extension shaft after encoder installation to connect the assembly with the propeller shaft.

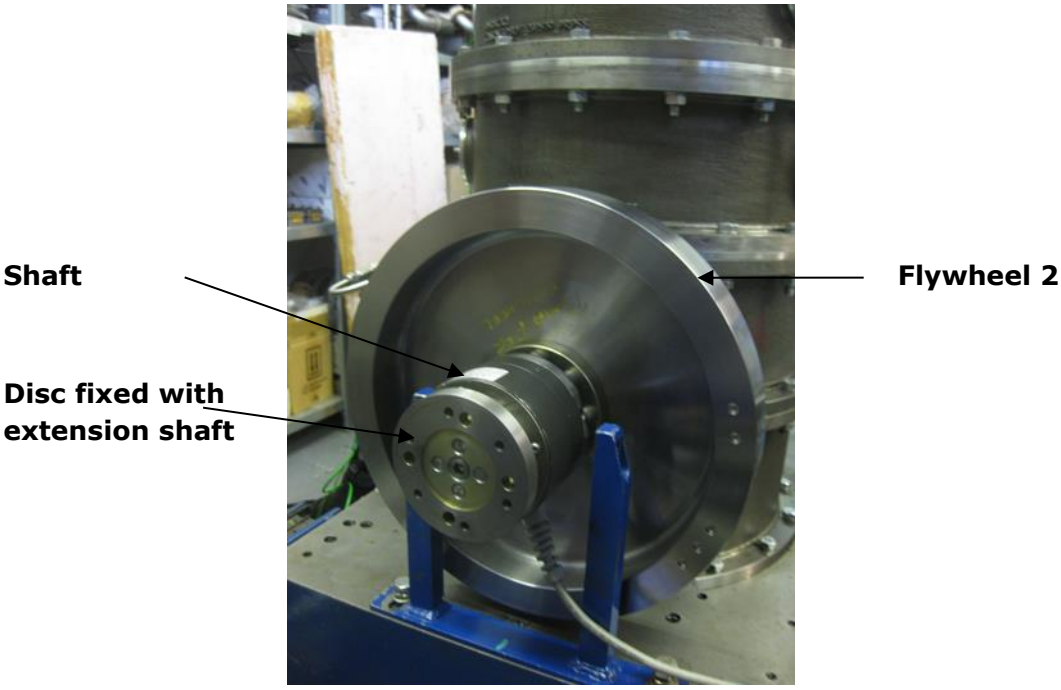

Figure 3.15: Shaft Encoder fixed on the driveline

The oil circuit was designed to supply the oil to the journal bearings, piston cooling jet and liner oil jacket. This circuit operates in a closed loop and is illustrated in Figure 3.16. A 12 litre rectangular open top vessel serves the purpose of oil reservoir and oil is heated inside by a Watlow 240V 2kW FIREBAR® heating element. This double –ended heating element of Alloy 800 has a nominal watt density of $25.5x10^3$ Watts/square meter. Moreover, the heater is fully submerged in the oil to avoid any smoke formation and the temperature is controlled by a PID controller.

Oil is delivered to the oil gallery manifold and liner oil jacket separately by two variable displacement centrifugal pumps of the same capacity. The pumps supplied by TEC Electric are powered by 400 V, 0.55 kW 3 phase electric motor and the speeds of the motors are controlled separately by ABB ACS150 inverter

driver units. The maximum flow rate achieved by each pump is 10 litres/min. Flow rate of pump 1 is adjusted to achieve a minimum oil supply pressure of 2 bars at the oil gallery manifold for the safe operation of the crankshaft bearings. From the manifold the oil is directed to three main bearings and piston cooling jet (PCJ) through the crank casting block channels. Another channel inside the crank allows the oil to flow from middle main bearing to the big end bearing.

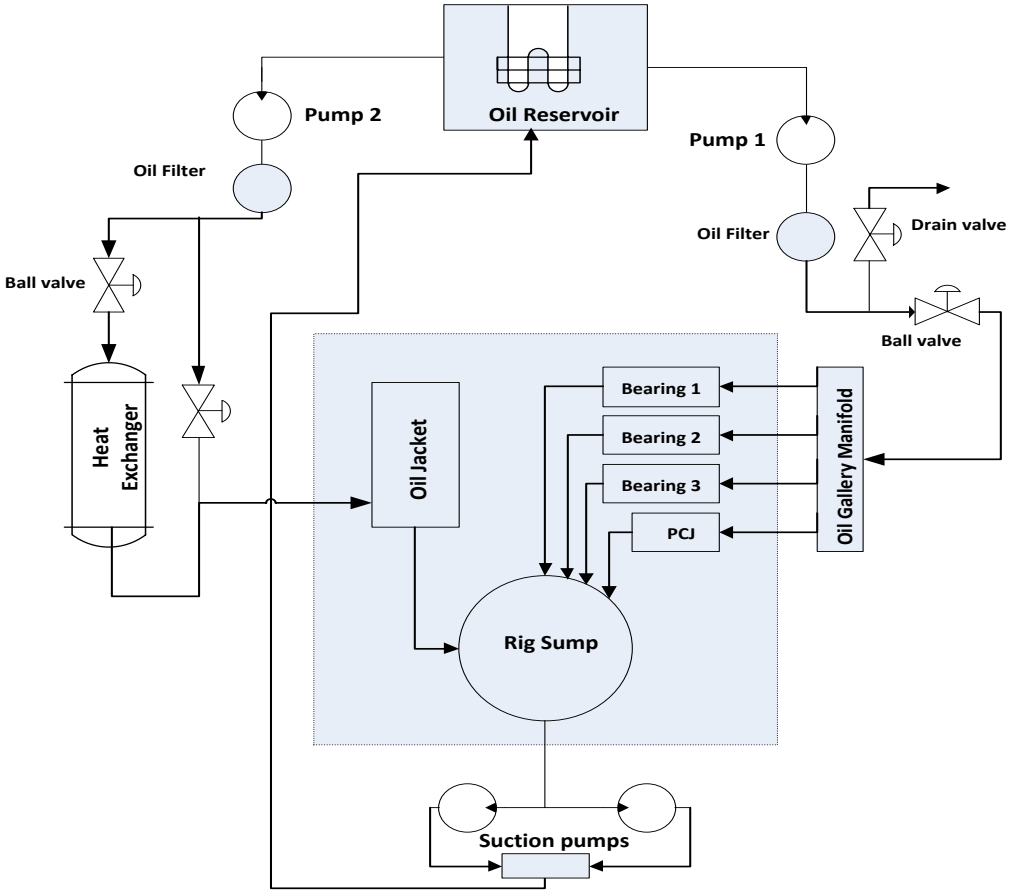

Figure 3.16: Oil circuit diagram

Oil supplied by pump 2 passes through a shell and tube water cooled heat exchanger to allow cooler oil to be supplied to the oil jacket during rig cooling. Ball valves are fitted in this flow to divert the hot oil directly to the jacket when needed. Ball valves are also fitted in gallery oil flow to facilitate oil draining. Ford standard oil filters are integrated in each pump supply to ensure cleaner oil delivery.

Oil supplied to the rig components drains to the sump at the bottom of the rig casting by gravity. Two 12V DC Mocal TCP1 diaphragm pumps connected in parallel completes the loop by drawing the oil from the sump and delivering it to the reservoir. Each of these pumps has maximum capacity of 6litres/min at a pressure of 3-4 bars with a maximum operating temperature of 130°C. Two pumps were chosen over one to balance the in and out flow of the oil from the oil reservoir. This avoids exposure of heating element above oil level and consequently eliminates chances of smoke formation by burning oil.

3.6 Instrumentation and Data acquisition

The temperatures, pressures, friction forces, speed and crank position data are acquired through the instrumentation of 10 thermocouples, 2 pressure transducers, 2 load cells and a shaft encoder. National Instruments (NI) data acquisition and control system acquires these data and controls the operating conditions such as motor speed, cylinder peak pressure and oil heater temperature through LabVIEW software installed in a computer.

3.6.1 Load cells

Friction forces in the floating liner assembly are measured by two 2 kN XFC200R force sensors supplied from Measurement Specialties ™. These stainless steel load cells were fitted opposite to each other along the crank axis underneath the bottom diaphragm. Force measurements in the load cells are undertaken by strain gauges with high stability. High stiffness of 7.3×10^8 N/m, miniature size and desirable operating temperature range of -40 to 120°C facilitates dynamic force measurements with the sensors. Moreover, they have high accuracy with less than ±0.5% of full scale non-linearity and hysteresis. A 10 V DC excitation voltage is provided to each cell to get a full scale output of 10 V DC.

3.6.2 Thermocouples and pressure transducers

K-type thermocouple probes were installed to measure temperatures at various locations in the rig. Six of them with a diameter of 1 mm were inserted at different depths in the liner at thrust and anti-thrust sides. This type of thermocouple has been chosen for its wide operating range of -100 to 1300°C, low cost and high accuracy of ±1.5°C. Moreover, the probes could be bent or twisted without affecting performance due to their mineral insulated construction. Three other 1 mm thermocouples measure the temperature of the gallery, oil reservoir and seal plug. A 3 mm diameter thermocouple is used to measure ambient temperature.

A Kulite ETL-CS-190M-150BARA pressure transducer fitted in the seal plug measures in cylinder pressure. This transducer has a compensated temperature range of 20 to 450°C and nominal pressure measurement capacity of 150 barg. Excitation voltage of 12-16 V DC is provided to the transducer to achieve a full scale output of 5V DC. Calibration was undertaken to measure the pressure to ambient reference or gauge pressure.

Another GE Druck PMP 4311 amplified output pressure transducer was fitted to measure gallery oil pressure. It has maximum pressure measurement capacity of 10 barg with an operating temperature range of -30 to 175 °C. Excitation voltage of 12-16 V DC is provided to the transducer to achieve a full scale output of 10V DC.

3.6.3 Shaft Encoder

A Hohner LPX series shaft encoder is used to measure the speed and crank position of the running rig. The 114 mm hollow encoder of 50 mm bore is fixed in the driveline with a locking collar after adjusting the TDC position. The encoder gives out two different pulse signals; one at every rotation for TDC and another

720 pulses at every rotation named as PPR (pulses per revolution). These 720 pulses enable the measurements with a 0.5 degree crank resolution. The TDC signal triggers the force and cylinder pressure measurements while the PPR synchronise the crank position with those measurements. Maximum output frequency and speed of the encoder are 150 kHz and 3000 rpm respectively. A 12 V DC power is supplied for the encoder operation.

3.6.4 LabVIEW data acquisition and control

LabVIEW data acquisition and control is comprised of two NI data acquisition (DAQ) devices: NI PCI–M10-16XE-10 and NI cDAQ-9172. These DAQs facilitate the system to control, acquire, process, display and save the data in a computer. All the analogue and digital signals from the rig are acquired through the DAQs in separate channels and then processed to monitor and save them in a computer with LabVIEW software. Moreover, output signals are also fed through these devices to the motor inverter, oil heater controller and air injection circuit. The floating liner data acquisition and control is illustrated in Figure 3.17.

Digital TTL signals of TDC and PPR from encoder and analogue signals from load cells and cylinder pressure transducers are collected by an E series NI PCI–MI0-16XE-10 DAQ. This high performance DAQ is equipped with analogue and digital input/output (I/O) channels along with analogue and digital triggering channels. Moreover, it has a high sampling rate of 100kS/s making it capable of acquiring crank resolved friction force and pressure data for high speed operation of up to 3000 rpm. The TDC pulse fed into the DAQ is not only used as a triggering signal but also as a counter input to measure the rotational speed. On the other hand, PPR pulses are used as external clock to synchronise analogue measurements with crank angles. The data acquired are then transferred to the computer with the help of a PCI card.

NI cDAQ-9172 is a DAQ chassis with 8 slots compatible for C series NI digital and analogue I/O modules. Three NI modules 9205, 9213 and 9263 are integrated into the chassis for analogue I/O measurements. NI 9205 is a ±10V 16 channels differential/ 32 channels single ended analogue input module capable of a high sampling rate of 250 kS/s that acquires analogue signal from the gallery pressure transducer.

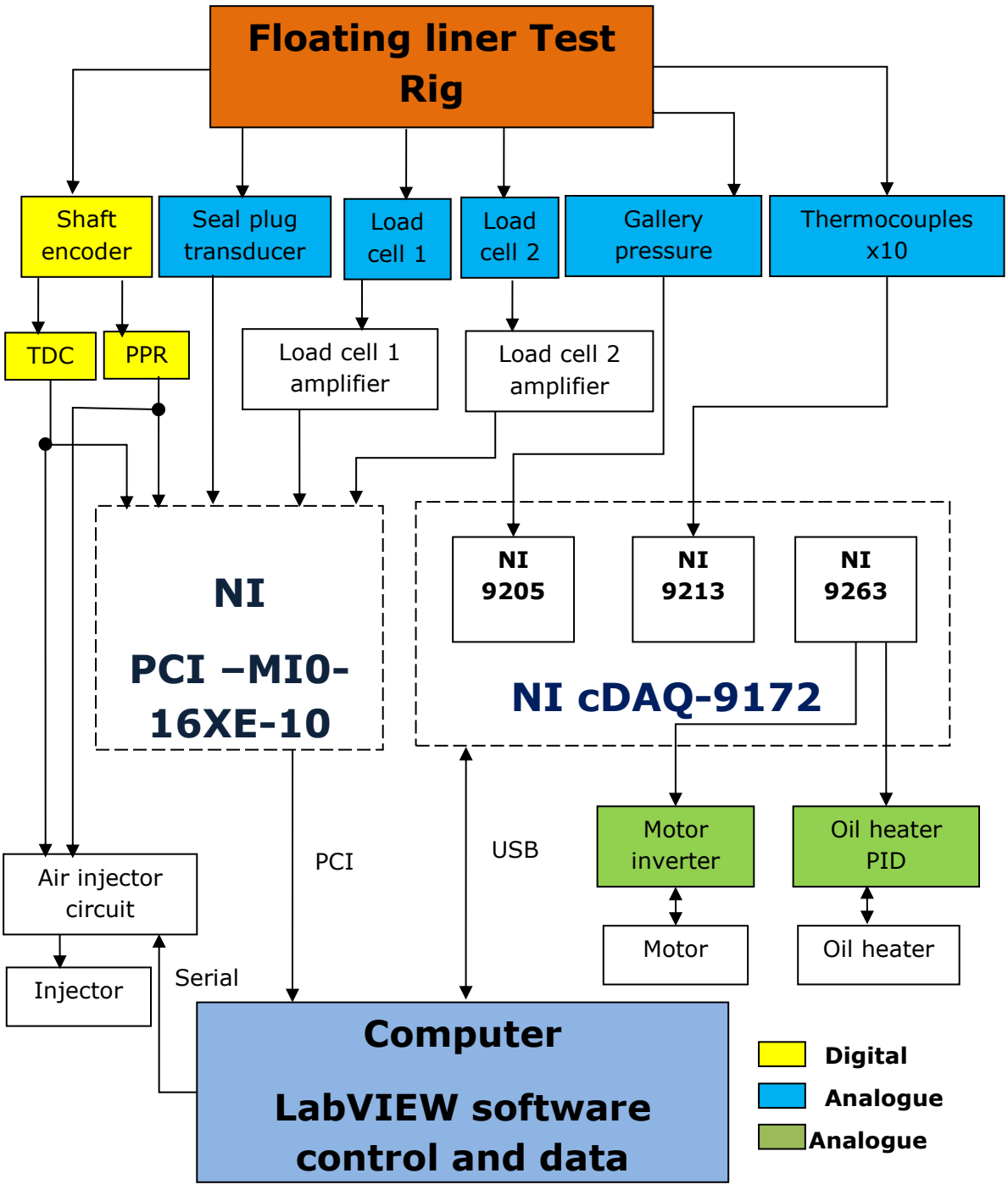

Figure 3.17: Floating liner data acquisition and control schematic

The 16 channel thermocouple module NI 9213 and 4 channel analogue output module NI 9263 have a sampling rate of 1.2 kS/s and 200kS/s respectively. The thermocouple measurements are acquired by NI 9213 whereas the motor speed and oil heater temperature are fed from NI 9263. Interface between the compact DAQ chassis and computer is achieved using a high speed USB 2.0 connection.

The data acquisition and control is operated by LabVIEW software. Virtual instrumentation (VI) is programmed to acquire and process the analogue and digital inputs as well as control the injection window, motor speeds and oil heater temperature. The acquired data are saved as spreadsheet files after the end of each test.

Air injection in the rig is controlled by a programmable interface controller (PIC) circuit which is powered by a 12V DC supply. This circuit utilises TDC and PPR signals from the encoder and a binary signal from the computer through serial port. The binary signal transfers the information of injection window to the circuit to control peak cylinder pressure.

3.7 Discussion

The design of an improved and updated floating liner rig compared to the previous existing setup [6] was described in this chapter. Compared to motored floating liner rigs described in references [98, 111, 115], it can operate at relatively higher peak pressures, 80 barg compared to maximum 50 bar without interrupting friction force measurement. Provision to study different liners and pistons micro and macro design features, without altering the whole engine setup is the biggest advantage over firing rigs described in references [25, 84].

Moreover, the operating conditions of a fired engine can also be simulated in this setup with higher confidence in isolating pressure force from the liner compared to some other fired floating liner setups [23, 25, 84, 109].The gas sealing in those

setups were achieved using a cylinder head, which can introduce an unbalanced pressure force in the liner and thus resulting in an error in friction force measurement. Sealing assembly designed in this reported study managed to isolate the direct application of pressure force on the liner by using a clearance seal separated from liner mounting as similar to setup designed by Gore et al. [111]. However, in Gore's design piston crown had to be modified to a stepped one to allow seal intrusion in the liner and only 20 bar of peak pressure was achieved due to a high clearance between seal and liner. In contrast to that, any modification in piston was avoided in this design due to extended liner height from TDC. Though the diametric clearance between the seal and liner is very large of 200 µm, still a better gas sealing is achieved by using the piston ring sealing. However, the influence of a proportional ring force to pressure on the liner due was compensated by the calibration method and will be further discussed in chapter 4 and 5. Similar pressure force calibration was also undertaken by Kunkel et al. [112].

The annular diaphragm used in this setup supports the liner at the top and suppresses lateral movement due to side thrust forces. The design ensures radial rigidity without stiffening it in axial direction. Compared to the designs with lateral supports in the middle of liner [23, 112], top sections support ensures minimal movement as similar to the setup of Yun et al. [98] and Ha et al. [25].

The load transfer mechanism used in this floating rig through the bottom end support was also implemented by most of the designers [25, 63, 102] . This high stiffness bottom diaphragm support ensures little/no movement in vertical direction to avoid the effect of liner inertia force on friction force measurement. Piezoelectric load cells were preferred above strain gauge cells due to their high stiffness in most designs [22, 23, 110, 111]. But they have higher error in linearity at a varied temperature [116]. The strain gauge type load cells were chosen due to their high stiffness as required by the design as well as the ability

to perform up to very high temperature of 120°C. With this bottom end design and stiff load cells maximum deflection of 1.5 microns was obtained similar to setup with piezoelectric load cells [23]. Moreover, only two load cells were installed in opposite end of motor axis instead of additional 2 load cells in transverse axis to avoid effect of thrust force on friction force measurement.

In this rig the effect of noise and vibration due to piston impulsive force (slap) was suppressed by adequate damping in the bottom diaphragm structure. Comparing to damping in lateral support [22, 23, 25, 98] this design ensures higher vibration elimination from load cell measurements. Further damping is provided by O-rings in the oil jacket around the liner.

High frequency data acquisition and control enables this rig to measure friction force and cylinder pressure at a high crank angle resolution of 0.5° as well as controlling cylinder pressure through air injection system. Further the oil circuit in the rig helps in undertaking tests at a wide temperature range, whereas it is impossible to take a lower temperature measurement in a fired engine.

Chapter 4 Operation and development of the facility

4.1 Introduction

In this chapter an overview of the use of the floating liner facility is presented. The systematic methods used to prepare the rig for a new test build which include component rebuild or oil flushing procedure for testing with a different batch of oil are discussed. Moreover, the in situ calibration processes and testing procedures are also included in the assessment. The assessment of the rig through operational behaviour has prompted further development of the rig and is discussed in section 4.5.

A key feature of the rig design described in the previous chapter is that it allows friction studies of various combinations of liner and piston components to be undertaken without manufacturing a new setup. The components in the assembly can be changed in relatively short time, typically 1-2 hrs to undertake tests with a different setup. Moreover, the formulations of the lubrication oil in the system can be changed to investigate the effects of this on friction, provided any surface layers on the liner and piston associated with previous oil use can be removed following a prescribed flushing procedure, making it more cost and time effective for parametric studies.

The tests were carried out using different liner-piston combinations. This allowed the study of different parameters; such changes include bore clearance, skirt & liner topography, operating speed and temperature. Static calibrations were undertaken to process the load cells responses into friction measurements. Repeatability was also built into the schedule to assess the reproducibility of the obtained results.

In this study, the friction force was measured at different liner temperatures, rotational speeds and peak pressure for each particular set of liner, piston and

lubricating oil setup. Aluminium and steel pistons were used in the setup with respective length of connecting rods. Pistons of different outer diameters were tested to study the effect of piston-liner clearance on friction. The diametric clearances ranged from 20 to 80 μm with an interval of 20 μm for the study of steel pistons. For the study of aluminium piston the clearance was kept at 60 μm clearance.

Two different grades of lubricating oil SAE 5W-30 and SAE 0W-30 were used in this study to investigate the effect of lubrication oil on piston-liner friction. The cylinder liners used for the studies were referred to as P1 and P2; both of them were plateau honed with a honing angle of 30° and Ra of 0.427 and 0.35 μm respectively.

4.2 Overview of use

The floating liner test facility can be used to investigate different micro and macro features in piston-liner assembly frictions. Moreover, the seal assembly can be alternatively installed and uninstalled in the rig to test in pressurised or uncompressed condition. The process of dismantling and assembling takes approximately 1-2 hours. However, working with a piston of different material requires the crank casting to be removed and installed with corresponding connecting rod. The driveline is also dismantled to accomplish this connecting rod changing step. Further oils are flushed from the system to study the effect of lubrication oil on friction. This section will describe the rig commissioning and component change method, and oil flushing procedure to facilitate testing procedures.

4.2.1 Rig commissioning and rebuilding changing components

Commissioning of the rig involves assembling the floating liner main assembly, driveline, oil circulation system, and finally instrumentation and data acquisition

system. An important feature of the test rig is the test unit is on a flexible bed, whereas the motor is fixed to the floor with the drive shaft connecting them.

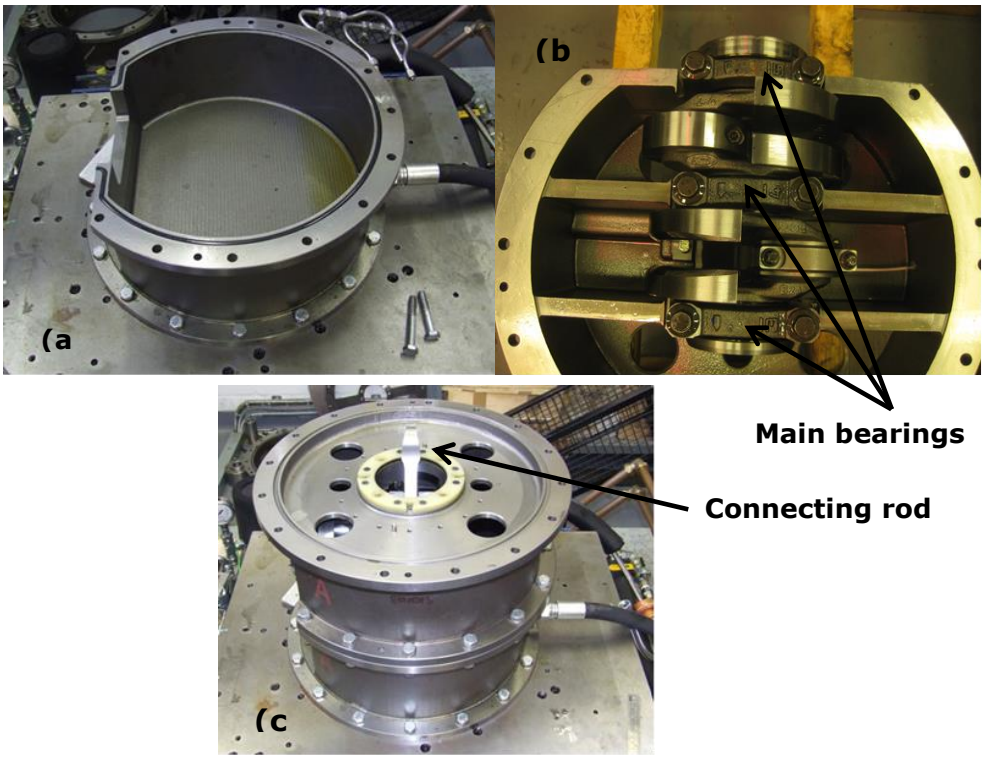

Figure 4.1: (a) Bottom casting/sump, (b) crank shaft with connecting rod assembled in crank casting, and (c) crank casting fixed on sump.

The assembly of the main rig is set out with the fixation of bottom casting or sump on the concrete block by 16, M10x40 bolts as shown in Figure 4.1a. This sump has slot in one side (left of the picture) to bring out the crankshaft through it and to connect with the driveline afterwards. The crankcase casting is then placed over the top of sump casting and fixed with 12, M10x60 bolts as shown in Figure 4.1c.The crank casting is the heaviest part of the assembly containing the crankshaft along with connecting rod and piston cooling jet. Three main journal bearings are used to support the crank shaft on the crank casting (Figure 4.1b). One of the two crank-throws in the crankshaft transfers the driving force to the connecting rod through big end bearing attachment. The other throw is left

unused and weight balances are used to impose dynamic balancing on the shaft. O-rings are fitted in the slot between each layer of casting drums.

The assembly of the piston-liner mounting arrangement proceeds with the fixing of third casting drum over crank casting. This layer is used to support the top diaphragm support of the floating liner. Before assembling the piston and liner, the load cells and bottom diaphragm ring base are fitted on the crank casting base as previously shown in Figure 3.14 of section 3.4. Electrical wires of the load cells are carefully taken out through the ring base gap to avoid any wiring failure. The bottom diaphragm is then fitted on to the base before connecting the piston with connecting rod.

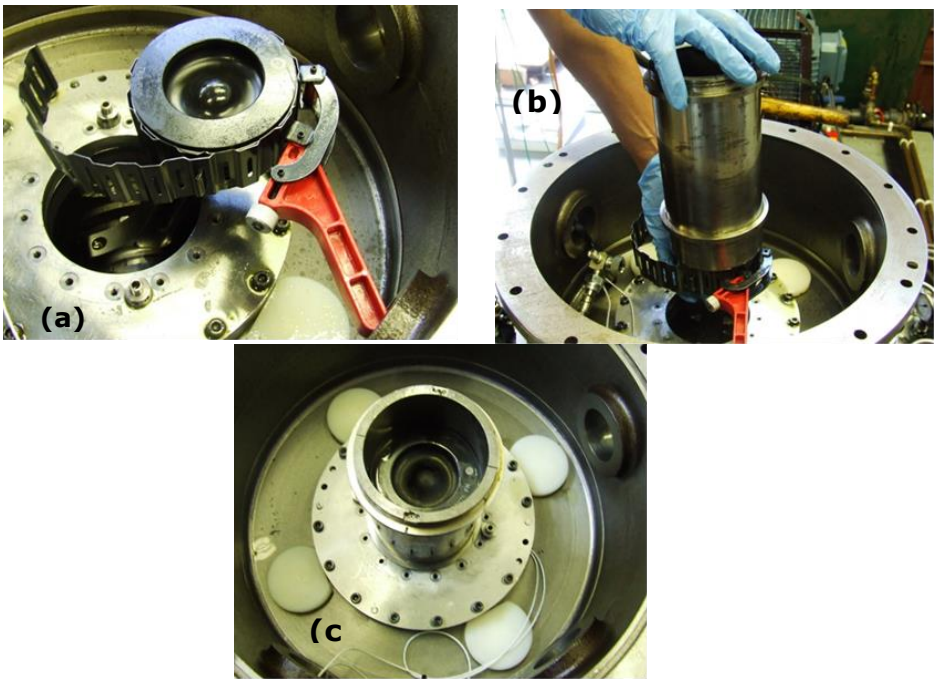

Figure 4.2: a) Piston clamped with ring compressor, b) piston inserted into liner, and c) Liner seating on the bottom diaphragm

Piston with piston rings is connected by inserting gudgeon pin through piston and connecting rod small end bearing. A circlip is used to lock the pin in the small end on the opposite side of motor while motor side is locked with a fixed clip. To insert the piston down the liner, rings are clamped with a ring compressor as shown in

Figure 4.2a. The ring compressor is removed once the piston is inserted and liner is pushed down afterwards to seat on the bottom diaphragm (Figure 4.2b and c).

The liner is fixed on the bottom diaphragm by two half-moon clamps with 14, M6x15 screws. A spacer is placed over the third casting drum to adjust the vertical position of top diaphragm support and afterwards another similar casting drum is dropped on it to fix the arrangements with 16, M10x60 bolts. Four M8x40 bolts are used to clamp the liner with the top diaphragm on its top flange. Preloading the loading screws is then followed by fixing the oil jacket around the liner. This jacket is equipped with several 2 mm O-ring chords on its inside grooves to damp any vibration transmitted from the liner during rig operation.

The driveline is assembled and connected with the crankshaft after sealing the gap between crankshaft and sump casting with an oil seal as shown in Figure 4.3. The smaller flywheel is connected with crank shaft via a 70 mm long spacer to avoid the flywheel face contacting the casting flanges. The assembly is followed by connecting the extension shaft and then fixing spacer, flywheel and extension all together on the crankshaft with high tensile 8, M12x110 bolts. Afterwards the shaft encoder is inserted on the extension shaft and fixed over it by a locking collar. This collar ensures rotation of inner shaft of the encoder during rig running while the outer body is fixed.

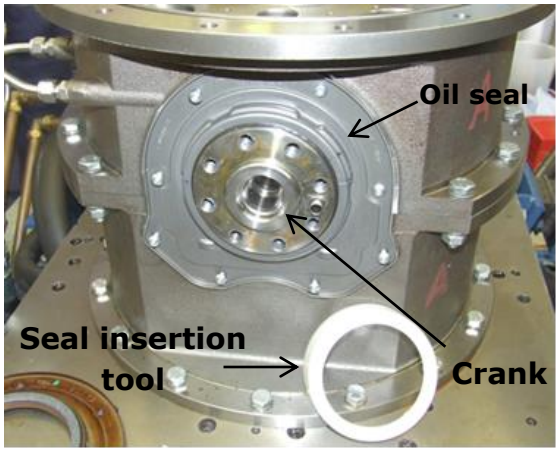

Figure 4.3: Crank shaft–casting gap sealed with oil seal.

Before connecting the propeller shaft, the motor centreline is aligned with crank axis by laser alignment tool. Afterwards the bigger flywheel is fixed on the motor shaft and the ball bearing is used to support it on the other side. The ball bearing housing is fixed on another bench over the concrete floor rail. The two ends of the driving shaft are finally connected with the motor side and rig side assembly of driveline to complete the setup.

The oil circuit has to be installed on the system before running the whole rig. Pumps and oil heater reservoir are fixed on the rig bed and proper pipe fittings are used to complete the circuit as discussed in section 3.5.2. Instrumentation with the thermocouples, pressure transducers and connecting them with data acquisition system finally completes the rig building.

At this stage the rig could be only run in uncompressed condition. To undertake some pressurised tests, the seal assembly is installed on the rig. One top piston ring at the bottom of seal plug is used to seal the air gap. This installation is undertaken while the piston is at TDC to use it as a datum position. Afterwards the top lid is placed on the seal assembly with the two guiding pins going through the lid interference holes. As well as guiding the seal, these pins act as alignment columns. The seal is fixed with the top lid and locking nuts, after fixing the lid on the top casting block with 16, M10X70 bolts. Clearance between the seal and piston is adjusted to test with a suitable compression ratio; this is accomplished by raising the air column relative to lid locking nut. The assembly process is concluded by locking with a final locking nut and connecting the regulated air supply as shown in Figure 4.4.

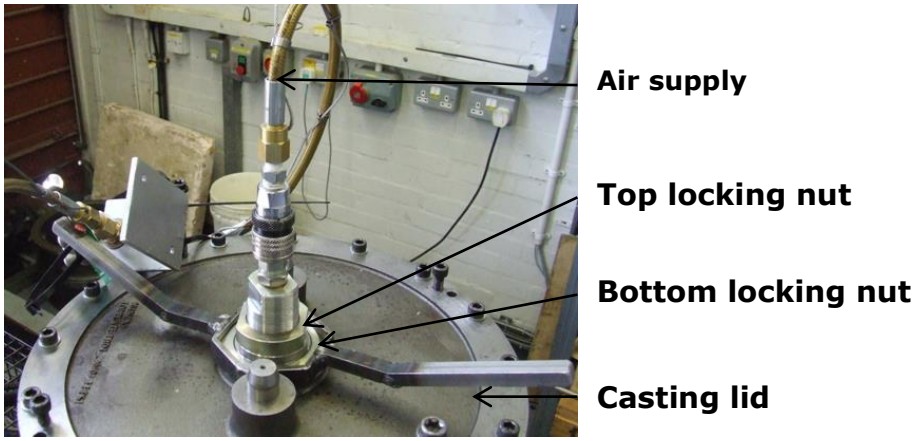

Figure 4.4: Fixation of seal assembly with the top casting lid

For testing with a different liner-piston combination only needs dismantling of the top two casting blocks along with top diaphragm, liner, oil jacket and piston. Thermocouples are also taken out from the liner during this component change process. The installation of new liner and piston are always undertaken by cleaning them in a paraffin bath to remove any dirt and grit from the surfaces.

4.2.2 Oil Flushing procedure

An oil flushing procedure is undertaken before examining with new oil or draining the old oil to clean the oil circuit. This procedure was defined by the oil supplier and followed to remove the previous oil and surface film laid down by the additives. Flushing oil is used to facilitate the procedure.

The flushing operation is set out by draining the old oil from the reservoir. This is undertaken after warming the bulk oil up to 100°C by running the rig to minimise oil carry over effects. Residual oil at the bottom of the reservoir is then drawn out with a suction pump. Although major portion of oil is extracted out of the system by draining, still some quantity is left over in the oil circuit as well as inside the rig. For this reason flushing oil is flushed through the system few times before flushing with the new oil.

At every stage of flushing, the rig is run at 1000 rpm for 15 minutes without any air injection. It is then followed by further 15 minutes of operation under 30 barg peak cylinder pressure conditions. Afterwards oil is drained and two oil filters are changed in the circuit to complete each stage and the reservoir is filled with new oil. The system is filled twice with flushing oil to complete the first two flushing stages. In the next two stages new oil is used instead of the flushing oil.

4.3 Calibrations

4.3.1 Load cell calibration

The output from the load cell transducer measurements are in voltages. In situ static calibrations were undertaken to relate load cell load to output in Newton/Volts (N/V). These calibrations were carried out for every single build to avoid any effect of build to build variability. The calibration load was applied by placing weights on top of the liner. Because the liner is partly supported by the top diaphragm, the calibration is for the additional compressive force on the load cells. There are two important features of calibration:

- Apparent sensitivities of load cells are higher than actual sensitivity. As some of the forces are taken by top diaphragm support, the voltage outputs are lower than stipulated outputs. Thus sensitivities in N/V are higher in calibration.
- Calibration value also drifts with temperature and is almost linear.

Calibrations of force versus load cell output volts were determined through static loading of liner. Before undertaking calibration, compressive preloads were applied to each load cell to ensure the cells are always under a compressive load for in range force measurements around a cycle. Moreover, the piston was kept at TDC during calibration as it would avoid force transfer from connecting rod to piston at its vertical position.

For a particular build, calibrations were undertaken at different temperatures of liner; one at room temperature and afterwards from 40 to maximum 80 °C at an interval of 10°C or less. Temperature rise was achieved by heating up the oil in reservoir and supplying heated oil to both oil jacket and piston cooling jet. It ensures temperature rise of liner and piston at an equal rate. During calibration at each temperature, successive weights were applied on the liner and corresponding voltage responses were recorded to obtain sensitivities in N/V. Assumptions are made that loads on the liner are equally shared by each load cell. Voltage responses were also recorded during unloading to consider the effect of any hysteresis.

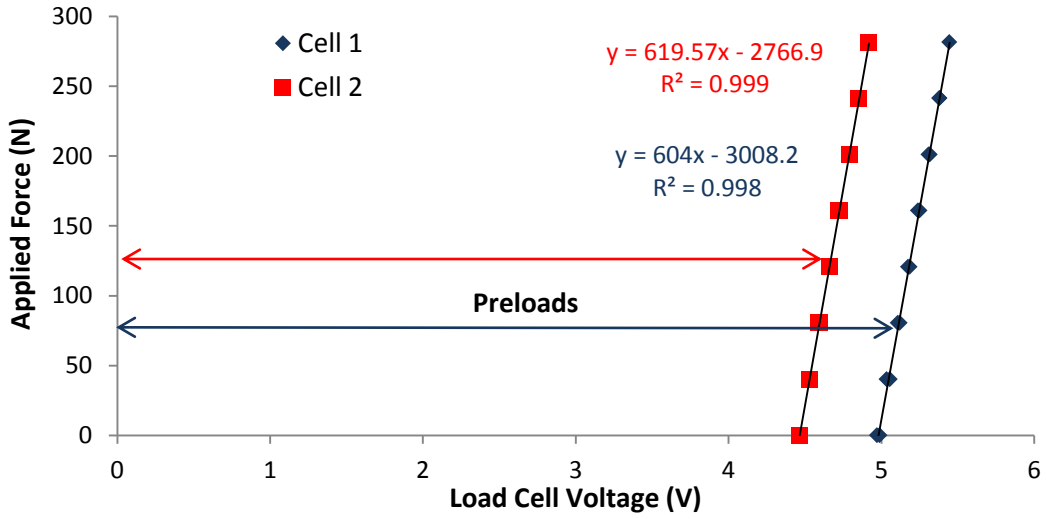

Figure 4.5: A load cell calibration at average liner temperature of 20°C

An example of static load cell calibration is given in Figure 4.5. Here first calibration was undertaken at room temperature of 20 °C and preloads of around 4.5-5 Volts were applied to load cells prior to calibration. Seven dead weights, each of 8200 g were loaded on the liner one by one and then again unloaded to complete the calibration. The load cells responses to loading showed a linear dependency with low drift and hysteresis as portrayed by R^2 value of above 0.99 for the trend lines. The slope of each line was taken to acquire the sensitivities of load cells at this temperature.

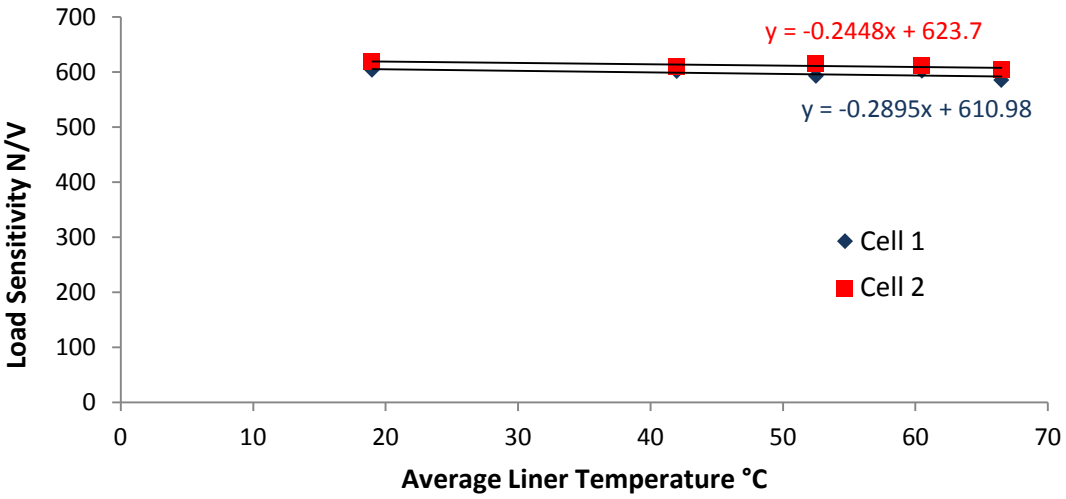

Figure 4.6: Variation in load cell sensitivities with temperature

Subsequent calibration were undertaken at average mid liner temperatures of 42, 52, 60 and 67 °C to obtain the variation in sensitivities with temperature as shown in Figure 4.6. The equations of the linear trend lines determined the load cell sensitivities as a function of temperature.

4.3.2 Seal force calibration

During pressurised rig operation, the sealing ring in seal assembly experiences an upward force by the application of cylinder pressure. A portion of this force is exerted on the liner and consequently the measured forces by the load cells are affected by it. This force has to be taken into account as it is not part of the actual friction force. However, sealing ring force is systematic and linearly dependant on cylinder pressure; thus calibrations were undertaken to obtain the force sensitivities in N/barg.

Similar to the load cell calibration, a seal force calibration was pursued under static condition at different temperatures. At each temperature condition, the piston was kept at TDC and cylinder pressure was raised to obtain the consequent load cells outputs. The variations in load cells' voltages with pressure were used

to calculate the sensitivities in V/barg. An example of seal ring force calibration is shown in Figure 4.7.

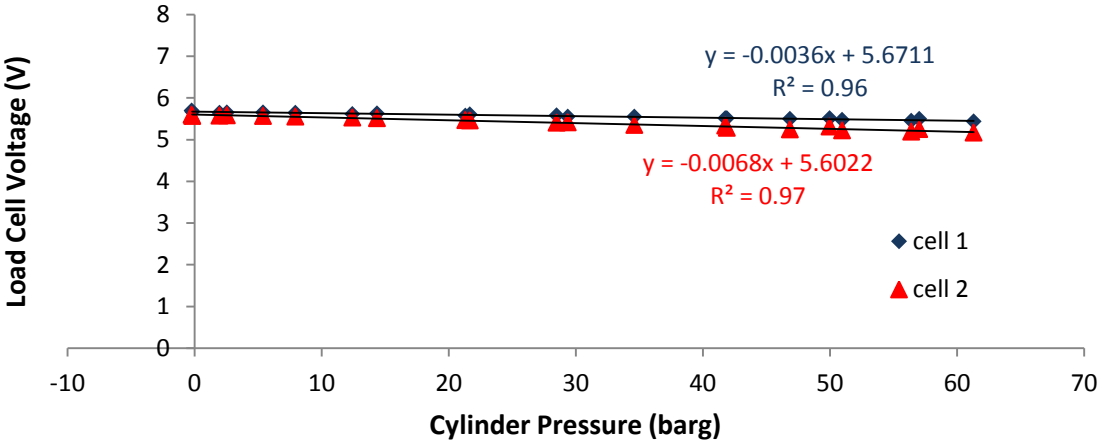

Figure 4.7: A seal ring force calibration at average liner temperature of 12˚C

In this calibration, the pressure rise was obtained by using a modified injector with the pin in the injector removed to get a free flow of air supplied from air bottle. The cylinder pressure was raised from partial vacuum condition to up to 61 barg by regulating the compressed air supply to the cylinder. The load cell voltages were recorded for different pressures and plotted to obtain the sensitivities in V/barg. As the pressure rise causes the ring to push the liner upwards, corresponding load cell voltages reduces as could be seen from Figure 4.7. Moreover, the dependencies of load cells voltages with pressure were found to be linear with a R^2 value of above 0.96. The sensitivities in V/barg are then converted to N/barg by using corresponding load cells sensitivities in N/V.

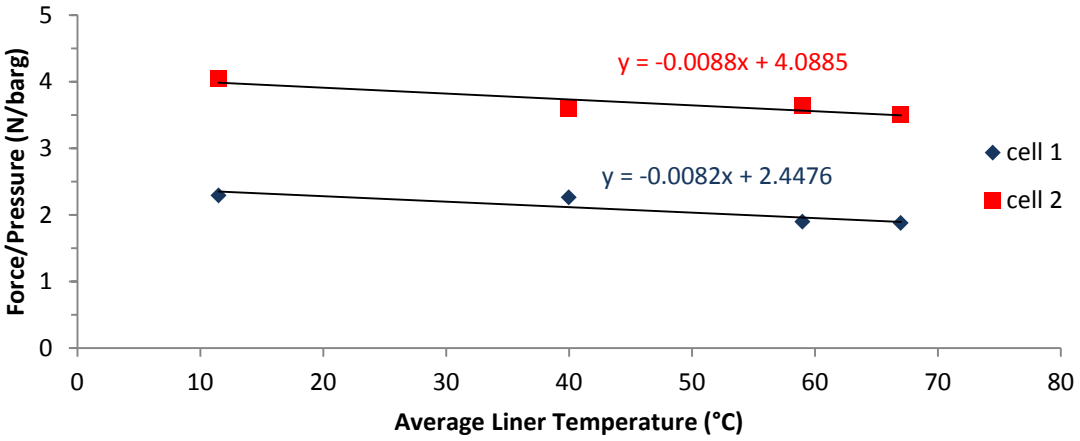

Figure 4.8: Variation in sealing ring force sensitivities with temperature

The calibration process was repeated for different liner temperatures and variations in force sensitivities with temperature showed linear dependencies as could be seen in Figure 4.8. The equations of the linear trend lines were calculated to obtain the force sensitivities as a function of temperature. Both calibrations are taken in to account when processing and analysing the data.

4.4 Rig Operation and test conditions

In the floating liner rig the friction force at the piston-liner interface are transferred from the liner to the diaphragm and consequently to the two load cells through the loading screws. During operation, the compression and expansion of air trapped in the cylinder produces a cyclic varying pressure on the piston which repeats in a two stroke, rather than a four stroke, cycle. This pressure variation was varied and raised by using the air injection system. The same system provides compensation of air to balance losses by leakage past the piston and the seal. The force measured by the load cells are resolved by a shaft encoder at 0.5° crank resolution thus enabling friction force measurement at different positions of the piston during expansion and compression strokes. The next section describes the test methodology and operating conditions to study the effect of different operating and design parameters on piston-liner assembly friction.

4.4.1 Test run methodology

In this study, each test run was undertaken at a fixed rotational speed for a range of mid-liner temperatures from ambient up to maximum 90°C and data were recorded for the entire duration of the test. Lubricating oil, heated in the reservoir was supplied through the piston jet and was used to heat the piston with warm oil, which transfers the heat to the liner. The combination of friction heating and heat from supplied oil, cause the liner surface oil film to rise. Thus the study was able to be undertaken at different liner temperatures ranging from room temperature to as high as 90°C at the middle of liner.

The seal assembly was removed during uncompressed operations while a piston-seal clearance of 5 mm was maintained to achieve a compression ratio of 10.5 during pressurised operations. For pressurised condition, the rig was first run up to the required speed and then air was injected to achieve required peak pressure. Peak pressure was achieved by controlling the injection window around BDC through the PIC circuit. Air was supplied from a 50 litres compressed air cylinder which has a maximum pressure capacity of 200 barg. Moreover, it was regulated before supplying it through air column of seal assembly. As the bottle pressure reduces along the test run, the injection window has to be adjusted accordingly.

Raw data of load cells outputs, cylinder pressure, temperature and speed were saved after completion of each test for post processing of results. To prepare the rig for next test, it was cooled by cooling the oil in the system and supplied through liner oil jacket. Oil from the reservoir was pumped through the heat exchanger before supplying it to oil jacket. The oil jacket is not equipped with any outlet rather it is has a gap between two halves of jacket. Thus oil is drained to the sump by gravity through the gap and then pumped back to reservoir to circulate in the loop. A fan blower was also used to assist the system cooling.

Once the temperature of the system is in equilibrium with ambient it is ready for the next test.

4.4.2 Operating conditions and characterisation of reference conditions

For a particular build, testing comprising a range of operating speeds, from 250 rpm resembling cranking speed up to 2000 rpm, which is currently an upper limit for the floating-liner rig. Average mid liner temperature was taken as reference oil film temperature because most of the frictional work takes place around the middle of the stroke where the lubrication regime is hydrodynamic. The load on the piston assembly is characterised by peak cylinder pressure which was adjusted by adjusting the injection window.

Pressurised condition resembles compression and power stroke respectively for upstroke and down stroke motion of the piston, whereas the uncompressed condition represents exhaust and intake stroke respectively as the pressure over the piston is atmospheric. As the rig is not fired, there is no pressure hike during power stroke and pressure variation along the cycle is symmetric for up and down stroke.

The range of operating speeds, average middle liner temperatures and peak pressures in this study were 1000-2000 rpm, 40-90°C and 0-80 barg respectively. Some low speed tests of 250, 500 and 750 rpm under uncompressed condition were also undertaken to study the effect of speed on friction. For pressurised condition, low speed operations produce high torsional vibration and thus were not pursued to avoid any catastrophic failure.

The parametric studies were undertaken for different combination of piston-liner setup and lubrication oil. Eight different test builds were used for this purpose as presented in Table 4.1. Liner P1 and SAE 5W-30 oil was used for different piston-

liner clearances tests with steel pistons. Performance of oil SAE 5W-30 and SAE 0W-30 were compared for both steel and aluminium pistons using liner P2 with a diametric clearance setup of 60 µm.

Table 4.1: Test builds for piston-liner friction study

Build No	Piston	Diametric clearance, µm	Liner	Oil
1	Steel	20	P1	SAE 5W-30
2	Steel	40	P1	SAE 5W-30
3	Steel	60	P1	SAE 5W-30
4	Steel	80	P1	SAE 5W-30
5	Steel	60	P2	SAE 5W-30
6	Steel	60	P2	SAE 0W-30
7	Aluminium	60	P2	SAE 5W-30
8	Aluminium	60	P2	SAE 0W-30

4.5 Rig development

In order to operate the rig at higher pressure condition and to achieve proper sealing method without interfering with the friction force measurement, the rig has gone through some developments and design changes over time. The developments were made on the sealing method and driveline assembly to bring the rig at current state as described below.

4.5.1 Sealing method

Initially, the pressure in the floating liner rig was achieved by using a Labyrinth seal system (Figure 4.9) where the minimum diametric clearance between the seal and liner was kept at 40 μm. Pressurised tests were undertaken at speed of 500 rpm and 1000 rpm, with a compression ratio of 16, which gave a cylinder peak pressure of up to 60 bars.

Figure 4.9 Installation of the Labyrinth Seal Plug

It was found that there was possibility of seal-liner contact at high temperatures which is shown in Figure 4.10 by the high friction values (also the values flattening out near the end of stroke). The contact occurred at high pressures and temperatures, the seal temperatures were more than 30-50° C higher than the liner and seal expanded so much that it ended up contacting the liner.

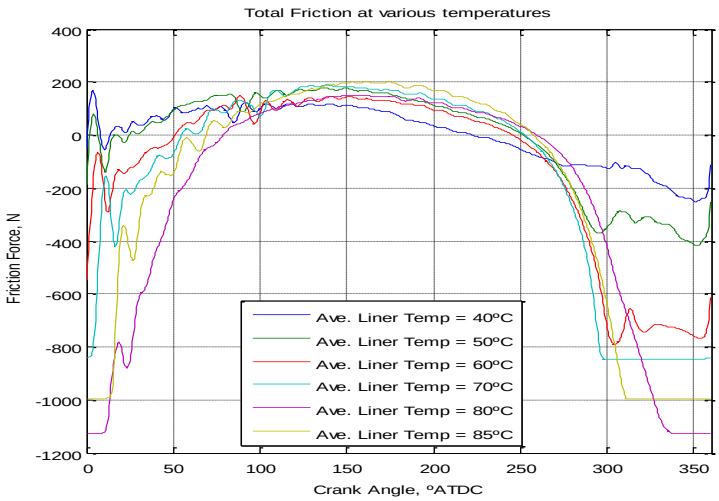

Figure 4.10 Friction force traces at 1000 rpm

The reduction of seal-liner clearance could also be seen from other experimental data, as the maximum pressure in the compressed test without any injection was found to vary along the test. The variation of pressure with temperature is shown in Figure 4.11. It can be seen that with the increase in temperature, pressure rises. This is an indication that the clearance between the seal and liner narrowed down, touching of the seal and liner was possible, as the temperature went higher which gave the pressure rise.

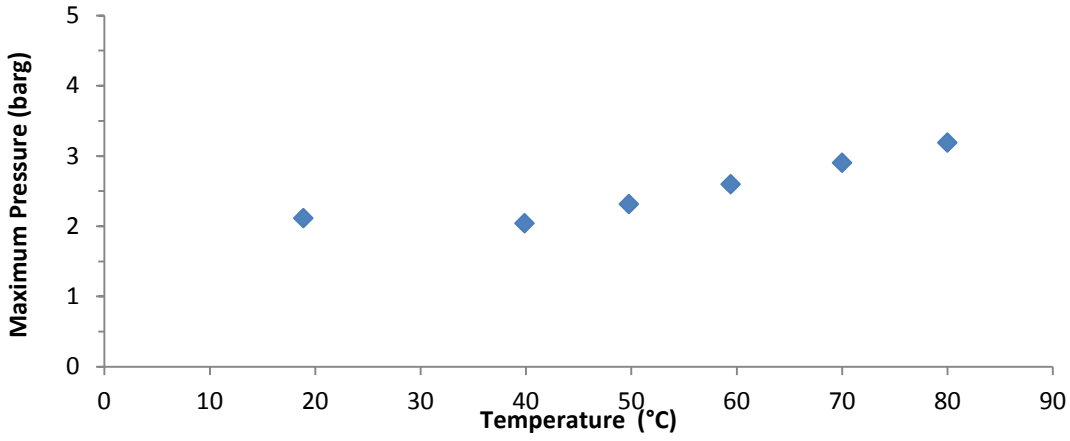

Figure 4.11 Maximum Pressure variations with temperature at 1000 rpm without any injection

As mentioned above, during pressurised operation the friction traces became erratic; it was highly probable that the seal came in contact with the liner, giving spurious friction traces. Moreover, the force exerted by the seal on the liner due to surface contact was irregular and impossible to calculate. To avoid this contact between the seal and the liner, the clearance between the seal and liner had to be found, such that at maximum pressure and temperature there would still be a gap between them. To find the minimum clearance, the expansion of the liner and the seal was studied out of the test rig. They were placed in an oven to heat up to 80-85° C and then taken out to cool down. The diameter measurements were taken at different temperatures and from there linear expansion coefficients were calculated. The calculated values of liner and the seal are 1.20 and 1.27 x 10^{-5} $°C^{-1}$ respectively at 18°C.

From Figure 4.10 it could be seen that the labyrinth seal would have touched the liner at some part of the test, which was confirmed to be after the average liner temperature reached 24°C from the expansion data. The contact between the seal and liner was due to the fact that, the Labyrinth seal was constructed out of mild steel, whereas, the liner is cast iron and expand at different rates when heated. For this reason a new design of seal was made, where the compression ring was used to seal liner as shown in Figure 4.12.

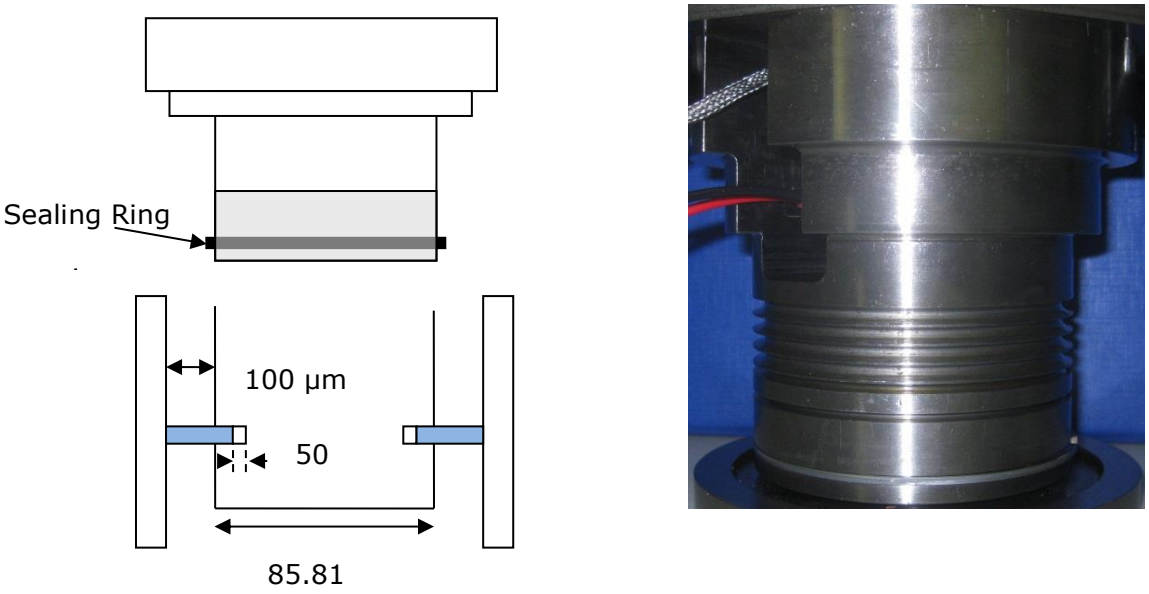

Figure 4.12: New liner/seal clearance and seal with sealing ring

During the higher pressure tests, 30-60 bars, it was found that the measurement of temperature at the top of the liner, where the seal was positioned, was up to 15° C higher than the rest of the liner temperature measurements of middle and bottom. This higher temperature at the top of the liner implies that the seal would be as hot if not hotter than the liner. With this in mind and using the expansion data, it was found that to prevent the seal coming into contact with the liner, the seal diameter should be minimum 70 µm smaller than the liner bore diameter. It was decided to have a radial clearance of 0.1 mm, as a compromise between not touching and engineering this. Test runs were performed on the new design of cylinder seal using a piston ring inset to a plug with a larger clearance to allow for differential expansion of the plug and liner and to ease location of plug in the cylinder. Traces as in Figure 4.10 were consequently avoided.

4.5.2 Modification to driveline assembly

The new sealing system was able to overcome the problem of erratic friction traces through irregular seal-liner contacts. As the new seal uses compression

ring to seal the air there was less chance of air leakage. This can be seen in Figure 4.13 where for similar peak pressure condition, the pressure variation was much steeper for labyrinth seal than the new seal. Thus the work at expansion stroke was much lesser for labyrinth seal than that of new seal (almost half).

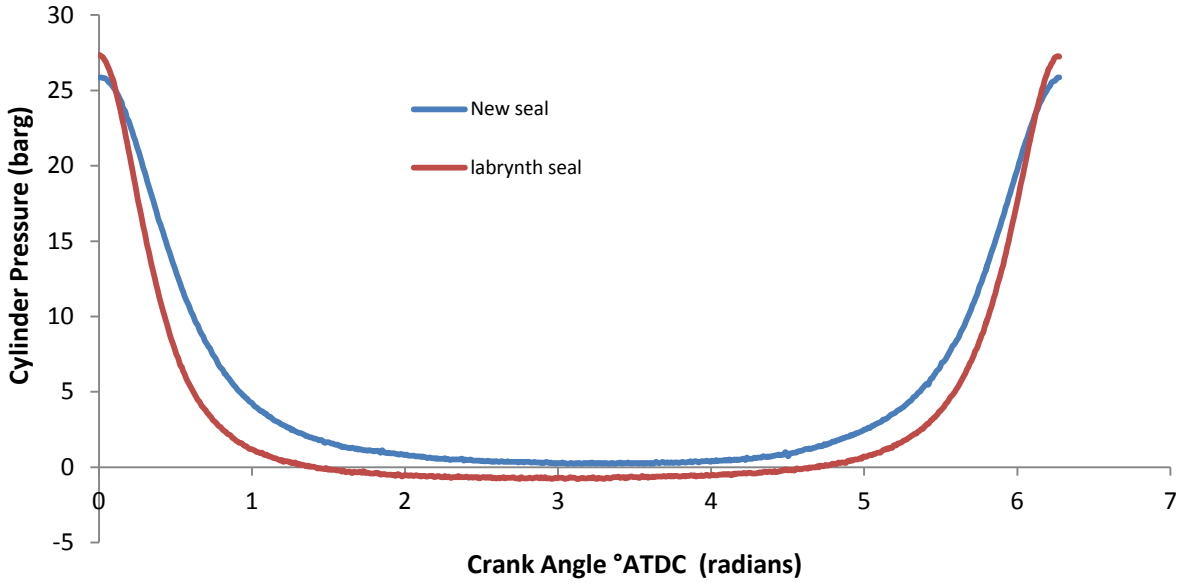

Figure 4.13 Pressure distributions over a cycle for different seal system at 1000 rpm

During the experiments it was found that the rig could work up to peak cylinder pressure of 25 bars without any interruption. But beyond that, motor was unable to supply adequate torque to drive the rig. This was due to the fact that the required motor torque to overcome that high cylinder pressure was higher than the maximum torque capacity of the motor. Also the flywheel with the inertia of 0.24 kg m^2 used at the system was not enough to store and supply energy when required at higher pressure.

Thus more development had to be done on the motor and flywheel for the system as the electric motor had insufficient torque to drive the test rig. The required motor torque (T_M) at different peak pressures is given by equation 4.1.

$$T_M = T_c - I\alpha \qquad (4.1)$$

Where T_c is crank shaft torque due to cylinder pressure, I is the flywheel moment of inertia (0.24 kg m^2) and α is the instantaneous angular acceleration ($rads^{-2}$).

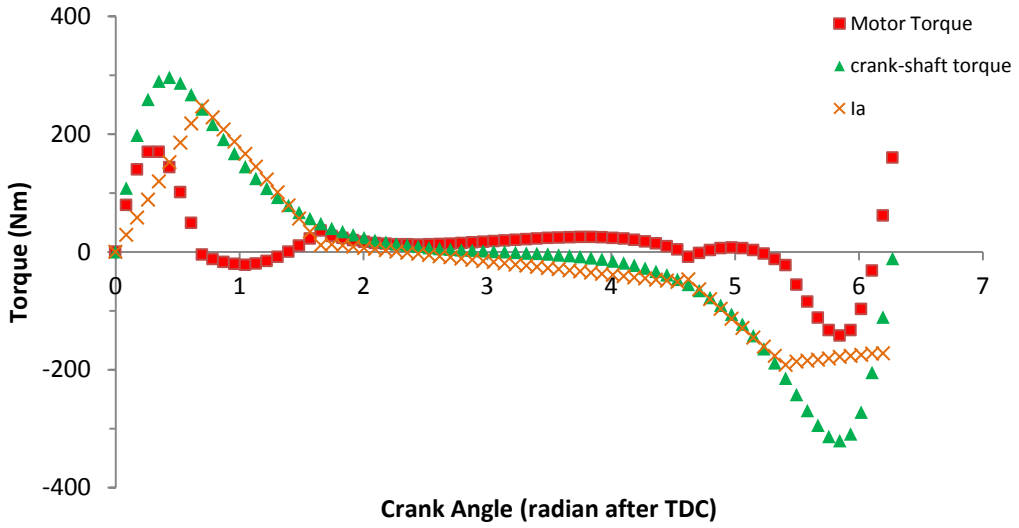

Figure 4.14 Torque curves for 1000 rpm with maximum cylinder pressure of 40 barg

An example of calculated result for the motor torque is given in Figure 4.14. It can be seen that at peak cylinder pressure of 40 bars the maximum required motor torque was 170 Nm which was higher than that of the nominal capacity (98 N m). Thus the system required higher capacity motor which could supply enough torque at higher pressures or another flywheel with more inertia, which could support the motor at similar situation. By the economic analysis it was found that it was cheaper to use a bigger flywheel. Thus a new flywheel of inertia of 1.07 kg m^2 was added with the system (Figure 4.16). It was placed near motor side of propeller shaft with the support of a bearing.

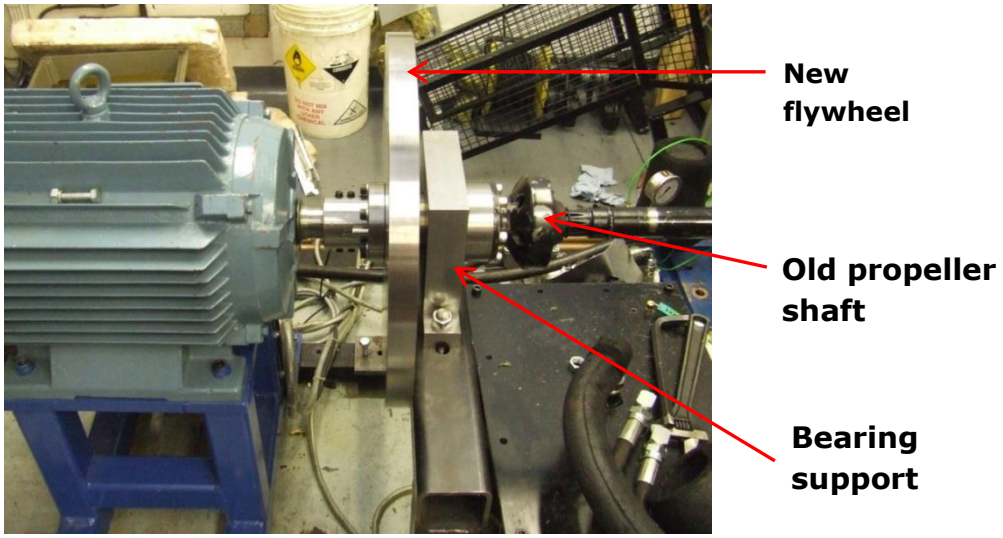

Figure 4.15 New Flywheel installed at the system

Several high pressure tests were undertaken with the new system and it could work up to peak cylinder pressure of 60 bars without any interruption. As the bigger flywheel was installed to the motor side of shaft, more energy was transferring through the shaft during high peak pressure operation. Eventually, the shaft failed at high pressure at a speed of 750 rpm where resonance occurs and excessive torsional vibration caused the rubber donuts of the shaft to break. A new improved rubber coupling shaft was thus installed in the system to cope with excessive loading. Moreover, the small flywheel near the rig was replaced with another flywheel of inertia of 0.42 kg m^2; consequently less energy was transferring through the shaft, a better balance between the two flywheels. With the current setup, the rig was able to run up to peak pressure of 80 barg without any catastrophic failure.

4.6 Discussion

Using the floating liner rig design described, changing the cylinder liner is relatively easier compared to fired rigs. Similar exchangeable liner design was implemented by O'Rourke et al. [110]. Exchangeable liner sleeve setup was also designed by Wakabayashi et al. [63] in a fired rig, but the installation of the cylinder head sealing takes longer time in their design. Moreover, the

performance of the rig can be effected by assembly and disassembly of the head as observed Gore et al. [111].

Calibrations undertaken for each build in the setup reported in this study minimise the uncertainty of the friction force measurement. Repeating the calibration exercise for a given build at various intervals showed calibrations were stable and the rig showed no propensity to change state. Though preloads in the load cells underneath the bottom diaphragm support were initially set in similar values for each build, they were observed to be drifting after top diaphragm installation. In situ calibration with the whole setup reduces the possibility of errors which will be further discussed in chapter 5 by observing the build to build repeatability.

Maximum 2% reductions in load cells sensitivities with liner temperature from 40 to 80°C were observed in the in situ calibration. The reason behind is, with increasing oil temperature the system components expands which includes the liner and clamping bolts. Study by Jaglinski et al. [117] suggests, with rise in temperature clamping force in a bolted joint is reduced because of thermal expansion. Thus lesser load is transferred to top diaphragm causing the calibrations to drift downwards. However, linear variations in the sensitivities with temperature make it easier to apply calibration in force measurements across the temperature range.

During pressurised operation maximum 9% of the total force on the sealing ring is transferred to the liner. Calibration of force contribution from seal to liner facilitates higher accuracy in friction force measurement by deducting this contribution from the total force measurement. Similar to load cells calibrations, linear responses with temperature were observed with 10% reduction from 40 to 80°C. This predictable behaviour eliminates uncertainty in friction force measurement compared to cylinder head sealing designs where unpredictable pressure force contributions were observed [22, 25, 98]. Further cooling

mechanism at the seal assembly reduces expansion of the seal and consequently lesser drift in the seal force sensitivities.

The operating conditions in this rig can simulate similar fired engine conditions. For example, the compression heating can cause the temperature of air to rise to 450°C for the compression ratio of 10.5:1, assuming the compression is isentropic which is closer to gas temperature in a fired engine [2]. Average temperature of middle of the liner was taken as the reference temperature for oil for two reasons. Most of the frictional work takes place around mid-stroke and high thermal diffusivity through cast iron liner gives little or no difference in temperature between the oil film and thermocouple positions. Moreover, the local oil film viscosity at a particular temperature rather than the supplied oil viscosity dictates the oil film thickness and pressure, consequently friction. Similar temperature referencing was used by some other researchers [85, 110].

Modification in sealing assembly not only managed to eliminate effect of spurious force interruption through liner-seal plug irregular contacts but also improved the air leakage. An improvement of 35% to 8% from previous design [6] was achieved in air loss thus reducing cost of running. A running speed of 750 rpm was avoided in the system due to resonance in the whole assembly. Yun et al. [98] also observed this behaviour in their design at speeds of 750 and 1500 rpm. Modification in driveline assembly though an additional flywheel ensured high peak pressure operation. But in process lower speed tests at 250 and 500 rpm could not be undertaken as fluctuation of speed in pressurised condition occurred at those speeds due to the higher inertia flywheel.

Chapter 5 Test results and presentation

5.1 Introduction

This chapter is concerned with the processing and interpretation of test results obtained during piston-liner friction parametric studies. The conversion of crank resolved raw data (in volts) measured by load cells into total friction force by using relevant calibration data is described in section 5.2. The two different force analysis options- crank resolved friction force and average loss in fmep are described in section 5.3. Interpretation of friction force for a four stroke operation through the use of two stroke pressurised and uncompressed data is discussed in section 5.4. In section 5.5 and 5.6 the repeatability of test results and the viscosity -temperature relation of the two lubricants SAE 5W-30and SAE 0W-30 are analysed.

5.2 Force measurements

The forces measured by the load cells is comprised of friction force, the compressive preloads from loading screws and sealing ring force as presented in Figure 5.1. Friction force in the piston-liner interfaces is transferred to the load cells through loading screws. Although the down stroke results in downward compressive loading, during up stroke the force direction changes. Therefore preloads were applied to ensure force measurements were in the range of the load cell capacity during both the down and up stroke. Moreover, during a pressurised test, an upward force from sealing ring due to cylinder pressure is transferred to the liner, consequently to the load cells. Thus this force was also taken into account before calculating the actual friction force.

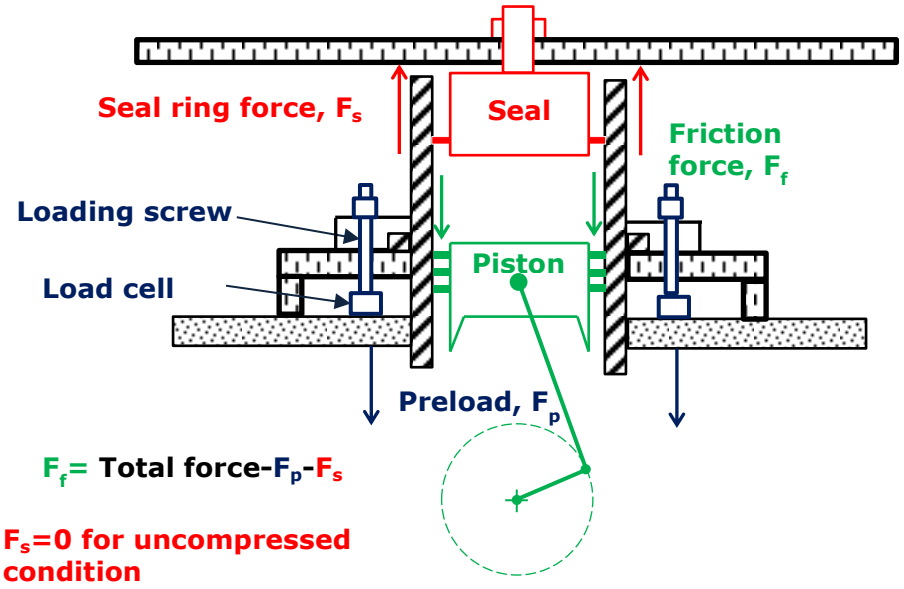

Figure 5.1: Force measured by load cells in floating liner arrangement

The compressive loading on the load cells varies in a cycle and also along the test depending on the friction force and sealing ring force. These variations are indicated by voltage variations in the range of positive 0 to 10V. Load cell calibrations were used to convert those voltages into force in Newtons. The cyclically varying sealing ring force due to varying cylinder pressure was calculated afterwards to obtain the corrected forces. Moreover, a zero force offsetting method was applied to differentiate between downward and upward force. Downward force was indicated by increase in voltages whereas decreases in voltages resulted from upward force. Finally, the forces measured by load cells were added to calculate total friction force. A MATLAB script given in Appendix A was programmed to implement these steps and it uses raw data of load cell voltages to process into actual friction force. The basic algorithm for this data processing method is shown in Figure 5.2.

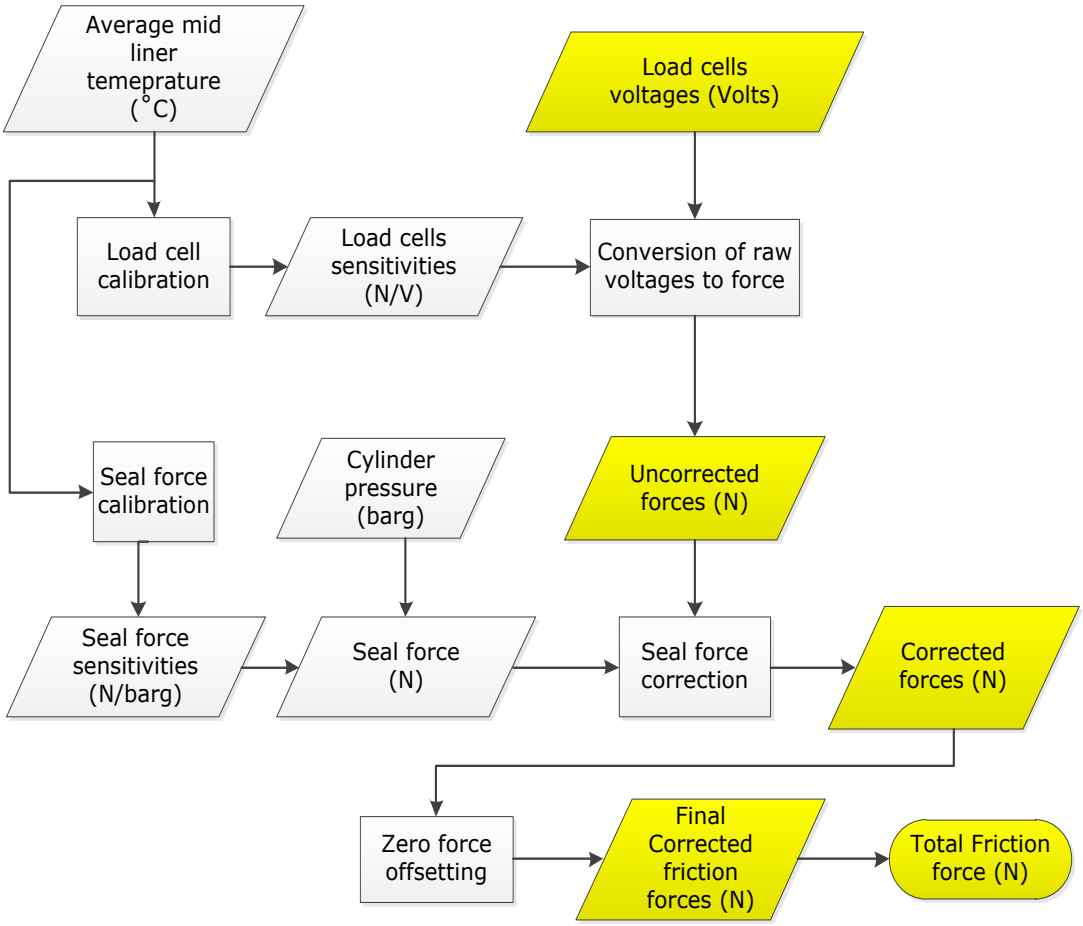

Figure 5.2: Algorithm to convert raw data into friction force

The test data of load cell voltages, temperatures and cylinder pressure, acquired through data acquisition system were saved in the spreadsheet files every single second during a test and afterwards fed into the script for data processing. In the processing method, average mid-liner temperature and cylinder pressure data were used to calculate the corresponding load cell and seal force sensitivities. These sensitivity values were utilised to convert the crank resolved load cell raw voltage data to corrected crank resolved friction force. The three steps of data processing- raw voltage conversion to force, seal force correction and zero force offsetting are illustrated with an example below.

5.2.1 Conversation of raw voltages to forces

The crank angle resolved raw data of load cell voltages were acquired every second of each test and were saved in a 2-D array. Each row of the array represents data for every second and has 720 data points for every 0.5° crank angle, starting from TDC which is represented by 0° of crank angle. After 180° of crank rotation during downstroke the piston reaches BDC and again comes back to TDC after a full rotation of 360° during upstroke. Thus 0 to 180° crank angle after TDC represents down stroke and 180 to 360° represents upstroke of a two stroke cycle.

Table 5.1 Specifications of the test build for the example in 5.2

Liner	P2 (Ra 0.35 μm, honing angle 30°)
Piston	Steel
Liner-piston diametric clearance	60 μm
Lubrication Oil	SAE 5W-30
Compression ratio	10.5

During the first data processing step, the crank resolved raw data of load cell raw voltages were converted to force in Newtons by applying the load cell calibration values. An example of this step is given below where load cell voltages acquired for a test at 1000 rpm and 60±1 barg peak pressure for the test build presented in Table 5.1 were converted to force by using corresponding calibration values. The load cell voltages data acquired at 130s of the test run are presented in Figure 5.3 where the average mid liner temperature was 40°C.

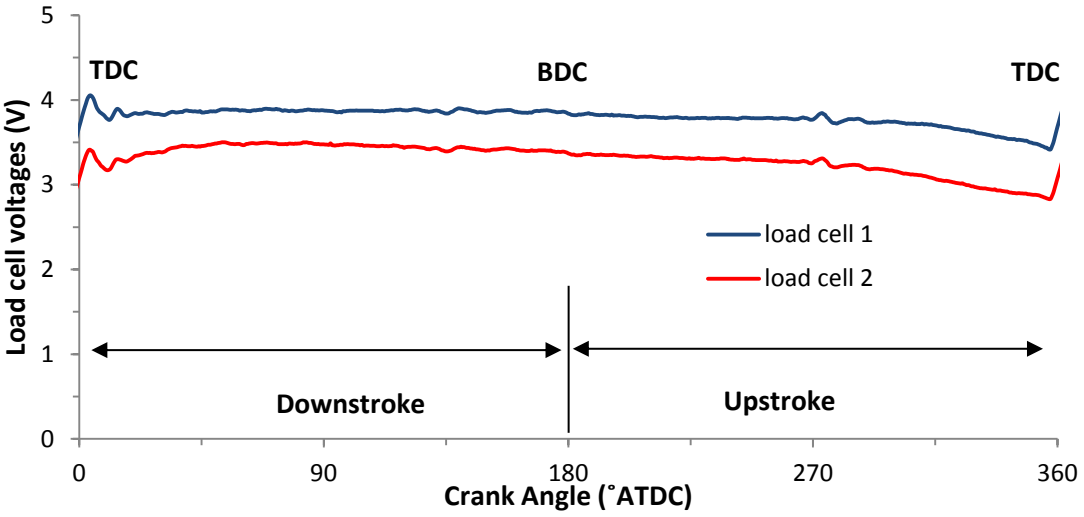

Figure 5.3: Crank resolved load cells output at 1000 rpm 60 barg peak pressure and 40˚C.

In this example, the load cells sensitivities were calculated for the corresponding average mid liner temperature and were employed to convert the voltages into force values in Newtons as presented in Figure 5.4. Shapes of both the load cell and corresponding force variation with crank angle are the same as same calibration values were applied across the cycle.

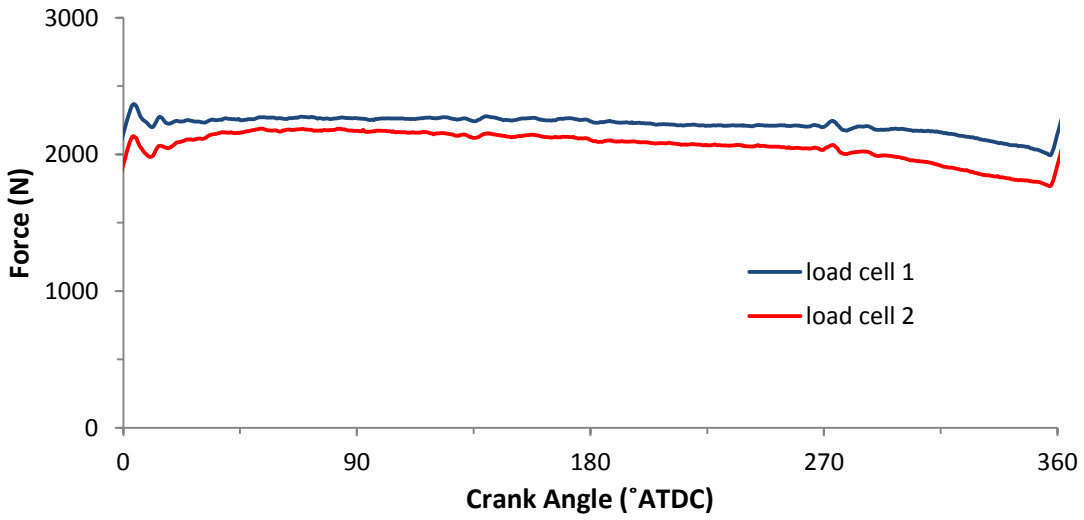

Figure 5.4: Crank resolved load cells voltages converted to force

5.2.2 Seal force correction

The force measured by load cells has a sealing ring force contribution during a pressurised operation. Thus the forces calculated in section 5.2.1 were corrected for a pressurised test data by using the seal force calibration described in section 4.3.2. At first, the seal force sensitivities in N/barg were calculated for the corresponding liner temperature and then the crank resolved sealing ring forces were obtained from the crank resolved cylinder pressure, presented in Figure 5.5.

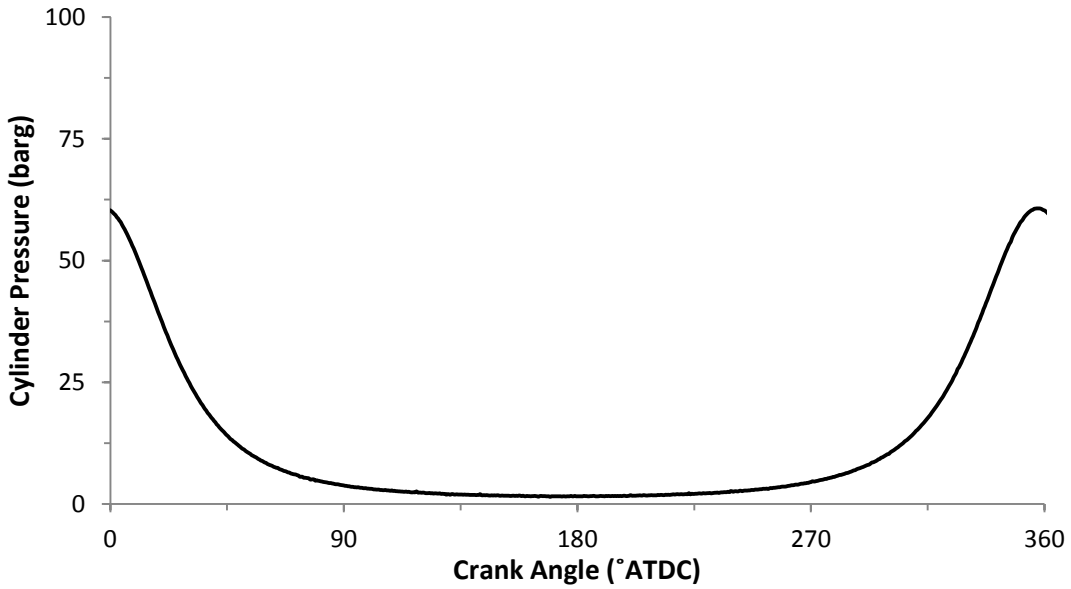

Figure 5.5: Crank resolved cylinder pressure

The calculated sealing ring force contributions towards each load cell measurement are presented in Figure 5.6. As the sealing ring force is directly proportional to the cylinder pressure, it varies along the cycle following the pressure. The cylinder pressure in this example varies from 60 barg peak pressure at 1-2° crank angle before TDC to near atmospheric pressure at BDC during down stroke and again same peak pressure before TDC at the end of upstroke.

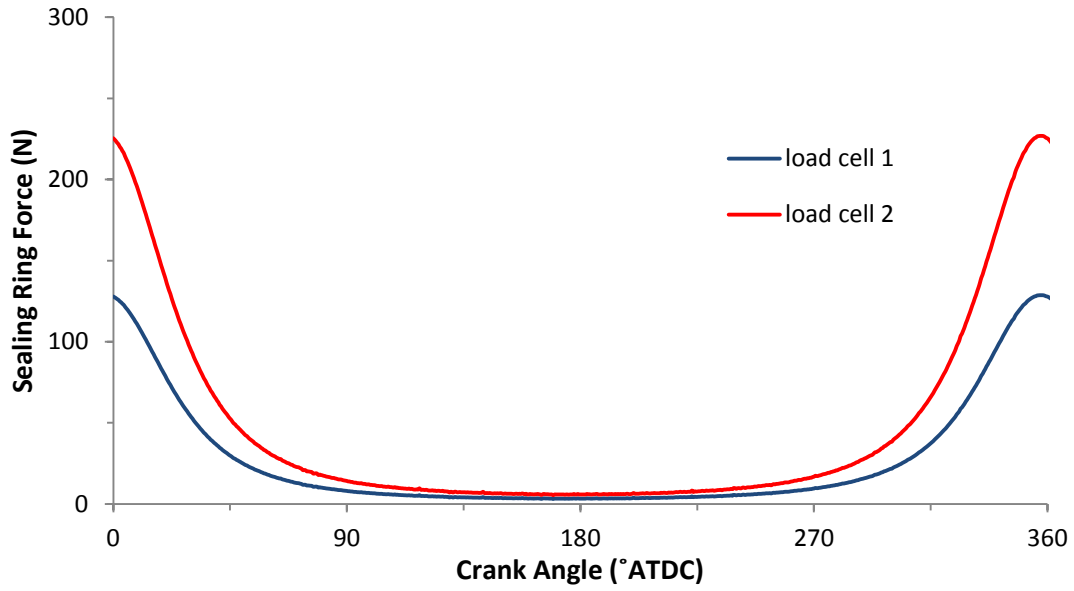

Figure 5.6: Sealing force contribution to measured load cells output

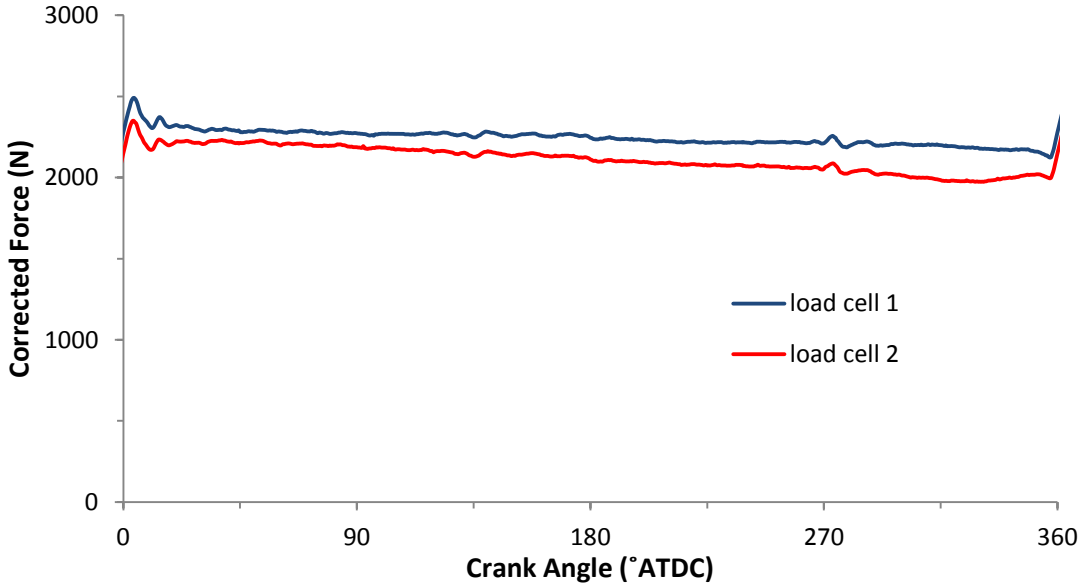

Figure 5.7: Corrected crank resolved forces

In this example, the maximum sealing ring force contributions to load cells 1 and 2 were 125 N and 225 N respectively. However, the forces decreased at high rates following the cylinder pressure and were minimum at 3N and 5N respectively at BDC. As the sealing ring force acts upwards, decreasing the measured force, its contributions towards load cells were added to the converted

force, presented in Figure 5.4. The corrected forces after seal force correction are presented in Figure 5.7.

5.2.3 Zero force offsetting

The corrected forces presented in Figure 5.7 indicate the variation around the cycle but not absolute values, as preloads are present in the values. The preloads varied with temperature because of clamping force reduction as mentioned in section 4.3.1 and they were not the same for both load cells. Thus the final friction force corrections were undertaken using a different method, zero force offsetting.

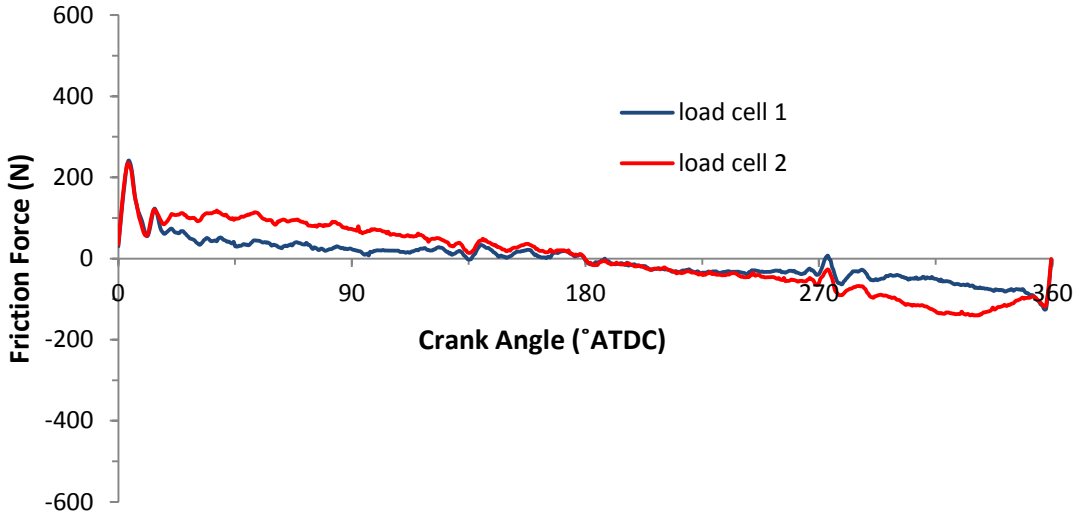

Figure 5.8: Final corrected crank resolved friction forces

This method is based on the theory that force direction changes after the end of each stroke at TDC and BDC. Therefore force would go past zero point near the dead centres. However, near TDC, pressure variations were very steep thus causing sudden changes in friction forces and consequently produce uncertainty in the zero offsetting method. Whereas, near BDC, the pressure traces were flatter and thus it was easier to apply an offsetting process.

In this step of data processing, the force values at 5° crank angles before and after BDC were averaged to calculate the zero force line. The method was applied individually to each of the load cell measurements and final corrected friction forces are presented in Figure 5.8. Finally, the final corrected friction forces measured by load cells were added to obtain the crank resolved total piston-liner assembly friction forces as presented in Figure 5.9.

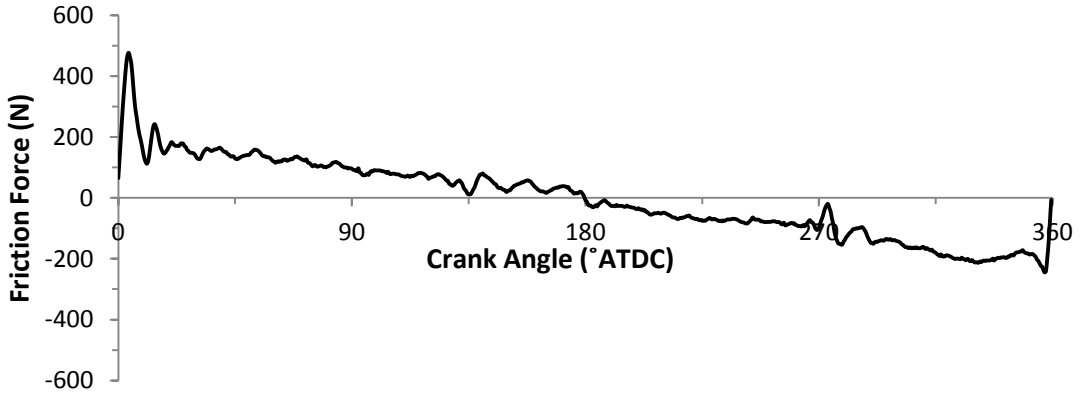

Figure 5.9: Total crank resolved friction force output at 1000 rpm 60 barg peak pressure and 40˚C.

5.3 Analysis options and presentation format

The crank angle resolved friction forces measured at a fixed operating speed and peak pressure condition along a test run, were analysed to compare friction forces at different average mid liner temperatures. In this study the friction forces were compared for temperatures from 40°C to a maximum of 90°C depending on the load and speed condition. For higher loads and speeds, temperatures below 40°C were difficult to obtain as temperature creeps up quickly because of high friction forces. Whereas, for lower speed and loads, temperatures higher than 80°C were arduous to achieve as friction force and oil heating were not adequate to reach higher temperature. The friction forces obtained at different temperatures were further analysed to obtain fmep and an instantaneous Stribeck diagram at different temperatures for a test run. fmep data indicate average work done in a

cycle whereas the Stribeck diagram was used as a tool to analyse changes in lubrication regimes along a cycle. The test results were presented as crank resolved friction forces at different temperatures, fmep variation with temperature and Stribeck diagram for particular operating condition-speed, temperature and peak pressure as described below.

5.3.1 Crank resolved friction forces

Friction forces obtained at different crank angles allow force characteristics around a cycle to be examined and differences in friction in various parts of the cycle to be distinguished. The friction forces at different temperatures were obtained by taking averages of data of different cycles around each temperature. The averages were taken from crank resolved data for temperatures ±1°C and peak pressure ±1 barg to obtain crank resolved friction data for a particular temperature and peak pressure. For the example of test run in section 5.3, 1000 rpm and 60 barg peak pressure, the crank resolved friction forces were obtained for temperatures 40 to 90 °C at an interval of 10°C. The friction forces for 40 and 80°C are presented in Figure 5.10.

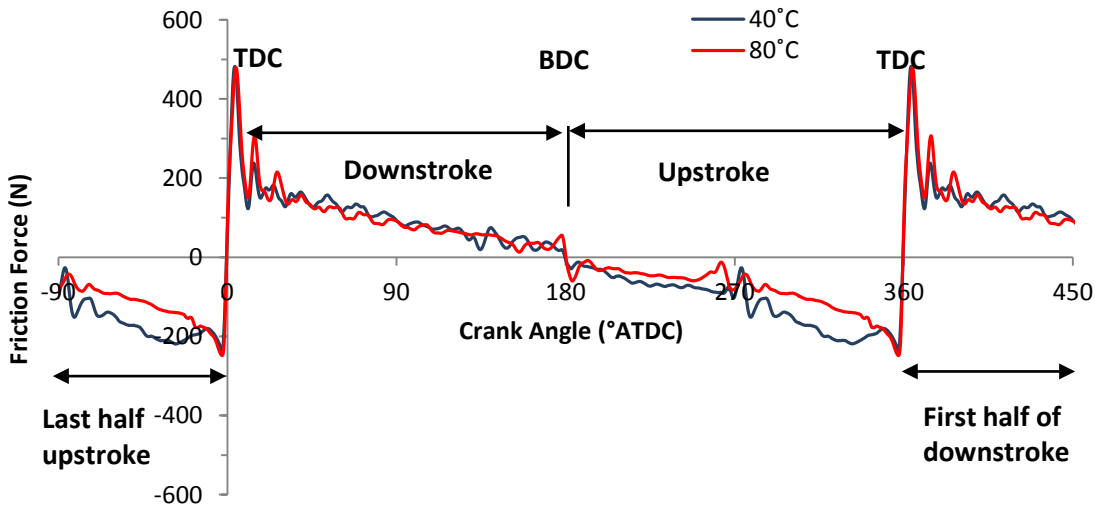

Figure 5.10: Crank resolved friction forces at different average mid liner temperature for 1000 rpm and 60 barg peak pressure.

In the graph of Figure 5.10, the friction forces were presented for -90 to 450° of crank angle. Crank angles from -90 to 0° represents last half of upstroke as indicated by negative friction forces whereas 360 to 450° represents first half of down stroke, indicated by positive forces. This representation of crank resolved friction forces further enables friction force analysis at the start and end of strokes near TDC. The data for 40°C were obtained from average of 30 cycles whereas for 80°C, data from 80 cycles were considered to obtain the average data. This is because temperature rise takes longer time at higher temperatures compared to a lower temperature as average frictional heat dissipation is lower at higher operating temperature. This is further illustrated in the next section by the analysis of fmep data.

5.3.2 Friction mean effective pressure

Crank angle resolved friction data for a particular temperature in a fixed speed and peak pressure condition were further analysed to calculate friction mean effective pressure (fmep). As the rig operates in a two strokes cycle rather than four strokes, the total frictional work in a cycle was doubled to obtain the equivalent fmep for the four stroke cycle assuming the friction force repeated every revolution. The fmep was calculated by using the equation 5.1 and the variation in fmep with temperature are compared as presented in Figure 5.11.

$$\mathbf{fmep} = \frac{\mathbf{2xTotal\ friction\ work\ \ in\ a\ cycle}}{\mathbf{Swept\ volume}} \qquad (5.1)$$

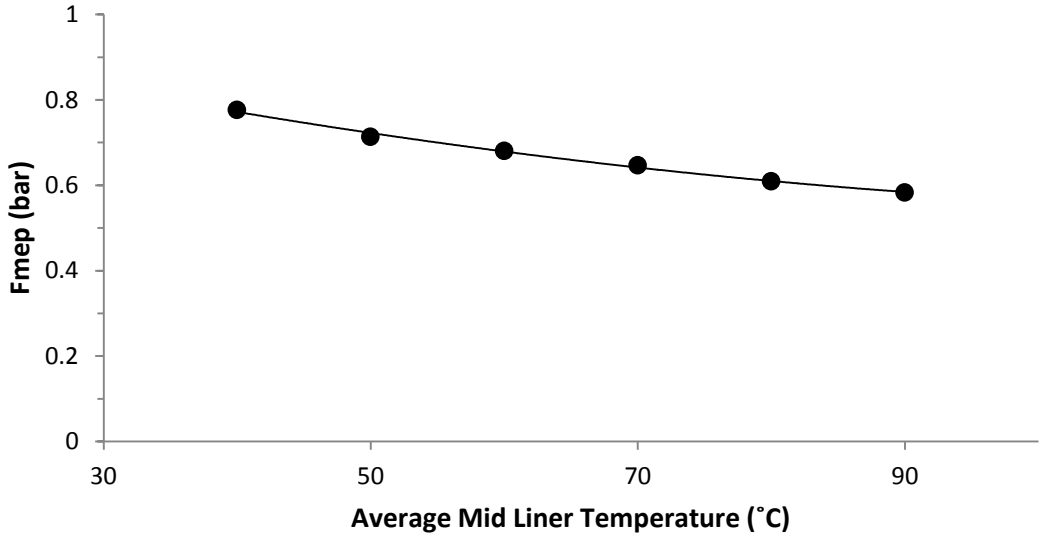

Figure 5.11: Variation of fmep with temperature for 1000 rpm and 60 barg peak pressure.

The fmep data presented in Figure 5.11 shows, fmep decreased with increasing temperature and the variation follows a second order polynomial. This indicates average friction work in a cycle was lower at higher temperature causing lower frictional heat dissipation, consequently longer time for temperature rise in oil. The fmep variation with temperature were also analysed for different speeds and peak cylinder pressures. Thus the analysis of average frictional work could be undertaken for different operating conditions for a particular rig build. The effects of operating conditions on piston-liner friction are discussed in details using crank resolved friction and fmep data in chapter 6.

5.4 Interpretation of data for an engine four stroke cycle

The friction forces data obtained from the test setup could also be used to infer fmep for a firing four stroke cycle by combining one revolution (two strokes) of uncompressed data to represent intake and exhaust strokes and one revolution of pressurised data to represent expansion and compression strokes. As described by Heywood [2], in a four stroke engine, the cylinder pressure is close to

atmospheric during intake and exhaust strokes whereas during compression and expansion strokes it can increase several folds depending on the load and engine type. Munney [118] stated that, peak cylinder pressures can be as high as 50 bara and 140 bara for petrol and diesel engine respectively.

The down and up stroke friction data from the uncompressed condition (without air seal assembly) were used to represent intake and exhaust respectively. Expansion and compression strokes are represented by down and up stroke respectively from a pressurised operation. A four stroke representation of piston – liner friction forces is shown in Figure 5.12. In the graph, 0° crank angle represents the start of the cycle at TDC and the cycle was completed after two full rotations of 720° crank angles. Thus the full four stroke cycle was presented in order of intake, compression, expansion/power and exhaust strokes.

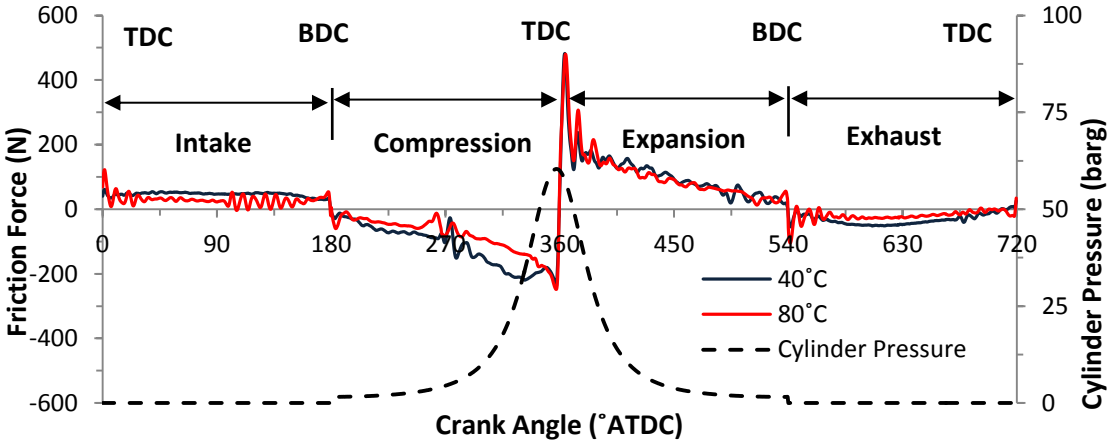

Figure 5.12: Four stroke representation of crank resolved friction data for 1000 rpm and 60 barg peak pressure.

In the Figure 5.12, the friction data from an uncompressed and 60 barg peak pressure tests at 1000 rpm were combined together to obtain the four stroke crank resolved friction forces at different temperatures for 1000 rpm and 60 barg peak pressure. fmep was calculated from the interpreted four stroke data as

presented in Figure 5.13 and follows similar variation with temperature to uncompressed or pressurised two stroke operation.

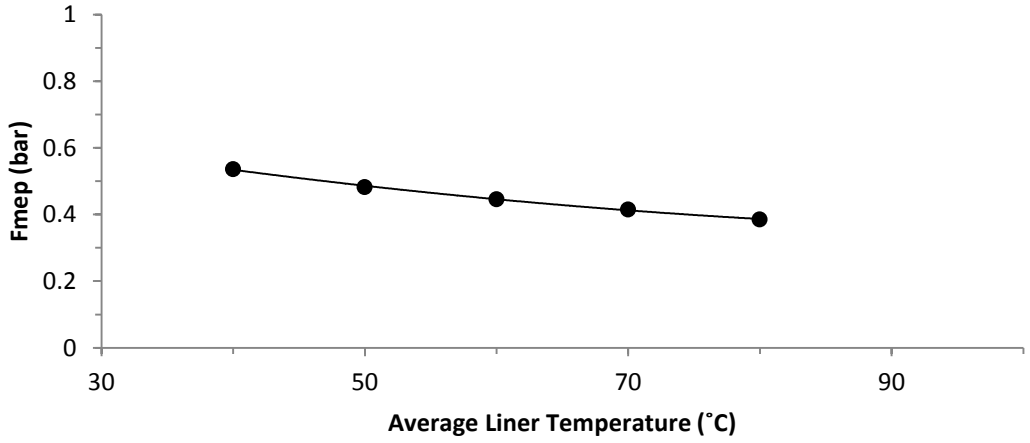

Figure 5.13: Fmep variation with temperature for four stroke cycle at 1000 rpm and 60 barg peak pressures.

5.5 Repeatability of test results

Tests were undertaken with different builds of the same liner-piston and oil combination under similar operating conditions to investigate the reproducibility of friction force results. Moreover, repeat tests also were undertaken with the same build to study the repeatability.

Table 5.2 Specifications of the test build for the example in 5.5

Liner	P2 (Ra 0.35 μm, honing angle 30˚)
Piston	Aluminium
Liner-piston diametric clearance	60 μm
Lubrication Oil	SAE 0W-30
Compression ratio	10.5

In the repeatability analysis the liner, piston and rings were removed and reinstalled and then tests through the same cycle were undertaken. Results of repeat tests with two different builds at uncompressed and pressurised condition

of 60 barg peak pressure for 1000 rpm and 40°C, for test build in Table 5.1 are presented in Figure 5.14.

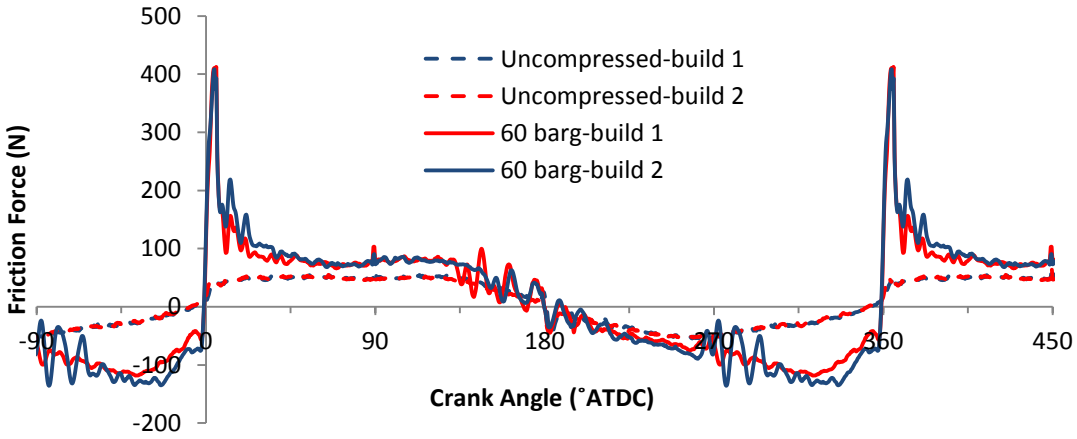

Figure 5.14: Friction force repeatability under uncompressed and 60 barg peak pressure condition at 1000 rpm and 40°C

From Figure 5.14 it can be seen that, highly repeatable friction force results were obtained with both pressurised and uncompressed condition. Two test build results obtained differences of 1 and 5% in fmep for uncompressed and 60 barg peak pressure conditions. Further, repeatability of test results were investigated for different peak pressure conditions from 0 to 80 barg. Fmep results for three different builds, including repeat tests were compared for different peak pressure conditions at 40 and 80°C, 1000 rpm as presented in Figure 5.15. Maximum differences of 5 and 7% between highest and lowest fmep results were obtained at 40 and 80°C respectively. At the higher peak pressure condition of 80 barg the maximum differences were 9 and 12% respectively.

Moreover, the repeatability of tests results for all peak pressures and temperatures were investigated with the analysis of average fmep results and standard deviation as presented in Figure 5.16.

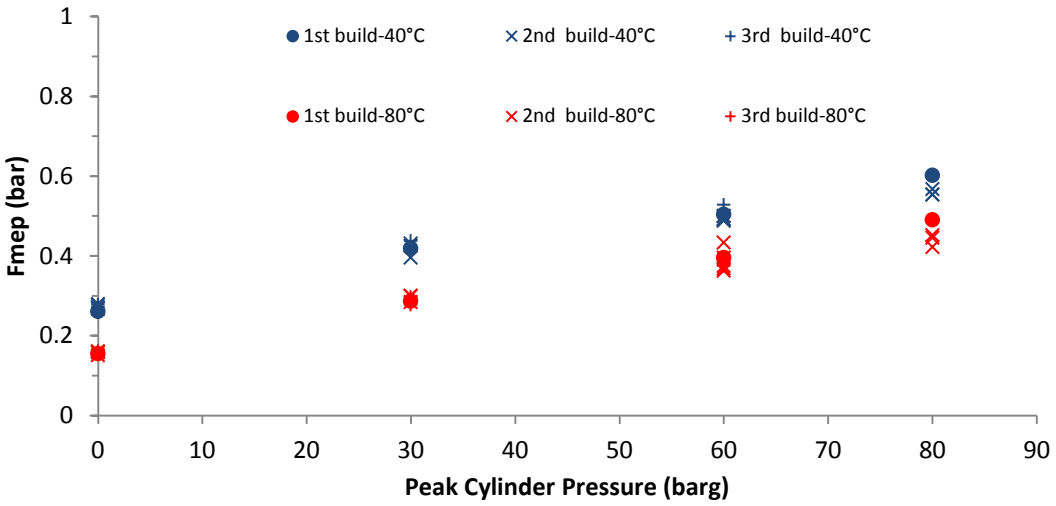

Figure 5.15: Fmep variation with peak cylinder pressure at 1000 rpm for different builds

From Figure 5.16 it can be seen that, variability in fmep results were higher for higher temperature and peak pressures. A maximum ±4% of standard deviation in fmep was observed for an uncompressed condition throughout the temperature range. However, higher standard deviations of ±5 and ±9% were observed at temperatures of 40 and 80°C respectively for pressurised conditions.

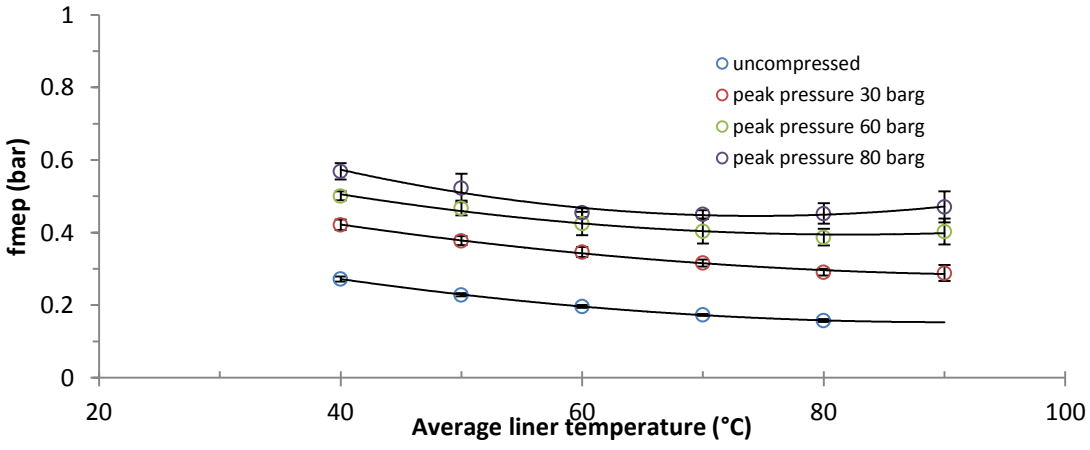

Figure 5.16: Average fmep variation with temperature with standard deviations at 1000 rpm

5.6 Lubricant viscosity analysis

The variations in lubricant viscosity with temperature were obtained for both the oils SAE 5W-30 and SAE 0W-30. The dynamic viscosities (μ) of both the oils at different liner temperatures were calculated by using Vogel's equation [46] in equation 5.3, where k_v , θ_1 and θ_2 are the Vogel parameters and T is the oil temperature.

$$\mu = k_v \exp\left(\frac{\theta_1}{T+\theta_2}\right) \qquad (5.3)$$

The parameters for individual oil were obtained by fitting a curve through the respective viscosity data provided by oil supplier. To consider the oil shear thinning effect, cold crank simulator (CCS) and high temperature high shear (HTHS) viscosity values were also imparted in the Vogel equation fit. Afterwards the Vogel parameters were adjusted to match the best fit curve.

Table 5.3: Physical properties of the lubricants

Properties	SAE 5W-30	SAE 0W-30
K_V (40˚C), cSt	37.58	31.4
K_V (100˚C), cSt	6.988	6.014
HTHS(150˚C), cP	2.97	2.99
CCS, cP	4006 (at -30˚C)	5572 (at -35˚C)
Density (15˚C), g/cm^3	0.8338	0.8338

The dynamic viscosities of the oils at 40 and 100˚C were calculated from the kinematic viscosities and density values presented in Table 5.3. Thus the parameters obtained with this method were used to predict dynamic viscosity at different temperature by taking account of both the low and high shear conditions. The Vogel parameters obtained for the oils SAE SAE 5W-30 and SAE 0W-30 are presented in Table 5.4.

Table 5.4: Vogel parameters for two lubricants

Vogel Parameter	SAE 5W-30	SAE 0W-30
k_v , mPas	0.0456	0.062
Θ_1, ˚C	1130	1020
Θ_2, ˚C	130	125

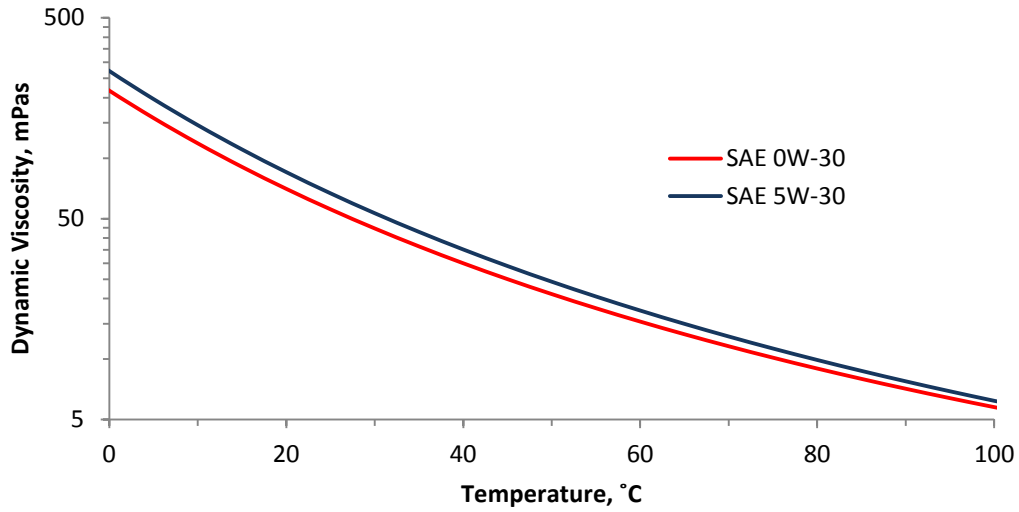

Figure 5.17: Dynamic viscosity (in logarithmic scale) variation with temperature for two oils at temperature range of 0 to 100˚C

Using the Vogel parameters for individual oil, the variations of dynamic viscosities with temperature were obtained as illustrated in Figure 5.17. It can be observed that viscosity of SAE 5W-30 oil is higher than that of SAE 0W-30 and the difference in viscosities reduces with temperature. At lower temperature of 40˚C the viscosities of SAE 5W-30 and SAE 0W-30 were 35 and 30 mPas respectively. At higher temperature, discernible difference in viscosities was observed; 9.9 and 8.9 mPas respectively for SAE 5W-30 and SAE 0W-30.

5.7 Discussion

In the friction force data processing, a zero force alignment method was applied around BDC where the friction value passes through zero point during piston reversal. Though piston reversal also takes place at TDC, rapid change in friction

force around TDC introduces some uncertainty in alignment method. However, the measurement of fmep which uses integration of frictional work around a cycle is independent of this zero point identification.

During pressurised operations, the peak pressure conditions 1-2° before TDC were observed which could be defined as 'thermodynamic loss angle' and was observed by different researchers [119-121]. Heat transfer through the cylinder liner during compression and mass leakage were identified as the main reasons behind this occurrence. It was observed that the pressure in the rig falls much more slowly than a real fired diesel engine. The compression ratio and air leakage past the piston and seal could be adjusted to mimic the condition of a fired engine. The compression ratio of 10.5 used in this setup could be increased to 16-18, closer to that of a diesel engine, which can help in achieving lower minimum pressure values and consequently more reduction in pressure for a particular peak pressure. However, the effect of higher air leakage compared to a real engine can be compensated by further increasing the compression ratio. Build to build repeatability analysed in section 5.4 shows the confidence in friction force measurement with a swift test specimen changeover.

Chapter 6 Results and discussion of friction parametric studies

In this chapter, the results of piston-liner friction parametric studies are presented and discussed. Section 6.1 is concerned with the study of operating conditions on friction. In section 6.2, the effects of lubricant viscosity on friction are discussed and section 6.3 deals with the effect of macro design features (piston-liner clearance and piston material) on piston assembly friction.

6.1 Friction at different lubrication regimes and operating conditions

The dependence of piston-assembly friction force on engine operating conditions of pressure, speed and temperature are presented in this section. The variation of friction with one particular parameter was studied by comparing results under similar other parameters. The comparisons presented in this section are based on the results obtained with the build specifications presented in Table 6.1.

Table 6.1 Specifications of the test build

Liner	P2 (Ra 0.35 μm, honing angle 30°)
Piston	Aluminium
Liner-piston diametric clearance	60 μm
Lubrication Oil	SAE 5W-30
Compression ratio	10.5

6.1.1 Friction variation in a cycle

In the piston-liner assembly, the transition from mixed/boundary to hydrodynamic lubrication in a cycle depends on the operating conditions, and lubricant and surface properties. The variation in friction and corresponding lubrication regimes were investigated using the floating liner rig under different operating conditions.

Under pressurised operation, ring force on and normal to the liner due to gas pressure on the back of the rings and ring tension vary depending on the gas load, but for an uncompressed condition this remains constant. Thus friction forces in a cycle for an uncompressed condition give the indication of lubrication regime transition. This is illustrated in Figure 6.1 where the variation of friction force, velocity and side thrust during down stroke at a speed 1000 rpm and average liner temperature of 80°C are presented for an uncompressed test.

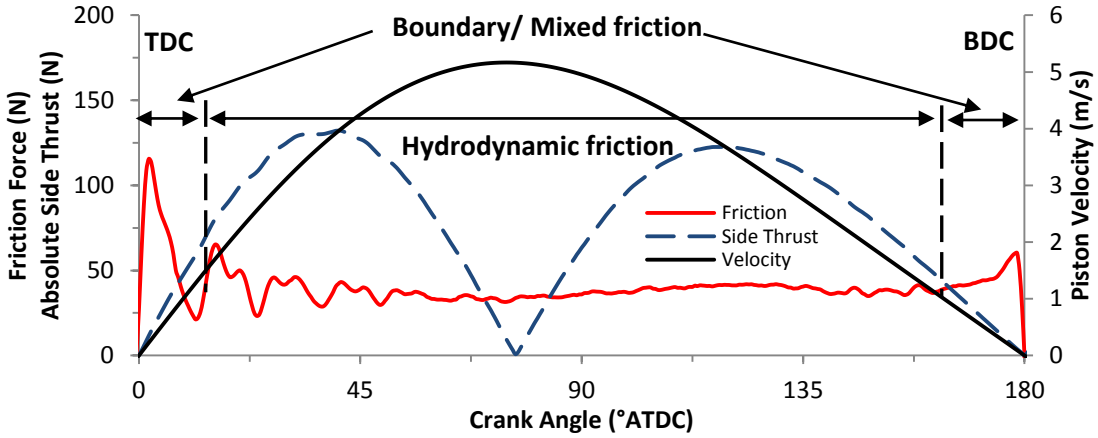

Figure 6.1: Transition through different lubrication regimes exhibited in one piston stroke (down stroke) at 1000 rpm uncompressed and 80°C.

The piston velocity (v) and acceleration (a) were calculated using the equations 6.1 and 6.2.

$$v = \pi SN\sin\theta\left[1 + \frac{\cos\theta}{(R^2 - \sin^2\theta)^{1/2}}\right] \qquad (6.1)$$

$$a = 2\pi^2 SN^2\left[\cos\theta + \frac{R^2\cos 2\theta + \sin^4\theta}{(R^2 - \sin^2\theta)^{3/2}}\right] \qquad (6.2)$$

$$R = \frac{l}{S/2} \qquad (6.3)$$

Where, S, N, θ are stroke, rotational speed and crank angle respectively and R is the ratio of connecting rod length (l) and crank radius (S/2). From the values of

acceleration (a) the calculation of corresponding side thrusts were obtained by using equation 2.1.

The friction force was highest at the beginning and end of the stroke. Near these dead centres piston velocities were very low and not adequate to develop a thick lubrication film which could separate the surfaces of the piston and liner. Here contacts between the piston assembly and liner interfaces are dominated by high asperity interactions, and as a result boundary lubrication regime occurs [49]. As the piston velocity increases, a film of lubricant can develop between the contact surfaces partly supporting the load at the interface; however some asperity contact can still exist. This was considered the mixed lubrication regime [115].

As piston velocity continued to increase, the side thrust is increasingly supported by the lubricant film and asperity contacts is diminished [21]. The hydrodynamic lubrication regime occurs when the lubricant film thickness is sufficient to prevent any asperity contact between the piston assembly and the liner wall. In the absence of asperity contact, the friction force produced is due to viscous shear of the lubricant. Since viscous shear is proportional to the relative velocity, a local maximum should have occurred near the mid stroke region. However, hydrodynamic friction is also dependent on film thickness which is strongly transient depending on the normal load. The side-thrust or normal load on the skirt was lower at the position of maximum speed (75° crank angle). Thus the film thickness would be higher in that position. Consequently, the effect of higher shear rate was reduced by side thrust at this point of the stroke. The position of maximum hydrodynamic friction with high speed and high side thrust was obtained at around 40 and 120° crank angle after TDC for this particular test condition.

6.1.2 Effect of gas loading on friction

The effect of gas loading on friction was investigated through tests covering peak pressure from 0 to 80 barg, at different speeds and temperatures. The variation of friction force in a cycle under different peak pressures for a speed of 1000 rpm and 80°C is presented in Figure 6.2 where uncompressed test represent 0 barg test.

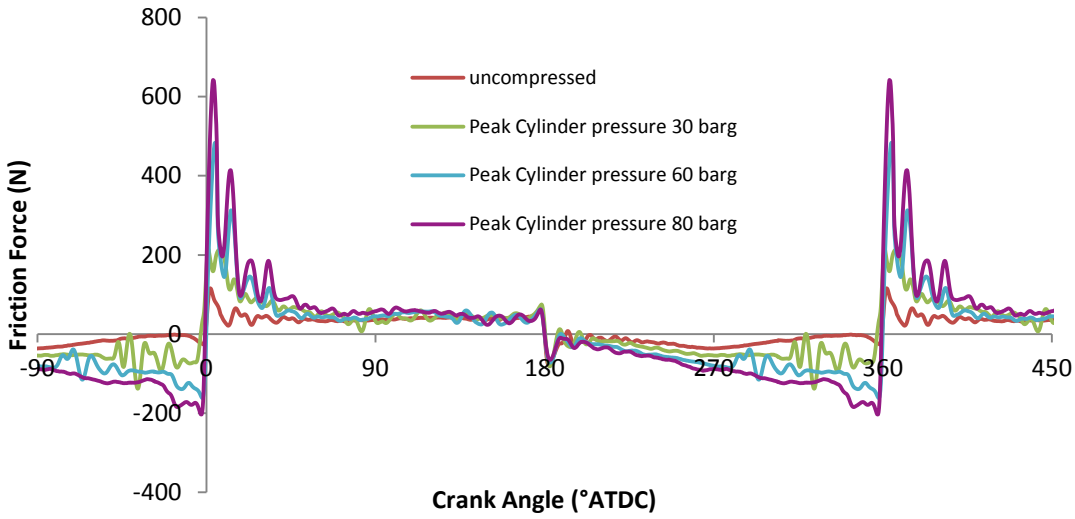

Figure 6.2: Friction forces at different peak pressure conditions at 1000 rpm and 80°C.

From Figure 6.2 it can be seen that friction forces increased with increasing peak pressure for similar speed and temperature conditions. Increasing pressure increases the normal load on the piston rings particularly at the top ring near TDC. Thus film thickness can reduce significantly to promote higher mixed/boundary friction. As the piston moved away from TDC, cylinder pressure reduced steeply and rate of reduction was higher for higher peak pressure as shown in Figure 6.3. Thus normal load on the rings reduced in a higher rate for higher peak pressures, resulting in higher mixed/boundary friction reduction.

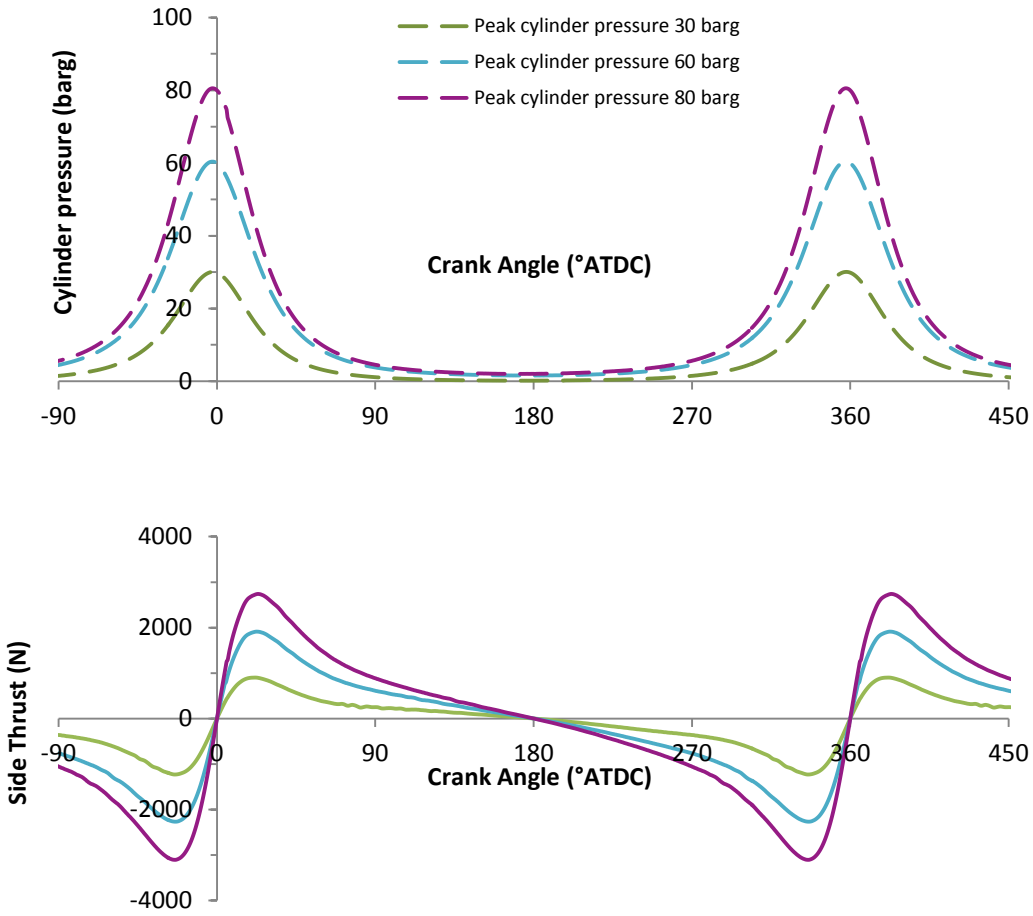

Figure 6.3: Variation in cylinder pressures and side thrust forces at different peak pressure conditions at 1000 rpm and 80˚C.

From mid-stroke to BDC for both of the strokes, the pressures were very close to each other for all peak pressures, resulting in similar normal loads on the rings. Consequently the film thicknesses at the rings-liner interfaces should be similar. As the velocities were the same for all peak pressure conditions similar hydrodynamic friction should occur in the ring packs. However, from mid-stroke to BDC, the side thrusts were higher for peak pressure of 80 barg than that of 60 barg even though the cylinder pressures were very close for both the peak pressure condition. Thus it resulted in a higher hydrodynamic friction in the skirt-liner interface, consequently higher hydrodynamic friction for the whole piston

assembly at higher peak pressure. Near BDC cylinder pressures were very similar and side thrust were close to zero, resulting in a similar mixed/boundary friction.

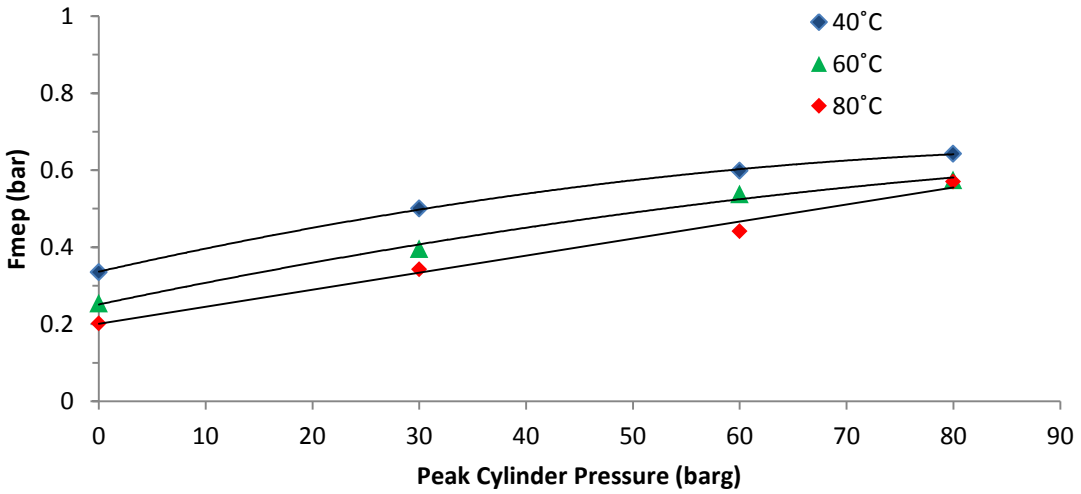

Figure 6.4: Variation in fmep with peak cylinder pressure for different temperatures at 1000 rpm.

The sensitivity of fmep to peak pressures was studied for different temperatures at 1000 rpm as presented in Figure 6.4. It was observed that fmep increased with increasing peak pressure following a second order polynomial. A decreasing gradient was observed as moving towards higher peak pressures. As with increasing peak pressures the increase in hydrodynamic friction was lower compared to mixed/boundary friction and most of the frictional work takes place in the hydrodynamic friction regions, thus rate of fmep increment reduced. However, at a higher temperature of 80˚C the occurrence of reduced gradient diminished as mixed/boundary contribution increased with temperature which is further discussed in section 6.1.4.

6.1.3 Comparison between down and up strokes

The friction forces during down and up strokes in one cycle were compared for different peak pressure conditions and at a speed of 1000 rpm. The comparison of individual stroke friction forces were first undertaken for the same piston positions as illustrated in Figure 6.5. The local operating variables such as velocity, side

thrust and pressures were also investigated to understand the development of lubrication film and frictional behaviour along each stroke.

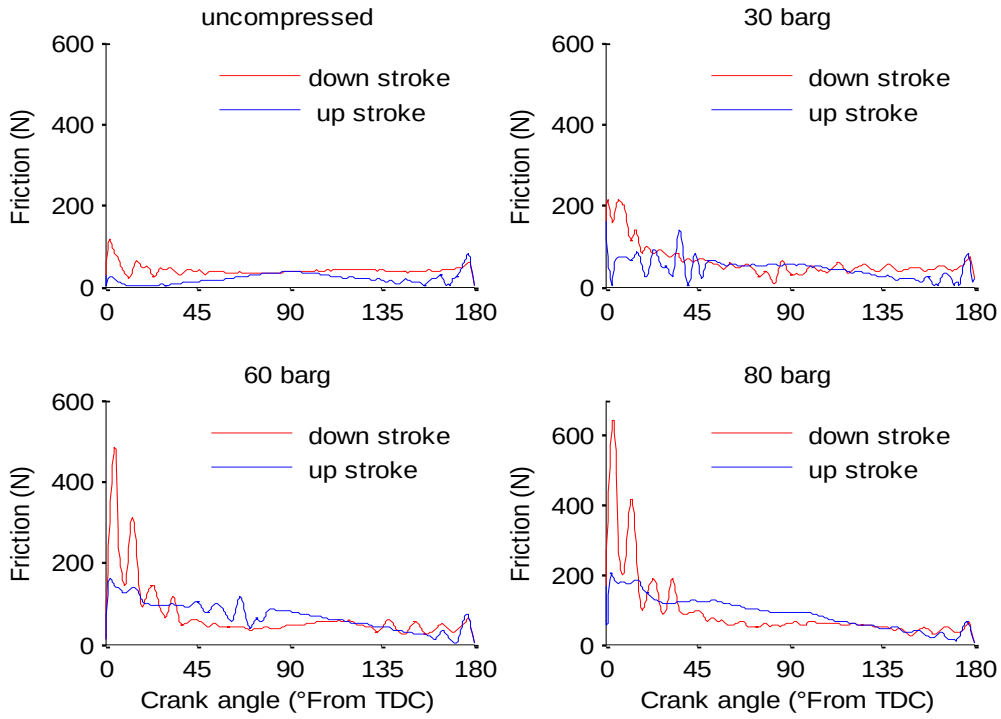

Figure 6.5: Comparison of down and up stroke frictions at different crank positions for peak pressures from 0 to 80 barg and 1000 rpm, 80˚C

An asymmetry of friction forces were observed between two strokes for the same piston positions. Higher Mixed/boundary friction forces were obtained during down stroke near TDC compared to upstroke for all peak pressure conditions. On the other hand, the hydrodynamic frictions were higher during up stroke around the mid-stroke regions for pressurised conditions. Moreover, near BDC similar mixed/boundary frictions were obtained. The biggest determinant of friction forces, cylinder pressure and velocity presented in Figure 6.6, were analysed to understand this behaviour.

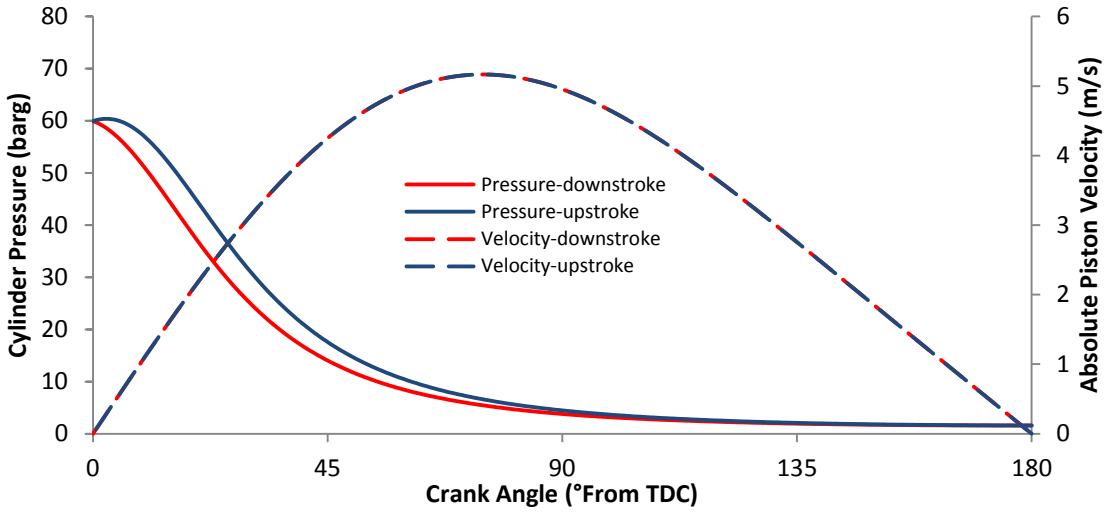

Figure 6.6: Comparison of down and up stroke cylinder pressures and velocities at different crank positions for 1000 rpm and peak pressure of 60 barg.

From Figure 6.6 it can be seen that, absolute velocities were similar for both strokes at same piston positions whereas cylinder pressures were slightly higher (maximum 6 barg) for upstroke from TDC to near mid-stroke region in a 60 barg peak pressure test. As the pressure dominates the side thrust forces, it was also higher for upstroke as presented in Figure 6.6. Thus higher hydrodynamic friction forces around mid-stroke region were obtained during upstroke. Moreover, the similar side thrusts, velocities and pressures from 135 to 180° crank angle resulted in similar hydrodynamic and mixed/boundary friction.

However, this mechanism was not followed at the first 15 to 20° crank angles near TDC. As for the same positions, down and up strokes were not in a similar motion thus the lubricant film formation was effected, consequently the friction.

The effect of piston motion on friction and lubrication was further investigated for an uncompressed condition where side thrust is not affected by cylinder pressure. Friction forces relative to displacement from start of each stroke (from TDC for a downstroke and from BDC for an upstroke) for a 1000 rpm uncompressed test at

80°C are presented in Figure 6.7. The comparison of forces relative to piston motion showed similar trend compared to asymmetric and dissimilar trend for a similar piston position analysis. The local absolute velocities, side thrust and acceleration for similar displacement were also investigated as illustrated in Figure 6.8 for in depth analysis.

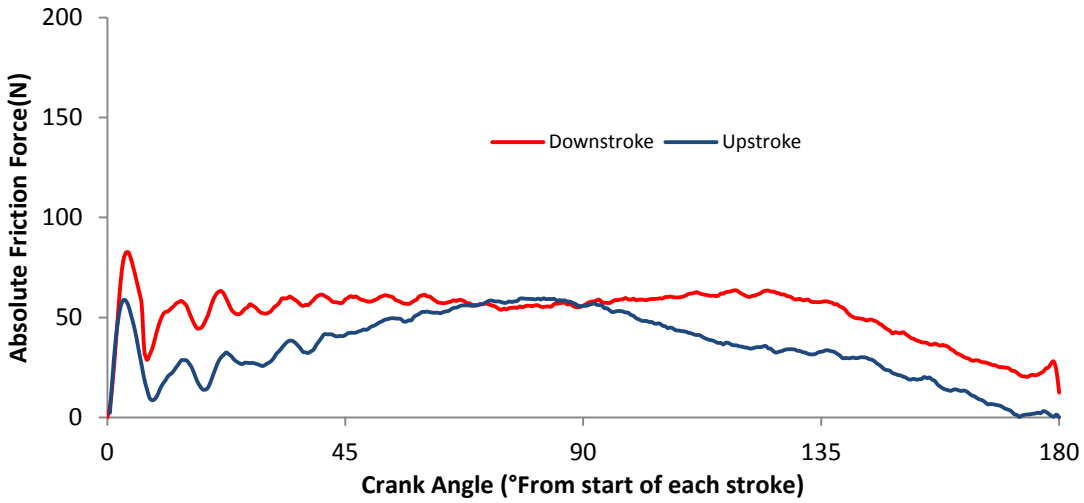

Figure 6.7: Comparison of down and up stroke frictions for uncompressed 1000 rpm test at 80°C.

For the comparison presented in Figure 6.7, piston was accelerated away from TDC and BDC for down and up stroke respectively and again decelerated when approaching BDC and TDC respectively. From the Figure 6.8 it can be seen that highest piston velocities were obtained after different crank angle rotation, around 75 and 105° crank rotation respectively. Thus dissimilar acceleration and deceleration were achieved, consequently resulted in dissimilar side thrusts.

At the early parts of each stroke, though piston was in acceleration for both the strokes, higher mixed/boundary friction was achieved during the down stroke due to higher side thrust. Up to the mid stroke region, down stroke had higher velocity, thus resulted in higher hydrodynamic friction. Though side thrust was higher for upstroke from 45 to 90° crank angles, but influences of piston velocity appeared to be dominant in determining hydrodynamic friction.

Similar hydrodynamic friction forces were obtained after half of the stroke because of similar velocity and side thrust for a similar motion. At the later half of the stroke, downstroke friciton was again higher compared to upstroke though piston velocity was higher for upstroke. At the latter half of the stroke, both the strokes were in deceleration and the side thrust and velocity was also lower for down stroke. However higher friction force was obtained during down stroke.

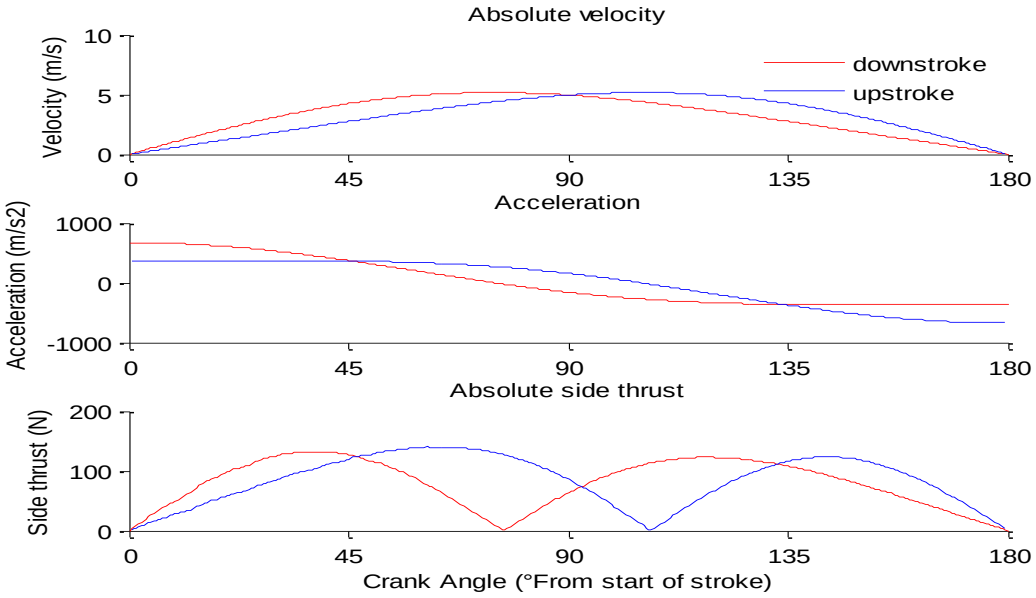

Figure 6.8: Comparison of down and up stroke velocities, accelerations and side thrusts for uncompressed 1000 rpm test at 80˚C.

6.1.4 Friction variation with temperature

The effect of oil film temperature on piston-liner friction was studied by investigating friction forces at different liner temperatures under different peak pressures and speeds. The friction forces for a 1000 rpm 60 barg peak pressure condition at different average mid-liner temperature of 40, 60 and 80˚C are presented in Figure 6.9.

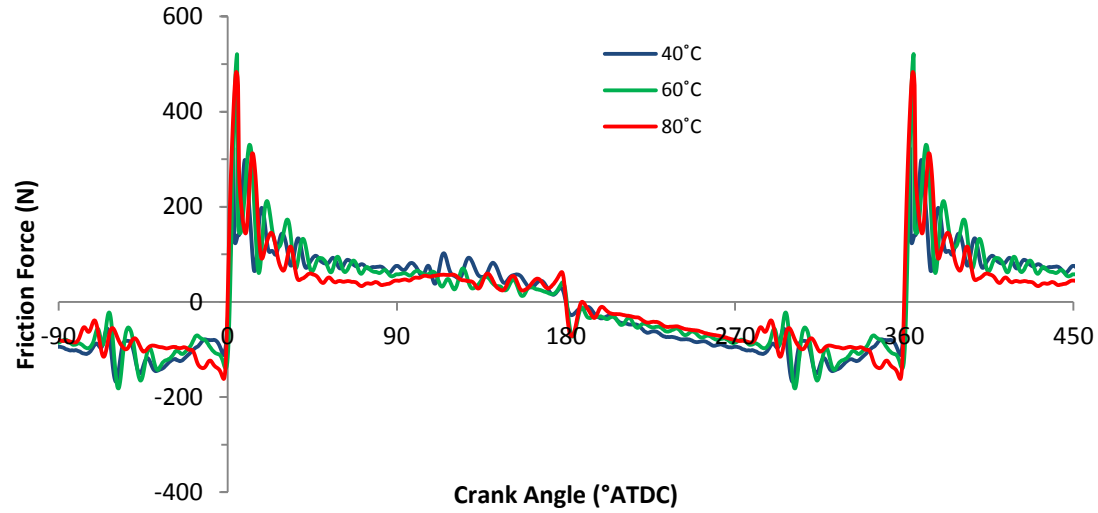

Figure 6.9: Friction force variation with temperature for 1000 rpm and peak pressure of 60 barg.

From the Figure 6.9 it can be seen that, with increasing temperature hydrodynamic friction reduced and mixed/boundary friction increased around BDC and near TDC for the compression stroke. Higher temperature reduced the viscosity of oil, resulted in a lower hydrodynamic shear force. As viscosity also determines the oil film thickness, thus a reduced film thickness occurred at higher temperature. Consequently higher mixed/boundary friction was achieved due to higher asperity contacts at higher temperature.

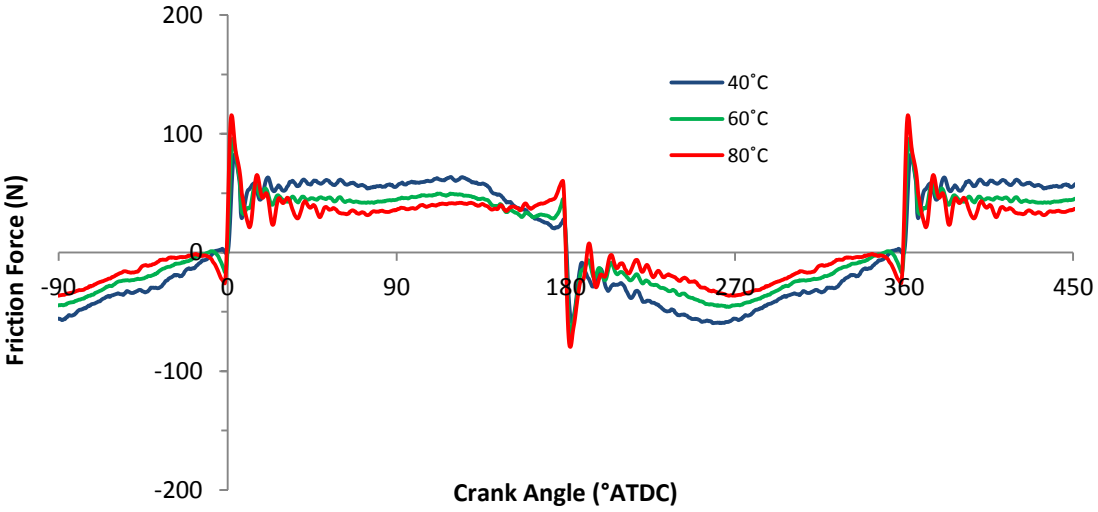

Figure 6.10: Friction force variation with temperature for uncompressed 1000 rpm test.

As pressure dominates the friction force around TDC during down stoke, the effect of thinner oil at elevated temperature was not evident. Friction forces at an uncompressed condition were compared to exclude the effect of pressure as illustrated in Figure 6.10. The effect of thinner oil on mixed/boundary friction was also observed near TDC during down stroke for this condition.

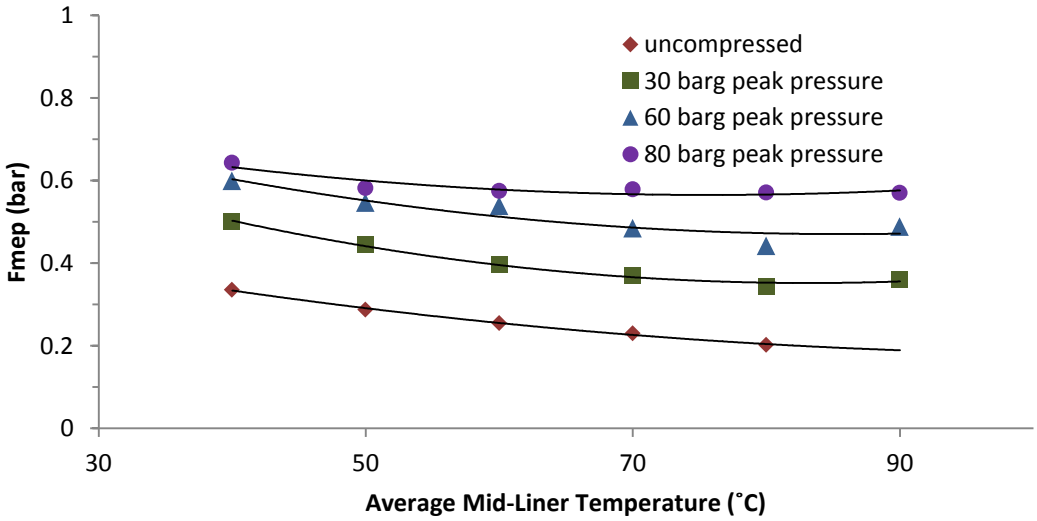

Figure 6.11: Variation in fmep with temperature for different peak pressure conditions at 1000 rpm.

The effect of temperature on fmep was observed for different peak pressure conditions as presented in Figure 6.11. Most of the frictional work takes place at the middle part of the strokes where friction is in hydrodynamic regime. Thus reduction of fmep was observed with increasing temperature due to reduction of hydrodynamic friction. The increase in boundary friction was not dominant in determining total frictional work. Moreover, sensitivity of fmep to temperature was reduced at higher peak pressure conditions. The combined effect of peak pressure and temperature were studied by analysing relative mixed/boundary and hydrodynamic contribution to fmep at different temperatures and pressures as illustrated in Figure 6.12.

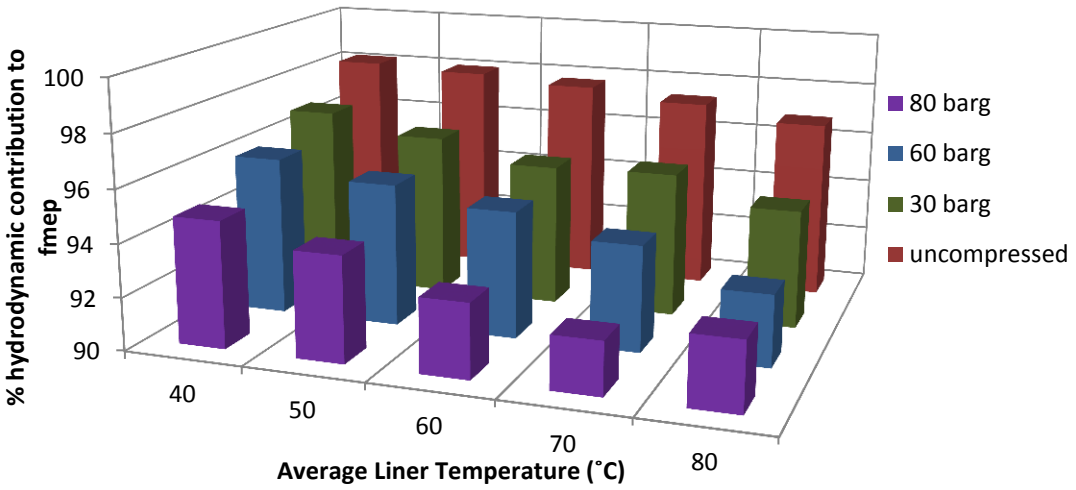

Figure 6.12: Relative hydrodynamic contributions to fmep at different temperatures and pressures for 1000 rpm.

The relative contributions from different frictional zones were obtained by calculating the frictional work at each zone. The mixed/boundary friction were observed to be occurring 10-15° crank angles before and after TDC. Thus frictional work in 15° crank angles before and after TDC were considered to calculate the mixed/boundary contribution and the rest of the cycle to calculate hydrodynamic contribution. From Figure 6.12 it can be seen that hydrodynamic contribution decreased with increasing temperature and pressure. For higher peak pressure, a contribution of hydrodynamic friction was lower compared to lower pressure. Maximum 3% of boundary contribution was obtained for uncompressed condition, compared to 8% for 80 barg condition. Thus boundary friction was more prominent at higher peak pressures, consequently lower fmep/temperature gradient was observed.

6.1.5 Friction variation with operating speed

The effect of operating speed on friction was investigated by undertaking tests at different speeds of 1000, 1500 and 2000 rpm for the pressurised tests. Some lower speed tests of 250, 500 and 750 rpm were also undertaken in addition to higher speeds for the uncompressed condition. The friction forces for different speeds for 60 barg peak pressure condition are presented in Figure 6.13.

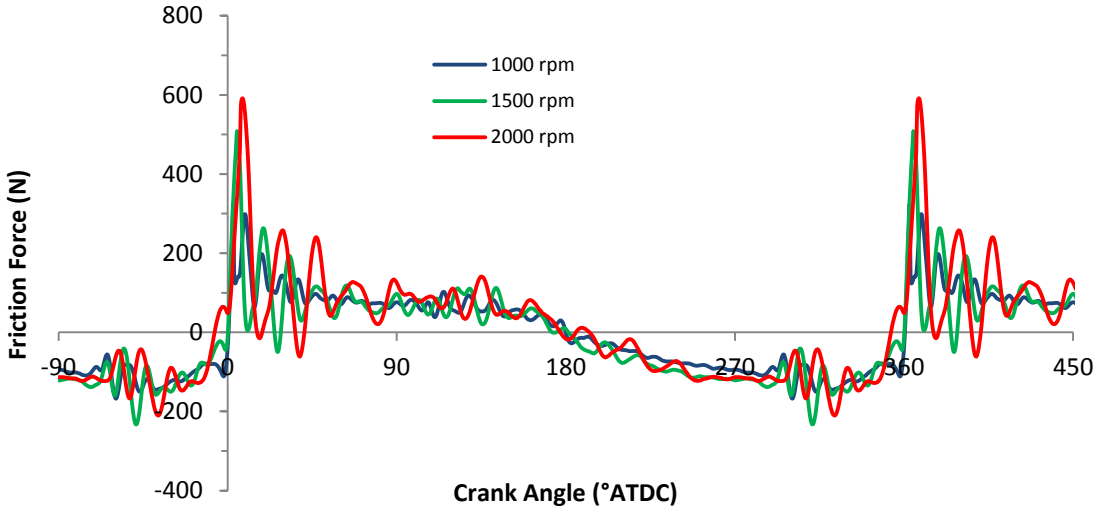

Figure 6.13: Friction force variation with speeds for peak pressure of 60 barg at 40˚C.

From the Figure 6.13 it can be seen that, with increasing speeds hydrodynamic friction increased and mixed/boundary friction reduced around BDC and near TDC for compression stroke. Higher speed resulted in a higher instantaneous velocity as presented in Figure 6.14, consequently higher hydrodynamic shear force and friction. The accelerations and side thrusts are also presented in Figure 6.14 to understand the combined effect of inertia forces and pressure during pressurised operation.

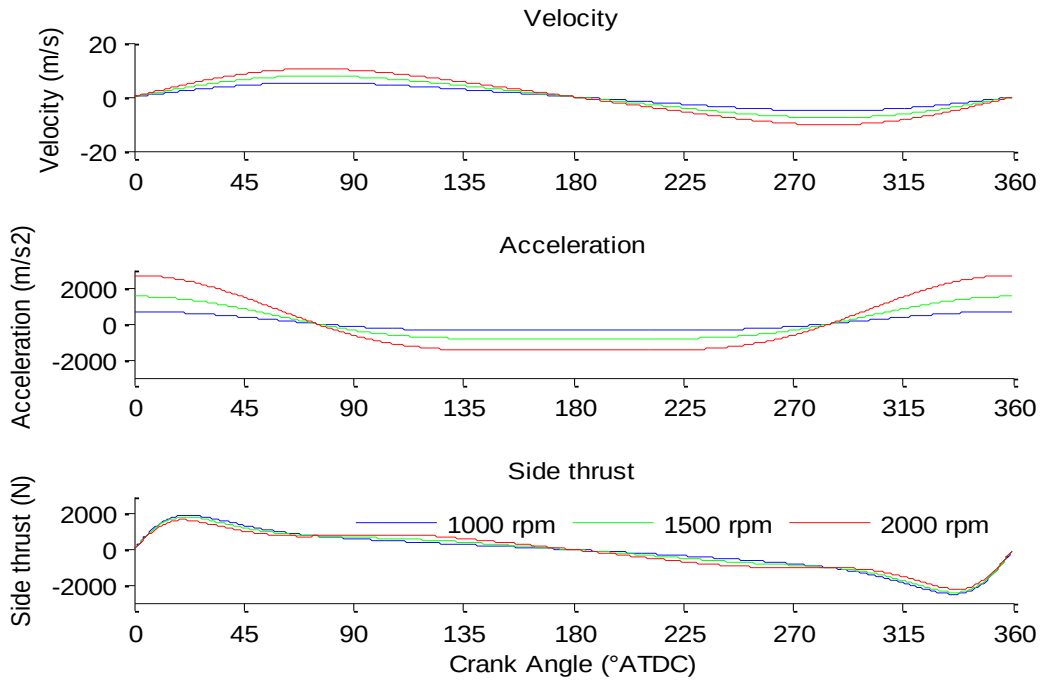

Figure 6.14: Comparison of velocities, accelerations and side thrusts at different speeds for peak pressure of 60 barg at 40˚C.

Higher piston velocity resulted in higher piston acceleration as presented in Figure 6.14, consequently higher inertia forces. As side thrust is more dominated by pressure force thus for similar peak pressure conditions, they were very similar. A 4 times increase in inertia forces from 1000 to 2000 rpm resulted in a maximum 1.5 times increase in the side thrust. Moreover, inertia forces negate the effect of pressure force on side thrust, thus higher side thrusts were obtained for 1000 rpm at the first and last quarter of down and up stroke respectively.

In the early part of down stroke mixed/boundary friction forces were higher for higher speed as acceleration and resulting inertia force was higher. In this region, for higher speed side thrust was lower, though the instantaneous velocity was higher. Consequently, they cancel each other out in altering film thickness, thus the dependency to inertia forces and resulting piston impulses were prominent on mixed/boundary friction in this region.

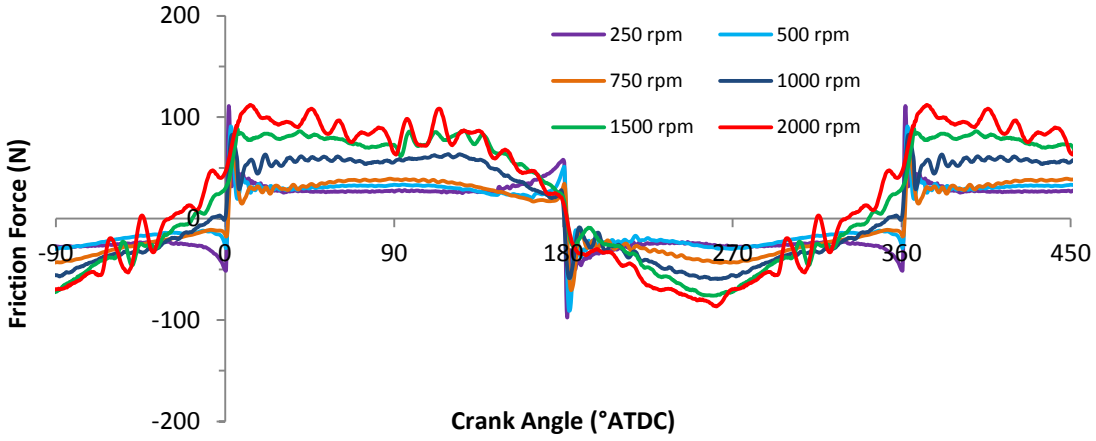

Figure 6.15: Friction force variation with speeds for uncompressed condition at 40˚C.

The effect of speed was further studied for an uncompressed condition to inhibit the effect of pressure as illustrated in Figure 6.15. Higher speed resulted in a lower mixed/boundary friction near the dead centres as it promoted oil film formation by wedge effect. Higher impulsive noises were also observed at higher speeds due to higher inertia forces. The effect of speed on fmep was observed for different temperatures and peak pressure conditions as presented in Figure 6.16.

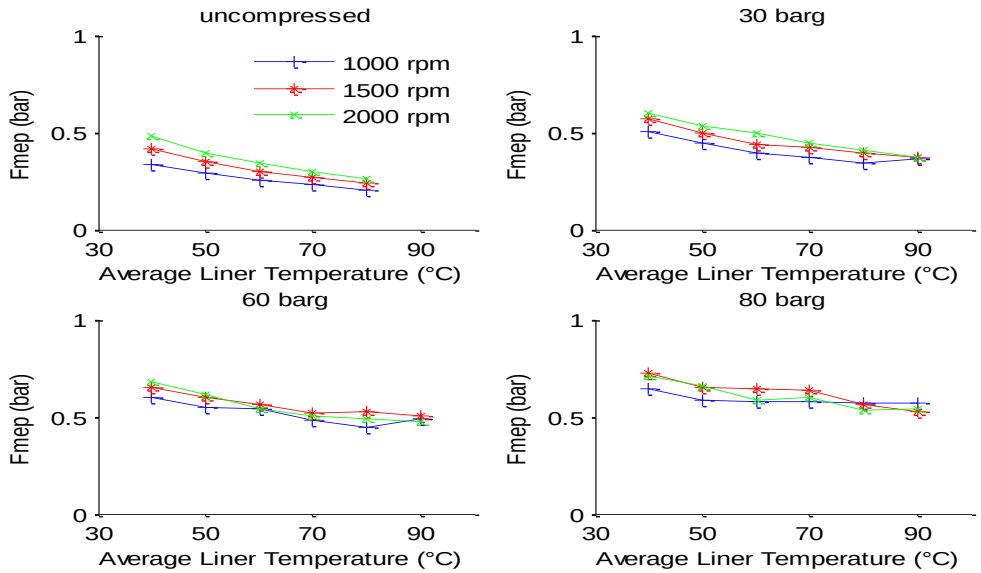

Figure 6.16: Fmep variation with temperature for different speed and peak pressure conditions

The combined effect of speed and temperature can be explained by the analysis of fmep variation for each particular pressure condition in Figure 6.16. Higher hydrodynamic friction is promoted by higher speeds and lower temperature. In contrast higher mixed/boundary friction is promoted by lower speeds and higher temperature. Thus with the increase in temperature, the rate of reduction of fmep was lower for lower speeds as higher mixed/boundary contribution was obtained compared to higher speed. Moreover, during higher peak pressure condition mixed/boundary contribution further increases. Thus convergence of fmep at different speeds were further promoted by higher mixed/boundary contributions. At very high peak pressure conditions of 80 barg, this behaviour was so prominent that the fmep was higher for 1000 rpm compared to 1500 and 2000 rpm at higher temperatures of 80 and 90˚C.

The combined effect of all three operating conditions on fmep could be observed from Figure 6.17 and will be discussed in section 6.1.7.

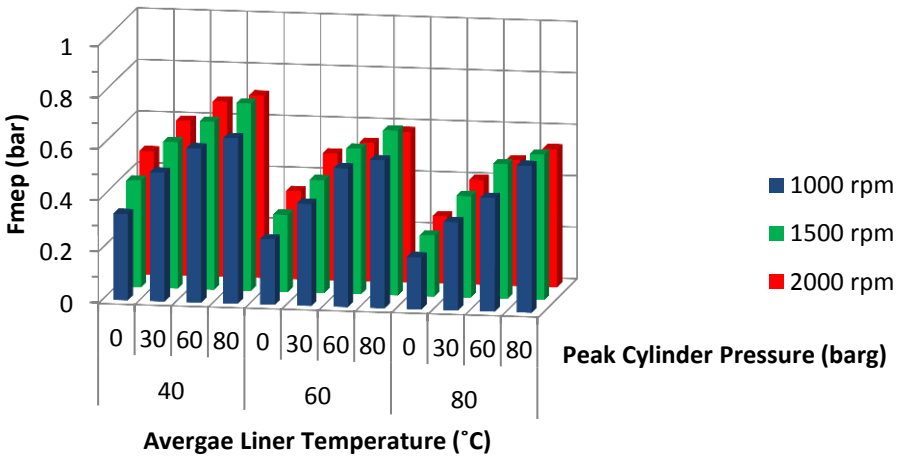

Figure 6.17: Combined effect of pressure, speed and temperature on fmep

6.1.6 Stribeck Diagram

Stribeck diagrams for the piston assembly were obtained for friction force variation in a cycle at 1000 rpm, 60 barg peak pressure and 80°C as illustrated in Figure 6.18. Though different friction components can operate in different lubrication regimes under similar operating conditions, still the diagram obtained for the whole assembly can give an indication of change of lubrication regime for bulk assembly components. The average coefficient of friction obtained at different positions of pistons in this analysis helps in understanding the dominating lubrication regime that exists at that particular position during the piston motion. Therefore the values obtained in this analysis cannot be compared with any theoretical coefficient of friction for a particular piston assembly component, but they can be used to predict the bulk assembly lubrication behaviour.

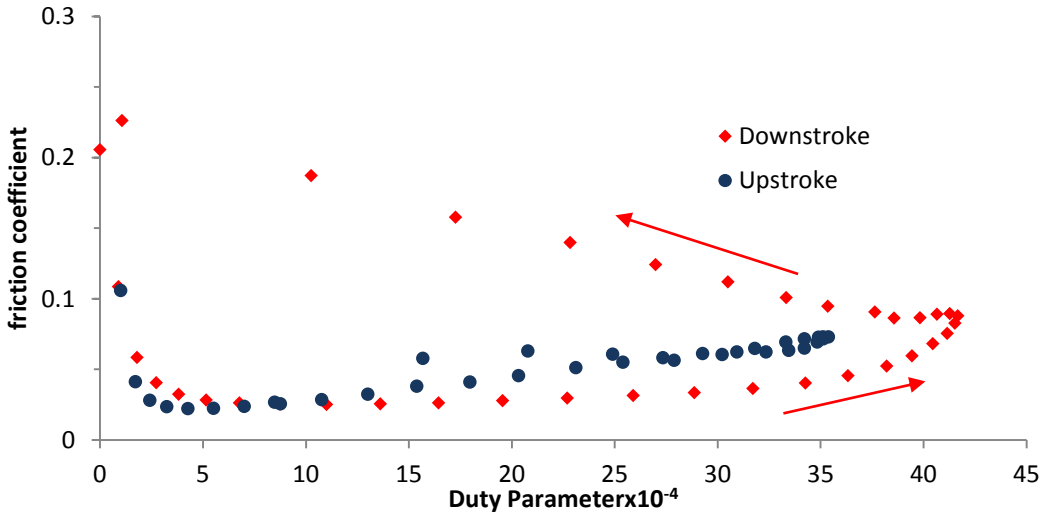

Figure 6.18: Stribeck diagram for 1000 rpm 60 barg peak pressure condition and 80°C

The instantaneous friction coefficients at every 5° of crank angle in the cycle and corresponding duty parameters were used to obtain the Stribeck diagram. An assumption was made that the average friction coefficients could be calculated by

dividing the instantaneous friction forces by total instantaneous normal loads (F_N), which is obtained from the equation 6.4. Instantaneous duty parameters (S) were obtained by using equation 6.5.

$$\mathbf{F_N} = \mathbf{F_{N_1}} + \mathbf{F_{N_2}} + \mathbf{F_{N_3}} + \mathbf{F_{N_s}} \qquad (6.4)$$

$$\mathbf{S} = \frac{\mu_{oil}|V_p|}{F_N/L} \qquad (6.5)$$

Where, F_{N1}, F_{N2}, F_{N3} and F_{Ns} are the normal loads for piston ring 1, 2 and 3 and piston skirt respectively. In equation 6.5, μ_{oil} and V_p represents oil viscosity and instantaneous piston velocity respectively. Moreover, piston characteristic length, L is defined as the total length of piston rings and skirt in contact with cylinder liner which is obtained from equation 6.6, where, L_1, L_2, L_3 and L_s are the characteristic lengths for piston ring 1, 2 and 3 and piston skirt respectively. The normal loads and characteristic lengths can be demonstrated by Figure 6.19

$$\mathbf{L} = \mathbf{L_1} + \boldsymbol{L_2} + \boldsymbol{L_3} + \boldsymbol{L_s} \qquad (6.6)$$

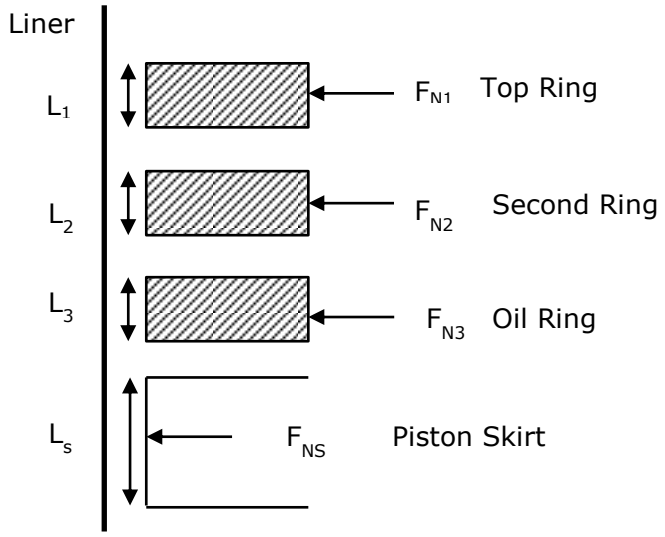

Figure 6.19: Representation of piston ring and skirt normal loads and characteristic lengths

The normal load on the rings and skirt were calculated by using equations 6.7 to 6.10 based on Taraza et al. [122] piston-assembly friction model.

$$\mathbf{F_{N_1} = 2T_1 + \pi D L_1 P_{cyl}} \qquad (6.7)$$

$$\mathbf{F_{N_2} = 2T_2} \qquad (6.8)$$

$$\mathbf{F_{N_3} = 2T_3} \qquad (6.9)$$

$$\boldsymbol{F_{N_s} = F_t} \qquad (6.10)$$

Where, T_1, T_2 and T_3 are the tensions for piston ring 1, 2 and 3 respectively. D, P_{cyl} and F_t are bore diameter, instantaneous cylinder pressure and thrust force respectively. The tensions and dimensions of the rings presented in Table 6.2 were used to calculate F_N and L where L_1, L_2 and L_3 were taken as 1.95 mm, 1.45 mm and 0.84 mm respectively.

Table 6.2: Specifications of the piston rings

Ring	Shape and Dimensions(mm)	Tension (N)
Top Ring	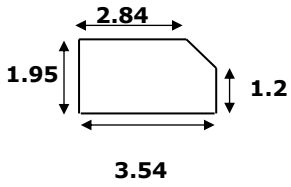	**33.5**
Second Ring	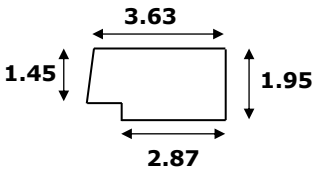	**17.1**
Oil Ring	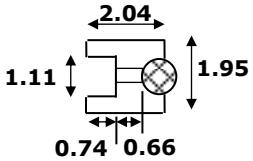	**14.9**

The maximum and minimum friction coefficients obtained during downstroke were 0.23 and 0.024 respectively. During up stroke a lower maximum and minimum of

0.11 and 0.022 was observed. The critical point of minimum friction coefficient was obtained at a crank angle of 20° before TDC where the duty parameter was $5x10^{-4}$.

The conjugal effect of speed and liner temperature on total frictional losses was observed through a modified Stribeck diagram as illustrated in Figure 6.20. In this diagram fmep values for different speeds of 250 to 2000 rpm at temperatures of 40-80°C were presented against mean duty parameter for uncompressed operations.

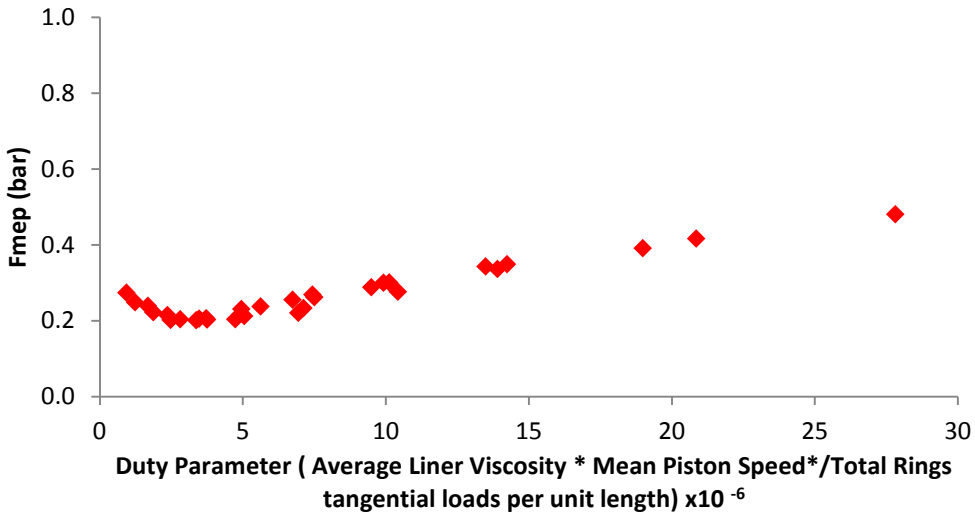

Figure 6.20: Modified Stribeck showing effect of speed and temperature on total friction under uncompressed condition

From the Figure 6.20 it can be seen that, at higher duty parameter (higher speed and lower temperature) friction is predominantly hydrodynamic and thus higher fmep was observed. As the duty parameter decreased (reducing speed or increasing temperature) fmep also reduced until reaching a minimum value of 0.2 bar. After that with decreasing duty parameter fmep started to increase as domination of boundary/mixed friction are obtained at low speed and high temperature conditions.

6.1.7 Discussion

The influences of operating conditions on friction and lubrication behaviour have been reported in this section. It was observed that cylinder pressure, speed and temperature had coupled effects on friction forces. Moreover, the pressure and velocity varied around the cycle, causing variation in friction and lubrication regimes. The local variation in friction and lubrication were further dependent on local variables such as instantaneous velocity, acceleration and normal load.

A higher friction forces near dead centres occurred due to mixed/boundary lubrication. A lower velocity of the assembly and higher normal load (due to pressure) of the piston rings resulted in a peak friction spike near TDC during downstroke motion. The increase in peak pressure further increased the amplitude of the force. Similar behaviours were observed by several researchers [23, 25, 99, 100, 105, 115] where they obtained an increasing friction force with increasing peak pressure at TDC in both firing and motored conditions. Merkle et al. [115] obtained a 85% increase in mixed friction force due to increase in peak pressure from 4 to 28 bar. A similar result was obtained in this study with a 350% increase in mixed/boundary friction near TDC for an increase in 0 to 80 barg peak pressure.

Higher peak pressure also obtained a higher hydrodynamic friction due to higher side thrust and consequently higher piston skirt friction. Kim et al. [105] observed thinner oil in the skirt area under higher load, which led to higher hydrodynamic shear force. A near linear increase in fmep with increasing peak pressure was observed in this study similar to the observation from Madden and Kim [100].

The effect of temperature on friction reported in section 6.1.4 showed a reduction in hydrodynamic friction with increased temperature due to reduced viscosity of oil. A 70% reduction in viscosity from 40 to 80°C resulted in a maximum reduction of 45% in the hydrodynamic friction during expansion stroke for a

pressurised operation of 60 barg at 1000 rpm. Moreover, a 100% increase in mixed/boundary friction near BDC was observed under similar condition. Ha et al. [25] observed similar behaviour with 100% increase in mixed/boundary friction and 50% decrease in hydrodynamic friction under a firing condition at 1200 rpm. Merkle et al. [115] also obtained a similar result under motoring condition and he further observed only 2% increase in friction for oil temperature from 35 to 90°C near TDC during down stroke of a pressurised operation. This conforms to the results obtained in this study.

Dominance of hydrodynamic friction resulted in a reduction of fmep with temperature. A 37% decrease in fmep was observed for the condition mentioned above. Leong et al. [85] and Kikuchi et al. [99] reported similar results of reducing fmep with increasing temperature.

Friction investigation under speed variation showed a lesser sensitivity from temperature and pressure. Under pressurised operation of 60 barg and low temperature of 40°C, a 20% increase in hydrodynamic friction from 1000 to 2000 rpm was observed due to decrease in oil shear velocity/ rate. Merkle et al. [115] reported a relatively lower rise of 2.5% in mixed/boundary friction with a reduced speed from 1500 to 1000 rpm near TDC during power stroke. They further observed higher rise of 17% in mixed/boundary friction at BDC. Similar results of decreasing friction near BDC were also observed in this study. Generally an increase in fmep was observed with increasing speed under lower temperature and pressure because of hydrodynamic lubrication dominance. Similar behaviour was also observed by Leong et al. [85] and Kikuchi et al. [99] under motoring condition.

The variations of fmep with speed and temperature vary with gas loading or peak cylinder pressure. Under different operating conditions, the balance between mixed/boundary and hydrodynamic friction finalise the total fmep. With increase

in peak pressure both the frictions increase. On the other hand mixed/boundary friction increases with increasing temperature but decreasing speed and vice versa for hydrodynamic friction.

A 40% increase in fmep from 1000 to 2000 rpm was observed for a low temperature of 40°C under uncompressed condition. With the increase in temperature under constant load the effect diminishes as the contribution from mixed/boundary lubrication becomes more dominating for lower speeds. After a certain temperature, the fmep started to increase for pressurised operation which was also observed by Kikuchi et al. [99]

At higher temperature of 80°C and higher loading of 80 barg, fmep increased with decreasing speeds as the domination from mixed/boundary increased sufficiently to negate the effect of increasing hydrodynamic friction by increasing speed and load. Madden et al. [100] reported similar findings on firing conditions with a very high temperature and peak pressure .

Comparison of friction forces between up and down strokes in one cycle showed dissimilar mixed/boundary and hydrodynamic frictions under similar pressures, ring normal loads and velocities. During down stroke for a pressurised operation, higher mixed/boundary friction near TDC was obtained. However, higher side thrust during the middle of the stroke resulted in a higher hydrodynamic friction during upstroke. Higher hydrodynamic friction during up stroke in a high peak pressure operation further resulted in a higher fmep contribution. Kim et al. [105] reported the variation in lubrication and corresponding friction behaviour during one cycle. A tilting in piston occurred at TDC during down stroke causing a bottom edge contact of the skirt. Thus higher mixed/boundary friction was obtained by the skirt edge-liner asperity contacts in addition to higher top ring normal load due to high pressure. Kim et al. further mentioned that bottom edge skirt contact squeezed the oil upwards. This oil collected at the top of the skirt, helped in

achieving higher film thickness at the rest of the stroke, causing decreasing oil shear rate and decreasing hydrodynamic friction during down stroke compared to upstroke.

Stribeck curve presented in section 6.1.6 showed different lubrication behaviour during up and down stroke for similar stribeck number. This curve obtained for the piston assembly does not show the transition of lubrication regime for each component. But still would give an indication of the transition behaviour for the bulk assembly. Higher mixed/boundary friction resulted in a higher friction coefficient during down stroke. On the other hand, lower hydrodynamic friction coefficients were obtained in most of the downstroke due to lower hydrodynamic friction forces. A similar curve to Ting [42] was obtained during the last half of downstroke where the lubrication regime was observed to be in the mixed region. Ting reported this curve for a piston ring, which proves the friction is more dominated by the ring packs especially the last half of downstroke. Moreover, the critical Stribeck number obtained in this study was $3x10^{-4}$ which is closer to the findings from Taraza et al. [122] of $1x10^{-4}$.

6.2 Effect of lubricant formulation

6.2.1 Friction dependence on oil viscosity

The effect of lubricant formulation on friction was studied by undertaking tests at different operating conditions with two different grades of oils. The dynamic viscosity of tested SAE 5W-30 and SAE 0W-30 oils were obtained for different temperatures through Vogel's equation as presented in section 5.6. The comparison of friction forces for these oils were undertaken for a speed of 1000 rpm and a peak pressure of 50 barg at both low and high temperatures of 40 and 80°C as presented in Figure 6.21 and 6.22 respectively. The test builds presented in Table 6.3 were used to perform the tests.

Table 6.3 Specifications of the test build for the study in section 6.2

Liner	P2 (Ra 0.35 µm, honing angle 30°)
Piston	Steel
Liner-piston diametric clearance	60 µm
Lubrication Oil	SAE 5W-30 and SAE 0W-30
Compression ratio	10.5

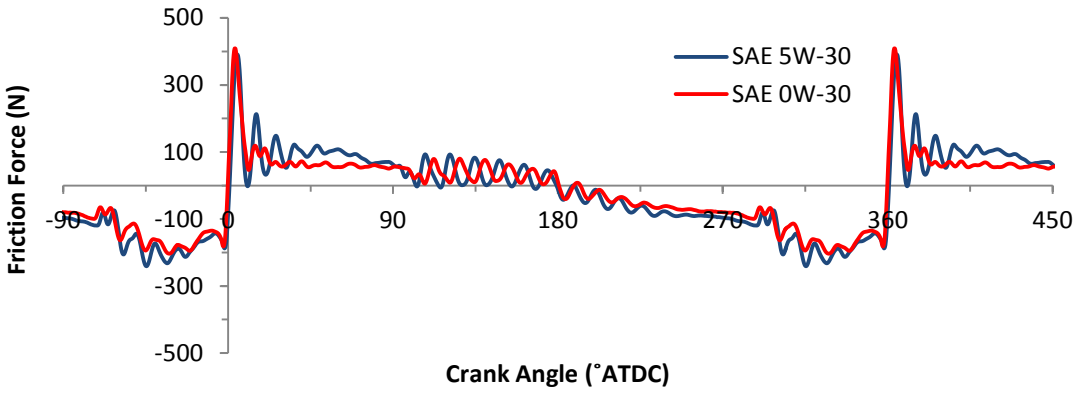

Figure 6.21: Comparison of friction forces for two different oils at 1000 rpm and peak pressure of 50 barg, 40 ˚C.

From the Figure 6.21 it can be seen that friction forces reduced in hydrodynamic lubrication regime for lower viscosity oil under similar operating conditions. A maximum 70% of friction force reduction was achieved in the expansion stroke for SAE 0W-30 oil at a temperature of 40°C. However, the mixed/boundary frictions were similar near TDC and BDC for both the strokes. For higher temperature of 80°C, the friction forces were very similar in both the strokes. A maximum 9% reduction of hydrodynamic friction force was achieved during expansion stroke as presented in Figure 6.22.

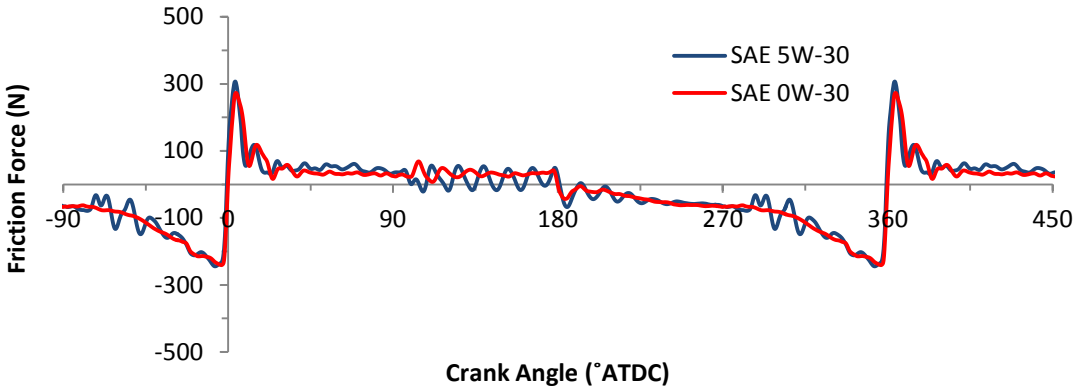

Figure 6.22: Comparison of friction forces for two different oils at 1000 rpm and peak pressure of 50 barg, 80 ˚C.

The analysis of oil viscosities shows a 15% reduction in viscosity for SAE 0W-30 oil at a temperature of 40˚C compared to 9% at 80˚C. As decrease in viscosity results in a decreasing hydrodynamic friction, thus lower hydrodynamic friction was achieved for lower viscosity oil. At higher temperature, the difference of viscosities narrowed down, resulting in a closer hydrodynamic friction.

The effect of reduced viscosity was not influential in mixed/boundary lubrication regime in this investigation. Lower viscosity should result in a lower film thickness, thus promoting higher asperity contacts and consequently higher mixed/boundary friction. But as the lubricating oils were formulated with similar additive packages, formations of boundary films were similar. Moreover, the effect of local variables such as velocity, temperature and pressure seemed to be more influential in determining mixed/boundary friction. Thus with similar operating conditions, similar mixed/boundary frictions were achieved for the two different grades of oil.

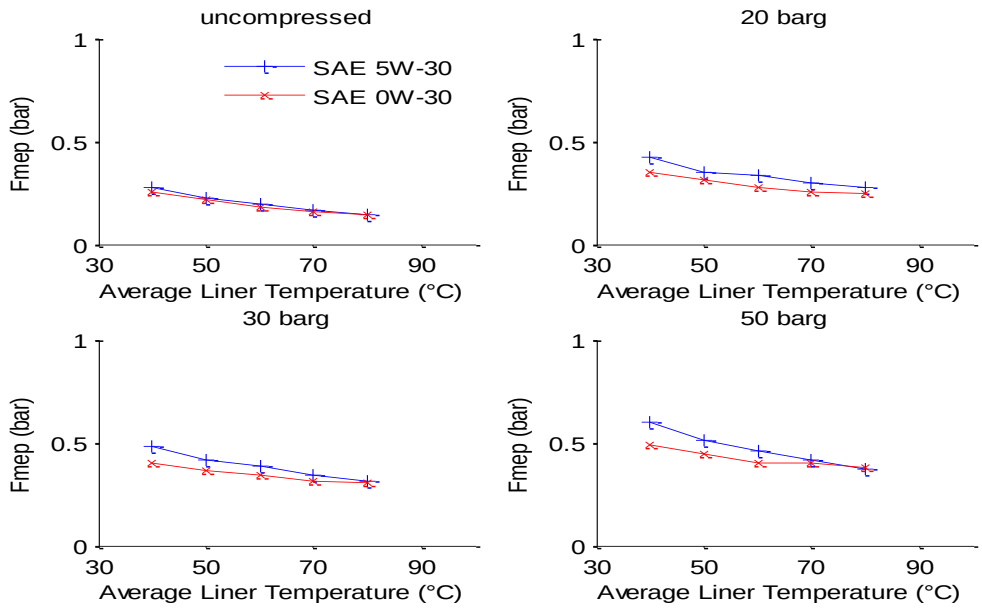

Figure 6.23: Comparison of fmep between two oils for 1000 rpm at different peak pressure conditions.

The variation in fmep with temperature was observed for different speeds and peak pressure conditions. In Figure 6.23 the comparison of fmep between the oils at 1000 rpm and different peak pressures of 0, 20, 30 and 50 barg are presented. A maximum reduction of 8% in fmep was observed at a lower temperature of 40°C for an uncompressed test. At higher temperature, difference in hydrodynamic friction for the oils reduced, resulted in a closer fmep.

Further from Figure 6.23 it can be observed that higher reductions in fmep were achieved at higher peak pressure condition. As with increase in peak pressure the hydrodynamic friction force also increases, thus higher reduction in fmep was achieved with low viscosity SAE 0W-30 oil at higher peak pressures. A maximum reduction of 18% in fmep was achieved for a peak pressure of 50 barg at 1000 rpm.

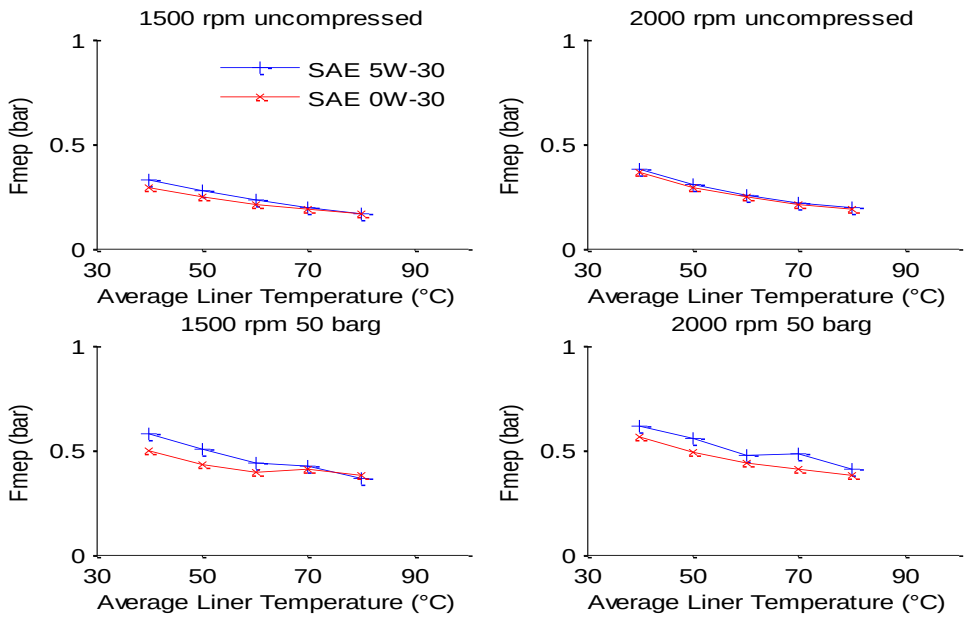

Figure 6.24: Comparison of fmep between two oils for 1500 and 2000 rpm at different peak pressure conditions.

The effect of oil viscosity was further analysed for higher speed conditions as presented in Figure 6.24. Higher speed results in higher hydrodynamic friction as discussed in section 6.1, thus more benefits should be achieved by reduced viscosity oil. But at higher peak pressure, the effect of speed is less dominant thus no further reduction was achieved at the higher speeds of 1500 and 2000 rpm. However, for an uncompressed test a higher reduction of 13% was achieved for 1500 rpm compared to 8% for 1000 rpm.

6.2.2 Discussion

The friction force characteristics for two different grades of oils were compared in this section. The SAE 0W-30 oil with lower viscosity obtained lower hydrodynamic friction force due to lower hydrodynamic shear force. However, the reduced viscosity of oil SAE 0W-30 did not have any impact on mixed/boundary friction. Koch et al. [109] observed reduced friction in both the mixed/boundary and hydrodynamic regimes with a lower viscosity oil .

Higher difference in viscosity at lower temperature resulted in a higher difference in hydrodynamic friction. With increasing temperature the viscosities of oils were closer, resulting in closer friction forces. At higher temperature mixed/boundary friction increases and the presence of friction modifier helps in reducing the friction in this regime as observed by Mufti et al. [92]. Both oils tested in this study were blended with similar additive packages or friction modifiers. Thus increased mixed/boundary friction with increasing temperature was not evident.

Reduction in hydrodynamic friction with oil SAE 0W-30 resulted in a reduced fmep. Similar results were obtained by Leong et al. [85] with reduced fmep from lower viscosity oil. Further higher reduction in fmep was achieved at higher peak pressure due to higher hydrodynamic friction force reduction with reduced viscosity. Moreover, no further reduction was obtained at higher speed under higher load due to a reduced impact of speed on friction under higher loads. Similar fmep reductions at 1500 and 2000 rpm under half load firing condition were reported by Mufti et al. [92].

6.3 Effect of macro design features

The influences of different macro design features on friction forces were investigated using the floating liner rig. Two different features, piston-liner clearance and piston design were analysed in this study. The effect of clearance was studied by undertaking tests with different builds of piston-liner diametric clearances ranging from 20 to 80 μm at an interval of 20 μm. Steel pistons with liner P1 were used, as referred to build specifications in Table 6.4. The effect of piston design and material was studied by undertaking tests with steel and aluminium pistons of 60 μm piston-liner diametric clearance as presented in Table 6.5.

Table 6.4 Specifications of the test build for the study in section 6.3.1

Liner	P1 (Ra 0.427 μm, honing angle 30°)
Piston	Steel
Liner-piston diametric clearance	20,40,60,80 μm
Lubrication Oil	SAE 5W-30
Compression ratio	10.5

Table 6.5 Specifications of the test build for the study in section 6.3.2

Liner	P2 (Ra 0.35 μm, honing angle 30°)
Piston	Steel, Aluminium
Liner-piston diametric clearance	60 μm
Lubrication Oil	SAE 5W-30
Compression ratio	10.5

6.3.1 Effect of piston-liner clearances

Tests to study piston-liner clearances were undertaken at speeds of 1000, 1500 and 2000 rpm, a temperature range of 40-80°C and peak pressure of up to 30 barg. The clearances mentioned above were referred to as cold clearance at room temperature of 15°. Friction forces for different clearances of 20, 40, 60 and 80 μm were compared for an uncompressed condition at 1000 rpm as presented in Figure 6.25.

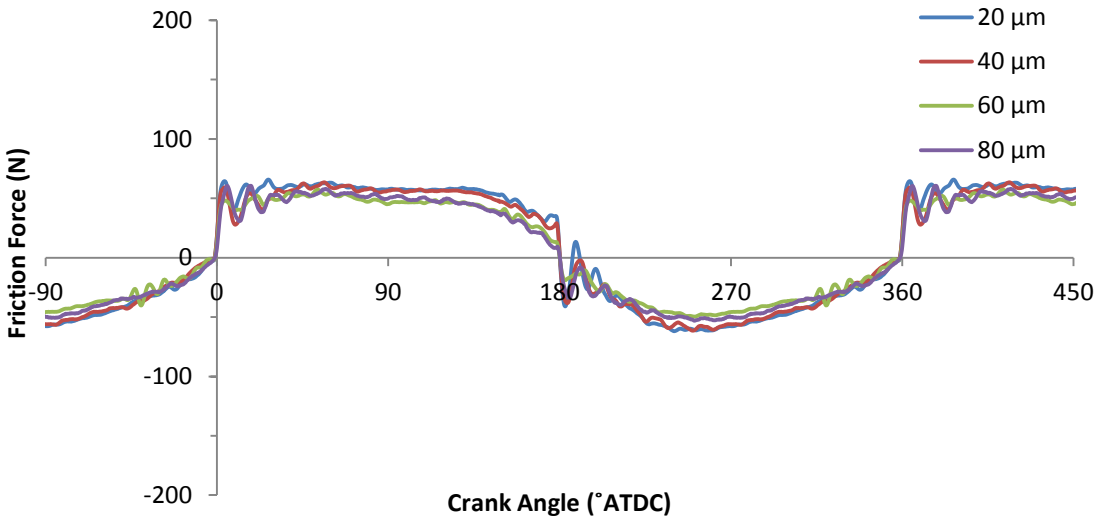

Figure 6.25: Friction force variation with clearances for uncompressed 1000 rpm and 40˚C

From the Figure 6.25 it can be seen that, friction forces decreased with increasing clearances in both mixed/boundary and hydrodynamic regime. With increasing clearances the surfaces were further separated from each other, resulted in a lower mixed/boundary friction. A maximum 20% reduction in mixed/boundary friction was achieved from 20 to 60 µm clearance. In the hydrodynamic regime, higher clearances promoted thicker oil film formation. Thus lower hydrodynamic shear forces were achieved with higher clearances. A maximum force reduction of 19% was achieved from 20 to 60 µm clearance in hydrodynamic regime.

Friction forces were further compared for a pressurised condition of 30 barg for 1000 rpm as presented in Figure 6.26. From the Figure 6.26 it can be observed that effect of clearances were not influential during downstroke for a pressurised condition. However, a maximum 11% reduction in friction force was achieved from 20 to 80 µm in hydrodynamic regime during upstroke.

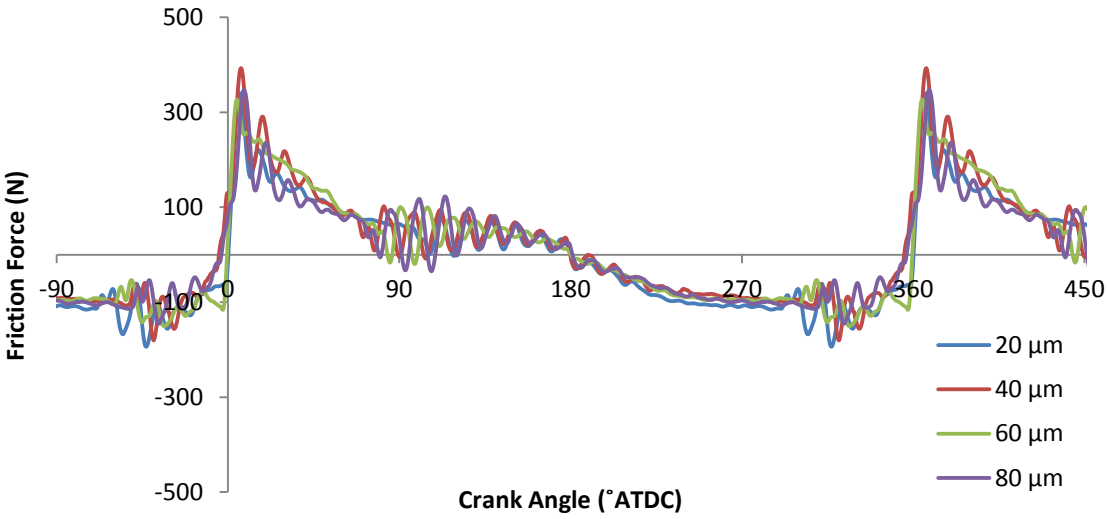

Figure 6.26: Friction force variation with clearances for peak pressure of 30 barg at 1000 rpm and 40˚C

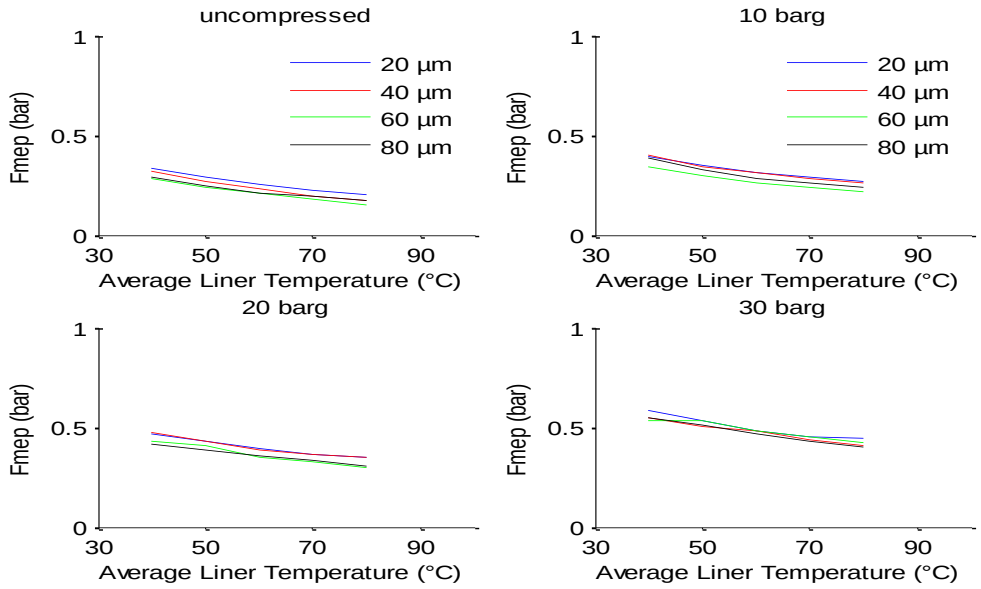

Figure 6.27: Variation in fmep with temperatures for different piston-liner clearances at 1000 rpm under different peak pressure conditions.

The effect of clearances on fmep was also observed for different speeds, peak pressures and temperatures. In Figure 6.27 variations in fmep with temperature are presented for different peak pressure conditions of 0, 10, 20 and 30 barg for a speed of 1000 rpm. A general trend in decreasing fmep with increasing clearances was observed. Though the reduction in friction with increasing clearances were

not visible in the friction force traces, still near constant reductions of around 0.4 bar in fmep from 20 to 80 µm were observed for all temperatures and peak pressures. As fmep reduced with increasing temperatures, the reduction was higher in percentages at higher temperature. Reductions of 12 and 7% were achieved for uncompressed and 30 barg conditions respectively at 40°C. At 80°C, 19 and 12% reductions were achieved respectively.

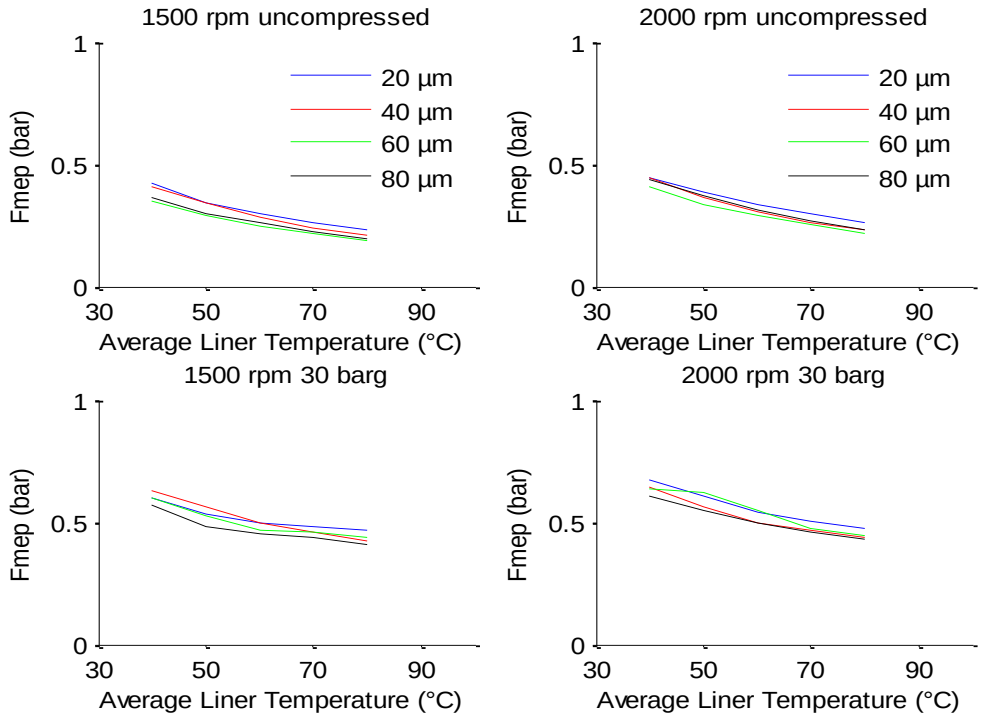

Figure 6.28: Variation in fmep with temperatures for different piston-liner clearances at 1500 and 2000 rpm under different peak pressure conditions.

Further comparisons of fmep were undertaken for higher speeds of 1500 and 2000 rpm as presented in Figure 6.28. Similar behaviour was observed at these speeds across the temperature and pressure ranges. Reductions of 0.4 bar fmep at all the temperatures and pressures were achieved from 20 to 80 µm clearances.

6.3.2 Effect of piston designs and materials

Comparison of friction forces between aluminium and steel pistons were undertaken for speeds of 1000, 1500 and 2000 rpm, temperature range from 40 to a maximum of 90˚C and peak pressure of up to 80 barg. Though the piston-liner clearances were same for both pistons, still they are not directly comparable because of different skirt lengths and ring-lands heights as mentioned in section 3.3. Thus all the factors jointly influenced the friction force behaviour and were discussed together.

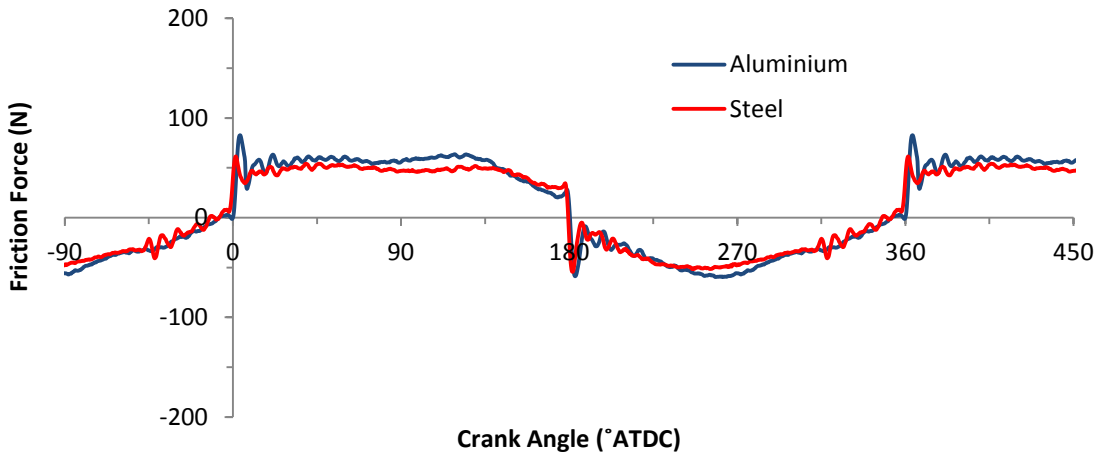

Figure 6.29: Comparison of friction forces for two different kinds of pistons at 1000 rpm uncompressed, 40 ˚C.

A comparison of fiction forces for an uncompressed condition at 1000 rpm is presented in Figure 6.29. A maximum reduction of 30% in mixed/boundary friction near TDC and similar reduction in hydrodynamic friction were obtained with the steel piston during downstroke. During upstroke, a maximum reduction of 20% was achieved in hydrodynamic friction. Mixed/boundary friction near BDC were similar in both the strokes.

Under similar operating speeds, almost similar velocities and accelerations were obtained for both the pistons even though connecting rod length was 6.5 mm

higher for steel piston. But inertia forces were higher (maximum 7%) for steel piston because of its 0.1kg higher reciprocating mass. Thus higher thrust forces were obtained for steel piston, yet even the friction forces were lower in the hydrodynamic regime. As piston skirt is 30% smaller in length for steel piston, less surface interactions between skirt and liner wall was achieved. Consequently lower skirt friction in hydrodynamic regime was obtained.

Moreover, steel has lower thermal expansion rate than aluminium. Calculations of relative thermal expansions between the liner and pistons show that the clearance between the aluminium piston and liner disappears at a temperature of 50°C. On the other hand, in the case of steel piston the clearance becomes zero at a higher temperature of 70°C. In the calculation, it was assumed that pistons temperatures were the same as the liner temperature, as no compression heating was achieved during uncompressed condition. From the results in section 6.3.1, it was observed that higher clearance promoted lower friction in both mixed/boundary and hydrodynamic regime. Thus lower clearance for steel piston at a similar temperature promoted lower frictional losses.

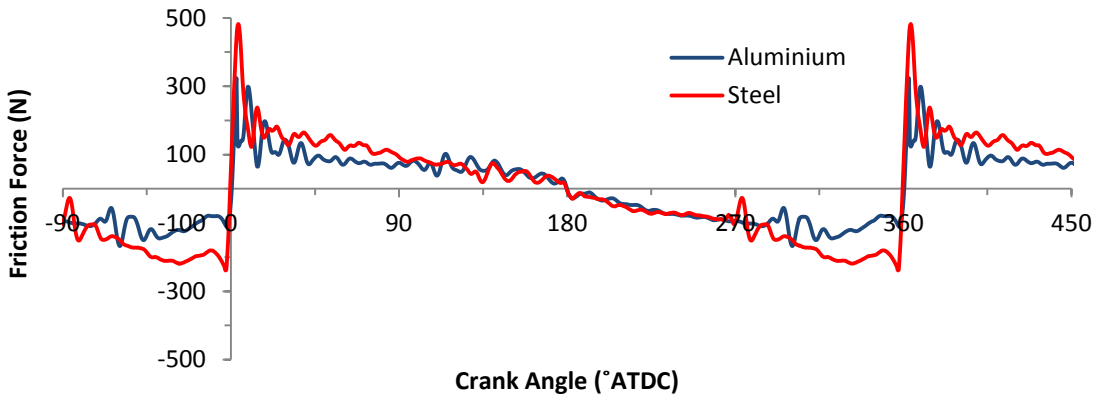

Figure 6.30: Comparison of friction forces for two different kinds of pistons at 1000 rpm and peak pressure of 60 barg, 40 °C.

The comparison of friction forces for pistons of two different materials were also undertaken for a pressurised condition as illustrated in Figure 6.30. In contrast to

the uncompressed condition, higher cylinder pressure resulted in both higher mixed/boundary and hydrodynamic friction in first and last half of down and upstroke respectively. A maximum 50% higher mixed/boundary friction near TDC was obtained for the steel piston in both up and down strokes at 1000 rpm and 40˚C. Similar 50% increase in hydrodynamic friction was obtained at the mid stroke region during downstroke. The side thrusts presented in Figure 6.31 were compared to analyse the friction variation during pressurised tests.

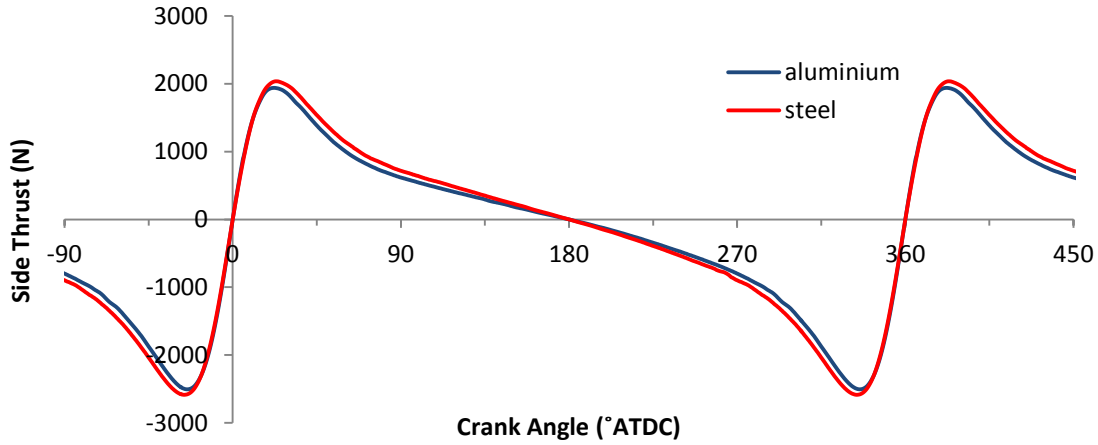

Figure 6.31: Comparison of side thrust for two different kinds of pistons at 1000 rpm and peak pressure of 60 barg, 40˚C.

From Figure 6.31, it can be seen that, maximum 5% higher side thrust was obtained with steel piston during pressurised condition. Thus higher hydrodynamic friction was achieved with steel piston. The fmep values were compared for pistons with two different materials at different speeds and peak pressure conditions. In Figure 6.32 variations in fmep with temperature are presented for different peak pressure conditions of 0, 30, 60 and 80 barg for a speed of 1000 rpm. A 13% reduction in fmep from aluminium to steel piston was observed at 1000 rpm and 40˚C under uncompressed condition. The variation was similar across the temperature range during this condition. The reduction in friction in both hydrodynamic and mixed/boundary regimes resulted in this fmep reduction.

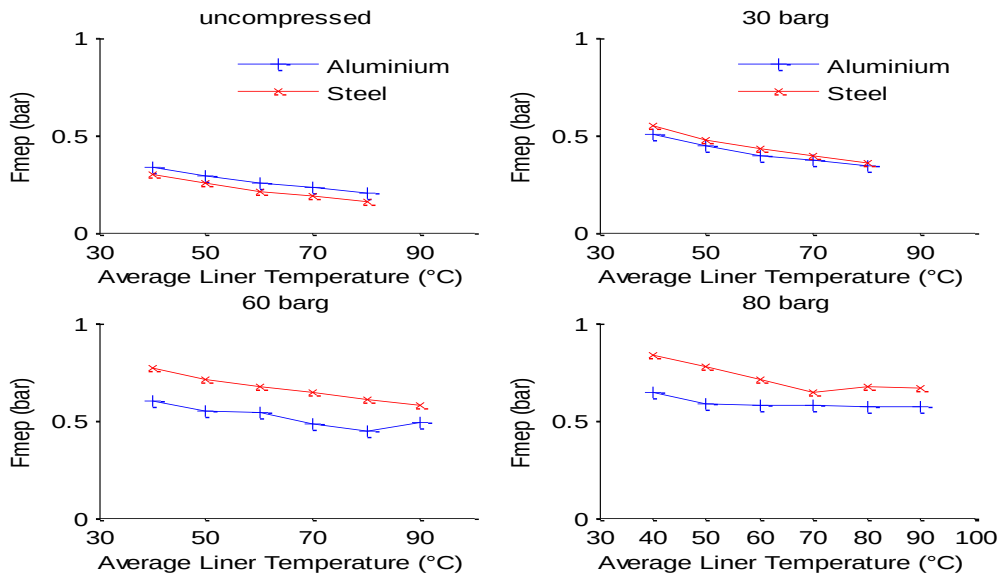

Figure 6.32: Variation in fmep with temperatures for two different kinds of pistons clearances at 1000 rpm under different peak pressure conditions.

However, under the pressurised condition fmep values were higher for the steel piston due to higher friction in all the lubrication regimes as shown in Figure 6.32. Moreover, sensitivity to pressure was higher for steel piston compared to aluminium piston due to increasing side thrust with increasing peak pressure. A maximum 30% rise in fmep was observed at a pressure of 80 barg and 1000 rpm.

The effect of piston material on fmep was further observed for higher speeds of 1500 and 2000 rpm as presented in Figure 6.33. Maximum increases of 17 and 18% were obtained at speeds of 1500 and 2000 rpm respectively under peak pressure of 60 barg. Increase in friction was observed in the first and last half of down and up strokes respectively where side thrusts were higher for lower speed. Thus higher increase in fmep was observed for 1000 rpm under pressurised condition. As the inertia force dictates the side thrust during uncompressed condition, higher reduction in fmep was observed for higher speeds in this condition. A maximum reduction of 20% was achieved with steel pistons with uncompressed condition at both the higher speeds of 1500 and 2000 rpm.

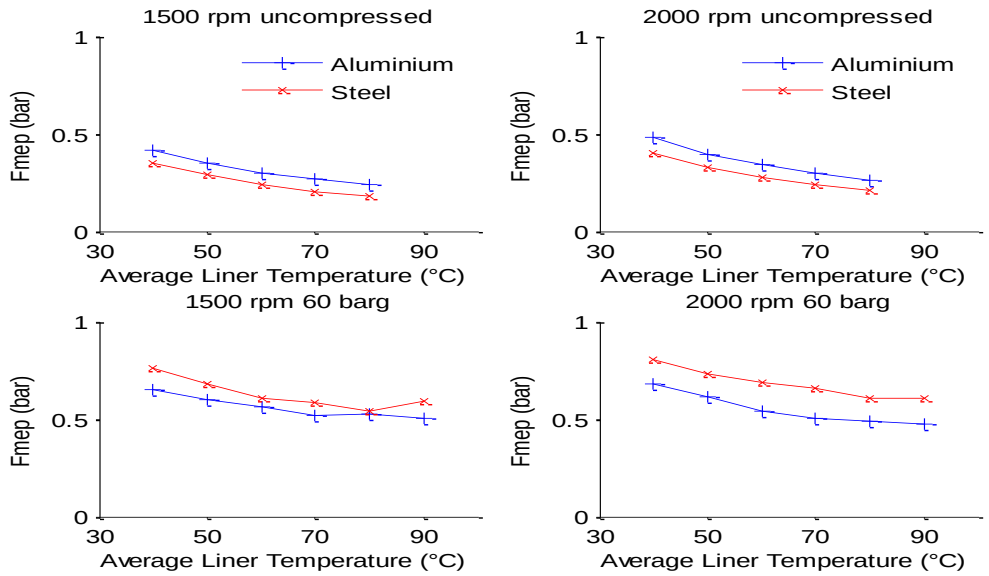

Figure 6.33: Variation in fmep with temperatures for two different kinds of pistons clearances at 1500 and 2000 rpm under different peak pressure conditions.

6.3.3 Discussion

The effects of piston-liner clearances and piston design and material on friction were investigated in this section. Higher clearances achieved both lower mixed/boundary and hydrodynamic friction due to less asperity contact and lower oil shear rate respectively. Similar results were reported by Ha et al. [25] with pistons of cold clearance difference of 20 μm.

Lower friction with higher clearances resulted in a lower fmep. However, some uncertainty was present in the trend where 60 μm clearances achieved lower fmep than 80 μm at lower peak pressure condition. At higher peak pressure, the trend was generally uniform with highest clearance of 80 μm obtaining the lowest friction. Higher clearances generally achieve less asperity contact but can experience unfavourable secondary motion in the form of slap, causing higher intermittent mixed/boundary friction as observed by Madden et al. [100]. They

further obtained a lowest fmep with an optimum clearance of 30 μm compared to 10 and 50 μm.

The effect of clearances on friction was also very prominent for analysis with steel and aluminium pistons. Lower expansion rate of steel achieved lower friction due to higher clearances at similar temperatures under uncompressed condition. However, the effect diminished under pressurised conditions due to the effect of side thrust on friction. Higher side thrusts were obtained for steel pistons due to higher inertia forces, resulting in a higher friction. A contrasting result was reported by Schneider et al. [123] where they obtained lower friction forces with a steel piston compared to aluminium under firing condition. But in their analysis the aluminium and steel pistons investigated had similar weights, unlike this study, and also the steel piston had lower inertia forces because of higher connecting rod length.

Another contrasting result was obtained by Kim et al. [113] which showed friction reduction with a steel piston. Better hydrodynamic lubricating condition with the steel piston was identified as the major reason behind their findings. Design of the piston played an important role in achieving this reduced friction.

The design of the piston skirt in this study was different to that of the study by Kim et al. [113]. Reduced skirt area of the steel piston could be ineffective in achieving reduced skirt friction as oil could be squeezed out of the bearing area, resulting in oil starvation and higher hydrodynamic friction [84]. Moreover, higher clearance of steel piston under similar temperature promoted higher tilting and slap of the piston, resulting in a higher mixed/boundary friction near TDC.

Chapter 7 Discussion and conclusion

7.1 Discussion

The development of a newly-constructed floating liner rig (FLR) and its application to the measurement and characterisation of friction between the piston and liner has been reported in this thesis. Developments of the setup included revisions to the air sealing method to improve gas pressure sealing without introducing uncertainty in the friction force measurement; and change to the drive assembly to facilitate higher gas loading operations similar to a fired engine operation. Parametric studies were undertaken using the updated rig to identify the potential areas of friction reduction.

The measurement of crank angle resolved friction force is necessary to understand the complex friction and lubrication behaviour at the piston-liner interface. The floating liner method is in principle well suited to the challenges involved. Compared to cycle-averaged measurements of friction torque or measurements derived from the analysis of forces on, and the acceleration of, the piston the floating liner approach has benefits. The earlier one cannot analyse friction force variation in a cycle whereas the later one provides higher uncertainty in friction force measurement.

Floating liner rigs have been used previously in both fired and motored test studies (such as [25, 84, 112] described in chapter 2). A motored rig enables investigation of a wider range of liner temperature compared to very high temperature condition in fired rig but achieving cylinder pressures similar to those in a fired rig are more difficult. In the rig described and used in the current work, the cylinder sealing and air injection approach offers a good route to achieving controlled cylinder pressures. Further, quick changeovers between piston-liner specimens are desirable to undertake the parametric study with lower cost and time savings in friction investigations. Thus the rig operation discussed in chapter

4 has addressed important requirements for friction studies. Though the changeover to different piston types needs the whole rig to be disassembled, still the total changeover time is a maximum of a working day or two. This rig can even adapt different sizes of bores and strokes within a limited range, with only some minor changes in assembly on the same assembly bed. Tests can be undertaken at different compression ratios to analyse friction for both CI and SI engine conditions.

Some of the major challenges faced in measuring friction with FLRs are to isolate gas pressure force from the liner, and to suppress the lateral movement and impulsive noise due to side thrust and piston secondary motion respectively. Designing a modified cylinder head to balance pressure force on the liner was implemented in several works (such as [22, 101, 102]) but still obtained some uncertainty in measurement. Lateral movement of liner was successfully suppressed by a lateral stopper, placed in the middle or top of the liner outer periphery as observed in the friction force results in chapter 5 and 6. Higher axial stiffness in the floating liner bottom end support as well as load sensors ensures no interference of inertia force on frictional force measurement as discussed in chapter 4. Moreover, higher radial stiffness of lateral support at the upper end minimises lateral movement, consequently less interference on measurement. Damping at the bottom end support rather than lateral support absorbs more impulsive noise as observed in the friction traces in chapter 5 and 6.

Using a clearance seal instead of cylinder head in FLR can avoid the application of pressure force on the top of the liner as reported in this study. Modification of the sealing assembly can further improve the sealing method as well as can gain confidence in friction force measurement through some static calibrations as reported in chapter 4. Undertaking calibrations for each different build ensures build to build repeatability, thus gaining further confidence in the friction results.

Though FLRs can simulate fired engine conditions, they are vulnerable to signal noise resulting from the impulsive impact of piston slap, which might limit the upper speed of operation. Inertia force of the liner-bottom diaphragm assembly excited by the axial vibration was identified to be higher at higher speeds [98]. Thus friction force measurement through load cells can have an additional inertia force effect. This effect was identified near the TDC and consequently force in the opposite direction at the end of compression stroke was observed for higher speeds in this study as shown in section 6.1.5. For an uncompressed operation where the friction forces are much lower near TDC compared to pressurised operation, this can have a bigger impact. During pressurised operation, the inertia force effect is much smaller compared to peak friction force, so consequently less impact. However, parametric studies would not be affected under similar operating conditions as similar behaviours are observed.

The resolution of friction force as a function of crank angle is an important aid to understand how the friction regimes changes over the engine cycle. Friction spikes near TDC were observed where ring normal load is highest due to high cylinder pressure as can be seen from section 6.1. The higher mixed/boundary friction force also causes temperature to rise near TDC compared to the middle of the stroke as discussed in section 6.1.7. Moreover, the higher friction spikes can be observed at higher peak pressure operations, resulting in a higher difference in temperature between top and middle part of the liner. In this study a lower difference of 2-3°C was observed for a peak pressure of 30 barg, compared to 8-10 $^{\circ}$C for 80 barg. Though the compression heating can increase the gas temperature to as high as 450 $^{\circ}$C, still much lower temperature of top of the liner shows less heat transfer from gas to the oil, and only frictional and external oil heating dictate the oil film temperature.

FLR with exchangeable piston-liner assembly can be used to analyse different micro and macro design parameters of the components affecting the friction.

Different macro features like piston-liner clearances, piston material and design and lubricant formulation have been analysed in this study along with analysing effect of operating conditions.

The different parameters can be studied separately but changes in friction in respond to changes in one particular parameter may be modified or even revised by changes in a second parameter. This coupling of effects complicates the interpretation of results and limits the possibility of summarising outcomes in simple, unqualified statements. For example, higher speed results in a higher frictional loss at lower temperature, but at very high temperature and peak pressure of 90°C and 80 barg respectively lower speed results in higher friction as observed in section 6.1.5. Piston motion can be a determinant factor for mixed/boundary friction near the dead centres along with local operating variables of gas pressure, oil temperature and instantaneous velocity as observed in section 6.1.3.

Gas loading characterised by higher peak pressure is the most influential operating parameter followed by temperature as observed for all different piston designs and lubrication formulation in chapter 6. Increasing peak pressure leads to near linear increase in fmep. However, a rather constant fmep was observed in a fired operation [124]. As with increasing load, temperature of the oil also rises for a fired engine, consequently the effect of increasing friction with increasing peak pressure is diminished by friction reduction though reduction in viscosity with increasing temperature. This further illustrates benefit of using motored FLR which can study the effect of a particular parameter under similar other operating parameters.

The friction force results from the FLR rig shows some sign of piston ring fluttering movement along with the noise and vibration due to impulses as observed in section 6.2 and 6.3. Fluttering in the rings can occur in both upstroke and down

stroke motion of the piston and is determined by the balancing act between gas pressure, inertia force and areas of the ring that pressure acts on [125]. Different fluttering behaviours in up and down stroke can lead to different oil transport, thus different film formation and friction. The profile of the piston rings also plays an important role in lubrication behaviour. Wedge profile in the second ring can promote film formation during upstroke due to liner surface converging towards the edge, and the opposite for downstroke. The different tilting action of piston near TDC during up and down stroke can also lead to different lubrication and friction behaviour. Thus not only the operating condition but also the conjugal effect of piston and rings design, and piston reciprocating and secondary motion effect the friction behaviour.

Friction reduction in piston assembly can be achieved by using technologies to reduce hydrodynamic friction, the dominant contributor to total frictional loss. Using lower viscosity oil can reduce hydrodynamic contribution but can also increase mixed/boundary friction due to lower oil film thicknesses. However, using required additive packages or frictional modifier in the oil can help formation of boundary film and the negative effect of viscosity on mixed/boundary lubrication and friction behaviour can be reduced as observed in section 6.2. Thus lower viscosity oil can be used to reduce piston assembly friction without increase in mixed/boundary friction and wear near TDC.

Friction reduction can also be achieved by increasing piston-liner diametric clearances. The reductions in fmep with a higher clearance piston skirt reported in section 6.3 are higher than the variability in friction results at those operating conditions, which imparts confidence in the study of this macro design feature. However, too high a clearance can lead to blow by losses [126] and higher noise and vibration due to the tilting action of the piston [100]. Higher noise and vibration were also observed for a clearance of 80 μm in this study compared to 20 μm clearance.

Steel pistons have a potential over aluminium piston in achieving lower friction due to lower thermal expansion and consequently higher piston-liner clearance as observed in the uncompressed tests in section 6.3.2. However, the weight of the piston is an important factor as higher mass and the resulting inertia of steel can result in higher mixed/boundary friction due to slap and piston tilt, and higher hydrodynamic friction in the skirt due to higher side thrust. Moreover, skirt design is also very important as too small a size of skirt can lead to oil starvation and consequently higher friction [84].

Investigating different friction parameters together using a FLR can help in identifying optimised micro-macro design features for reduced piston-liner assembly friction. The results can be incorporated in the existing piston assembly friction models [122, 127, 128] where currently only the ring profile, viscosity, pressure and speed are taken into account.

7.2 Further work

Piston expansion has been identified as a major influence in running clearance and resulting friction as discussed in section 6.3. In the existing floating liner rig the piston temperature is affected by compression, friction and oil heating cannot be measured. Thus introducing a dynamic piston temperature measurement system can help in analysing the relative expansion rate between liner and piston as well as undertaking comparison with fired engine. A previous telemetry system was installed to measure temperature of different positions in the piston but failed due to poor structural integrity and durability. A more robust system can be used to serve the purpose.

Friction force measurement was observed to be affected by inertia force of the liner bottom end mounting due to axial vibration. An accelerometer installed in this bottom support structure can measure this inertia force and subsequently can be imparted in the force measurement to further correct the friction force.

The air injection system used in the design uses fuel injector and needs a long injection duration (crank angle based) to achieve higher peak pressure. Longer injection duration led to occasional injector seizing and thus had to be stopped in the middle of the tests. The reduction in peak pressure in this non-injection period can cause different oil film formation and takes some extra time to obtain previous film formation after the retrieval of the required operating pressure. Installation of another injector could facilitate continuous operation under a constant peak pressure condition by switching between two injectors.

A second floating liner rig with larger bore and stroke has already been commissioned. This will allow for parametric studies to be undertaken using the FLR with different liner roughness, laser textures, honing patterns, nano surface coatings, ring profiles and piston designs. It will also allow for the effects of bore and stroke changes to be considered and should allow an extended operating range of cylinder pressure to be covered to simulate heavy duty engine conditions. The extended parametric studies can be utilised to obtain an improved piston assembly friction model through DoE.

7.3 Conclusions

The main conclusions drawn from the studies described in the thesis are as follows:

Rig Design and Operation

- A motored single cylinder, floating liner setup can be used for dynamic measurement of piston-cylinder liner assembly friction over a range of operating conditions, approximating those of a firing engine. The engine conditions of gas pressure, temperature and speed can be simulated by controlled compressed air injection with required gas sealing assembly, controlled oil heating with regulated supply and fixed rotational speed

operation through a driveline with an inverter controlled motor respectively.

- Using a gas sealing assembly with a clearance gap between the sealing plug and liner, and further separating sealing assembly from floating liner support can isolate the direct application of gas pressure on the liner; consequently irregular interference in friction force measurement is avoided.
- A multi-layer bottom diaphragm support for floating liner with an appropriate damper provides high axial stiffness as well as vibration damping. The axial stiffness of this support negates the effect of liner inertia force in friction measurement.
- Supporting the top of the liner with an annular diaphragm minimises lateral movement, thus the introduction of extraneous force in friction measurement can be avoided.
- A top piston ring is used to seal the air gap between sealing assembly and liner and consequently can achieve higher peak cylinder pressure of 80 barg. However, a portion of sealing ring force due to cylinder pressure is exerted on the liner; undertaking a static sealing ring force calibration can measure this force contribution and is incorporated in the measurement to obtain the true friction measurement.
- The provision of changing liner and piston specimens allows parametric studies to be undertaken with cost and time savings. Further applying a specified oil flushing procedure facilitates the study of lubricating oil in piston assembly friction without imparting oil carry over effect.
- The repeatability of test results is characterised by a maximum standard deviation of ±4% from average fmep for low peak pressure condition. However, a higher standard deviation of maximum ±9% was obtained at high peak pressure and temperature of 80 barg and 80°C respectively. This higher uncertainty in measurement at high pressure condition is

avoided by keeping constant gas pressure loading and allowing sufficient time for development of oil film before acquiring any data.

Friction data sets

- Friction results from two stroke uncompressed and pressurised operations can be combined together to interpret to a 4 stroke operation; down and up stroke of uncompressed operation represents intake and exhaust strokes respectively, whereas expansion and compression stroke respectively are obtained from pressurised operation.
- Parametric studies show peak cylinder pressure is the most influencing factor in determining piston assembly friction. Increase in peak pressure from 30 to 80 barg can obtain maximum 300% increase in boundary/mixed friction spikes near TDC for a compression ratio of 10.5:1. Maximum 60% increase in hydrodynamic friction around mid-stroke region can further be obtained for similar peak pressure rise.
- Around 7 times higher friction force near TDC compared to friction force in mid-stroke for a peak pressure operation of 80 barg can result in an 8-10°C higher temperature of oil film and liner in the TDC region.
- Piston secondary motion along with cylinder pressure influence the friction force near TDC. Higher mixed/boundary friction near TDC during down stroke compared to upstroke can be obtained due to the tilting action of piston and consequent poor lubrication.
- Lower hydrodynamic friction during down stroke compared to up stroke can be obtained due to better lubrication or oil retention by piston skirt.
- Fmep generally decreases with increasing mid-liner temperature. The gradient of fmep sensitivity to temperature also reduces with increasing peak pressure and upward variation can be obtained at higher temperatures during higher peak pressure operations.

- Increasing speed results in an increasing fmep for lower temperature and peak pressure operation. However, at higher temperature and peak pressure the opposite behaviour is observed.
- Lower viscosity oil SAE 0W-30 can obtain a maximum reduction of 18% in fmep compared to SAE 5W-30 oil at a lower temperature of 40°C and peak pressure of 50 barg.
- Higher piston-liner diametrical clearance can result in a lower friction. A near constant reduction of 0.4 bar in fmep is obtained with higher clearance of 80 μm compared to 20 μm at all peak pressure and temperature conditions.
- Steel has the potential to achieve lower frictional losses compared to aluminium due to lower expansion rate as observed only in uncompressed operation. However, contrasting result is reported during pressurised operations. The effect of heavier and shorter skirt length of steel piston can influence in this result.

References

1. Holmberg, K., Andersson, P. and Erdemir, A., *Global energy consumption due to friction in passenger cars.* Tribology International, 2012. **47**: p. 221-234.
2. John, B.H., *Internal Combustion Engine Fundamental*. 1988: McGraw-Hill Inc.
3. Lars Eriksson, Lars Nielsen, *Modeling and Control of Engines and Drivelines*. 2014, Chichester, UK. : John Wiley and Sons Ltd.
4. Ciulli, E., *A Review of Internal Combustion Engine Losses Part 1: Specific Studies on the Motion of Pistons, Valves and Bearings.* Proc. IMechE, Part D: J. Automotive Engineering,, 1992. **206(4)**: p. 223-236.
5. Plint, A.G. and Plint, M.A., *Test procedure for rapid assessment of frictional properties of engine oils at elevated temperatures.* Tribology International, 1984. **17**(4): p. 209-213.
6. Law, T., MacMillan, D., Shayler, P., Kirk, G., Pegg, I., Stark, R., *A New Floating-Liner Test Rig Design to Investigate Factors Influencing Piston-Liner Friction.* SAE Technical Paper 2012-01-1328, 2012.
7. Allmaier, H., Priestner, C., Sander, D.E. and Reich, F.M., *Friction in Automotive Engines*, in *Tribology in Engineering*, D.H. Pihtili, Editor. 2013.
8. European Comission, Climate Action. *Road transport: Reducing CO2 emissions from vehicles*. [cited 2016 5-Jan]; Available from: http://ec.europa.eu/clima/policies/transport/vehicles/index_en.htm
9. EPA United States Environmental Protection Agency. *EPA's Fuel Economy Programs*. [cited 2016 5-Jan]; Available from: http://www3.epa.gov/fueleconomy/420f09067.pdf.
10. SMMT Driving The Motor Industry. *Tailpipe CO2 emissions* [cited 2016 5-Jan]; Available from: http://www.smmt.co.uk/industry-topics/environment/intro/tailpipe-co2-emissions/
11. European Comission, Climate Action. *Reducing CO2 emissions from passenger cars*. [cited 2016 5-Jan]; Available from: http://ec.europa.eu/clima/policies/transport/vehicles/cars/index_en.htm.
12. Fischer, C., Harrington, W. and Parry, I.W., *Should Automobile Fuel Economy Standards Be Tightened?* The Energy Journal, 2007: p. 1-29.
13. Car. *Budget 2015: how it affects UK motorists and what the Premium Car Tax means* [cited 2016 5-Jan]; Available from:

http://www.carmagazine.co.uk/car-news/motoring-issues/2015/budget-2015-how-it-affects-uk-motorists/

14. Committee to Assess Fuel Economy Technologies for Medium- and Heavy-Duty Vehicles; Board on Energy and Environmental Systems; Transportation Research Board; Division on Engineering and Physical Sciences; National Research Council, *Technologies and Approaches to Reducing the Fuel Consumption of Medium- and Heavy-Duty Vehicles*, 2010, The National Academies Press: Washington, DC .
15. Report of the European Expert Group on Future Transport Fuels, *Future Transport Fuels*. January,2011 [cited 2016 15-March]; Available from: http://ec.europa.eu/transport/themes/urban/cts/doc/2011-01-25-future-transport-fuels-report.pdf.
16. Coy, R.C., *Practical applications of lubrication models in engines 1.* Tribology International, 1998. **31**(10): p. 563-571.
17. Xin, Q., *Diesel Engine System design*. 2011, Cambridge, UK: Woodhead publishing
18. Hori, Y., *Hydrodynamic Lubrication*. 2006: Springer-Verlag.
19. Staron, J. and Willermet, P., *An Analysis of Valve Train Friction in Terms of Lubrication Principles.* SAE Technical Paper 830165, 1983.
20. Ofune, M., Banks, P., Morina, A., Neville, A., *Development of valve train rig for assessment of cam/follower tribochemistry.* Tribology International, 2016. **93, Part B**: p. 733-744.
21. Cho, S.-W., Choi, S.-M. and Bae, C.-S., *Frictional Modes of Barrel Shaped Piston Rings Under Flooded Lubrication.* Tribology International, 2000. **33:** p. 545-551.
22. Wakuri, Y., Soejima, M., Kitahara, T., Nunotani, M. and Kabe, Y., *Characteristics of Piston Ring Friction (Influences of Lubricating Oil Properties).* JSME International Journal, Series C 1995. **38(3)**: p. 593-600.
23. Furuhama, S. and Takiguchi, M., *Measurement of Piston Frictional Force in Actual Operating Diesel Engine.* SAE paper 790855, 1979.
24. Colin R. Ferguson, Allan T. Kirkpatrick, *Internal Combustion Engines: Applied Thermosciences*. 3rd ed. 2016, Chichester: John Wiley & Sons Ltd. .
25. Ha, K., Kim, J., Cho, M., and Oh, D., *Development of Piston Friction Force Measurement System.* SAE Technical Paper 2002-01-2902, 2002.

26. Johansson, S., Nilsson, H., Ohlsson, R., Rosén, B.G., *Experimental friction evaluation of cylinder liner/piston ring contact.* Wear, 2011. **271**(3–4): p. 625-633.
27. *Tribology Data Handbook: An Excellent Friction, Lubrication, and Wear Resource*. 1997, New York: CRC Press.
28. Furuhama, S., Takiguchi, M., and Tomizawa, K., *Effect of Piston and Piston Ring Designs on the Piston Friction Forces in Diesel Engines*, in *SAE Technical Paper 810977*. 1981.
29. Andersson, P., Tamminen, J., Sandström, C., *Piston ring tribology: A literature survey.* VTT Tiedotteita – Research Notes, Espoo 2002. **2178**.
30. Hewitt William, R., *Piston*. 1933, Patent US 1903216 A.
31. Gupta, H.N., *Fundamentals Of Internal Combustion Engines*. 2nd ed. 2013: PHI Learning Private Limited,Delhi.
32. Rakopoulos, Constantine D., Giakoumis, Evangelos G., *Diesel Engine Transient Operation-Principles of Operation and Simulation Analysis* 2009, London: Springer.
33. Dowson, D., Priest, M., Dalmaz, G., Lubrecht, A., *Tribological Research and Design for Engineering Systems*, *Tribology Series*, 2003. Elsevier. p. 913-921.
34. Rosenberg, R., *General Friction Considerations for Engine Design.* SAE Technical Paper 821576, 1982.
35. Takiguchi, M., Nakayama, K., Furuhama, S., and Yoshida, H., *Variation of Piston Ring Oil Film Thickness in an Internal Combustion Engine - Comparison Between Thrust and Anti-Thrust Sides.* SAE Technical Paper 980563, 1998.
36. Millington, B. and Hartles, E., *Frictional Losses In Diesel Engines.* SAE Technical Paper 680590, 1968.
37. Röhrle, M.D., *Pistons for internal combustion engines :Fundamentals of piston technology*. 1995: Landsberg/Lech, Germany. 70.
38. Chittenden, R.J. and Priest, M., *Analysis of the Piston Assembly, Bore Distortion and Future Developments*, in *Tribology Series*, C.M. Taylor, Editor. 1993, Elsevier. p. 241-270.
39. Soman, K., *Thermal Engineering*. Eastern Economy ed. 2011, New Delhi: PHI Learning Private Limited.
40. Bhushan, B., *Introduction To Tribology* 2002, New York: John Wiley & Sons, Inc.
41. *Stribeck Curves*, in *Encyclopedia of Tribology*, Y.-W.C. Q. Jane Wang Editor. 2013, Springer US. p. 3365-3370.

42. Ting, L., *Development of a Reciprocating Test Rig for Tribological Studies of Piston Engine Moving Components - Part I: Rig Design and Piston Ring Friction Coefficients Measuring Method.* SAE Technical Paper 930685, 1993.
43. Offner, G., Lorenz, N., and Knaus, O., *Piston Clearance Optimization using Thermo-elasto Hydrodynamic Simulation to Reduce Piston Slap Excitation and Friction Loss,.* SAE Technical Paper 2012-01-1530, 2012.
44. Meng, F.M., Zhang, Y.Y., Hu, Y.Z., Wang, H., *Thermo-elasto-hydrodynamic lubrication analysis of piston skirt considering oil film inertia effect.* Tribology International, 2007. **40**(7): p. 1089-1099.
45. Bolander, N.W., *Piston Ring Lubrication and Friction Reduction Through Surface Modification*. 2007, Purdue University West Lafayette, Indiana.
46. Stachowiak, G.W. and Batchelor, A.W., *Engineering Tribology (4th Edition)*. Elsevier.
47. Bilgin Hacioglu, Z.D., *Effect of Surface Texture on Compressor Piston Lubrication*, in *International Compressor Engineering Conference, Paper 2027*. 2010: Pardue.
48. Bhatt, D.V., Bulsara, M.A. and Mistry, K.N., *Prediction of Oil Film Thickness in Piston Ring - Cylinder Assembly in an I C Engine: A Review* in *Proceedings of the World Congress on Engineering*. 2009. London, U.K.
49. Werner, M., Merkle, A., Graf, S., Holzmüller, R., Wachtmeister, G., *Calculation of the Piston Assembly Friction: Classification, Validation and Interpretation.* SAE Technical Paper 2012-01-1323, 2012.
50. Bernard J. Hamrock, Steven R. Schmid, Bo O. Jacobson, *Fundamentals of Fluid Film Lubrication*. 2004, USA: Marcel Dekker Inc.
51. Hans Fishcher, Joseph Byrnes, *A New Look at Honing*, in *Honing Technology*. 1990, Society of Manufacturing Engineers: Detroit, Michigan.
52. Mezghani, S., Demirci, I., Yousfi, M., El Mansori, M., *Mutual influence of crosshatch angle and superficial roughness of honed surfaces on friction in ring-pack tribo-system.* Tribology International, 2013. **66**: p. 54-59.
53. Sato, O., Takiguchi, M., Takayuki, A., Seki, Y., Fujimura, K. and Tateishi, Y., *Improvement of Piston Lubrication in a Diesel Engine By Means of Cylinder Surface Roughness.* SAE Technical Paper 2004-01-0604, 2004.
54. Durga, V., Rao, N., Boyer, B.A., Cikanek, H. A. and Kabat, D.M. *Influence of surface characteristics and oil viscosity on friction behaviour of rubbing surfaces in reciprocating engines*. in *Fall Technical Conference ASME-ICE, 31(2), Paper No. 98-ICE-131*. 1998.

55. Galligan, J., Torrance, A.A. and Liraut, G., *A scuffing test for piston ring/bore combinations Part I. Stearic acid lubrication.* Wear, 1999. **236** (1-2): p. 199–209.
56. Dimkovski, Z., Cabanettes, F., Löfgren, H., Anderberg, C., Ohlsson, R., Rosén, B. G., *Optimization of cylinder liner surface finish by slide honing.* Proceedings of the Institution of Mechanical Engineers, Part B: Journal of Engineering Manufacture, 2012. **226**(4): p. 575-584.
57. Jocsak, J., Li, Y., Tian, T., and Wong, V., *Modeling and Optimizing Honing Texture for Reduced Friction in Internal Combustion Engines.* SAE Technical Paper 2006-01-0647, 2006.
58. Ishida, Y., Usami, H., Hoshino, Y. *Effect of micro dimples on frictional proper- ties in boundary lubrication condition*. in *Proceedings of the world tribology congress* 2009. Kyoto, Japan.
59. Kovalchenko, A., Ajayi, O., Erdemir, A., Fenske, G., Etison, I., *The Effect of Laser Texturing of Steel Surfaces and Speed-Load Parameters on the Transition of Lubrication Regime from Boundary to Hydrodynamic.* Tribology Transactions, 2004. **47**: p. 299-307.
60. Gabriel Arin Mihalcea, Leonard Mihăescu, *Structured Surfaces Used For Improving Tribological Behaviour For The Piston – Ring Cylinder – Liner Friction Couples In Internal Combustion Engines*, in *International Conference on Diagnosis and Prediction in Mechanical Engineering Systems (DIPRE'07)*. 2007: Galati, Romania. p. 77-87.
61. Sonthalia, A., Kumar, C.R., *The Effect of Compression Ring Profile on the Friction Force in an Internal Combustion Engine.* Tribology in Industry, 2013. **35**(1): p. 74-83.
62. Quillen, K., Stanglmaier,R.H., Moughon, L., Takata, R., Wong,V., Reinbold,E., Donahue, R., *Friction Reduction by Piston Ring Pack Modifications of a Lean-Burn Four-Stroke Natural Gas Engine: Experimental Results.* Transactions of the ASME, 2007. **129**: p. 1088-1094.
63. Wakabayashi, R., Kawanishi, M., Yoshida, H., and Ozaki, Y., *The Effects of Piston Rings and Liner Break-in on Lubricating Condition.* SAE Technical Paper 2007-01-1250 2007.
64. Ma, Z., Henein, N. A., Bryzik, W. and Glidewell, J. , *Break-in liner wear and piston ring assembly friction in a spark ignited engine.* STLE Tribology Transactions, 1998 **41(4)**: p. 497–504.
65. Priest, M. and Taylor, C.M., *Automobile engine tribology - approaching the surface* Wear, 2000. **241(2)**: p. 193–203.

66. Sui, P. C. and Ariga, S., *Piston ring pack friction and lubrication analysis of an automobile engine using a mixed lubrication model.* SAE Paper 931937, 1993.
67. Ryk, G. and Etsion, I., *Testing piston rings with partial laser surface texturing for friction reduction.* Wear 2006. **261** p. 792–796.
68. Erdemir, A., *Review of Engineered tribological interfaces for improved boundary lubrication.* Tribology International 2005. **38**: p. 249–256.
69. Holmberg, K. and Matthews, A., *Coatings tribology—properties, mechanisms, techniques and applications in surface engineering*. Tribology and Interface Engineering Series. 2009: Elsevier.
70. Erdemir, A. and Donnet, C., *Topical Review:Tribology of diamond-like carbon films: current status and future prospects.* Journal of Physics D: Applied Physics, 2006. **39**: p. 311–327.
71. Podgornik, B. and Vizintin, J., *Action of oil additives when used in DLC coated contacts.* Tribology - Materials, Surfaces & Interfaces, 2010. **4**(4): p. 186-190.
72. Enomoto, Y. and Yamamoto, T., *New materials in automotive tribology.* Tribology Letters, 1998. **5**: p. 13-24.
73. Tung, S.C. and McMillan, M.L., *Automotive tribology overview of current advances and challenges for the future.* Tribology International, 2004. **37**: p. 517-536.
74. Taylor, R.I. and Coy, R.C., *Improved fuel efficiency by lubricant design: A review. .* Proceedings of the Institution of Mechanical Engineers , PART J: Journal Of Engineering Tribology, 2000. **214**: p. 1-15.
75. Glidewell, J. and Korcek, S., *Piston Ring / Cylinder Bore Friction Under Flooded and Starved Lubrication Using Fresh and Aged Engine Oils.* SAE Technical Paper 982659, 1998.
76. Tung, S. and Tseregounis, S., *An Investigation of Tribological Characteristics of Energy-Conserving Engine Oils Using a Reciprocating Bench Test.* SAE Technical Paper 2000-01-1781, 2000.
77. Saini, M.S., Lockwood, F. E., Smith, T. R., Pridemore, D. and Grulke, E. A., *Statistical study of organomolybdenum compounds in an engine oil formulation and the results of engine testing.* Tribotest, 2001. **8(1)**: p. 27-44.
78. Ruijun Zhang, S.L., Yuansheng Jin, Yucong Wang, Simon C. Tung, *Tribological behaviors and molecular spectroscopic characterization of a lubricated piston ring/cylinder bore sliding contact under stepwise heating conditions.* Industrial Lubrication and Tribology, 2002. **54**(2): p. 69-73.

79. Spikes, H.A., *Low- and zero-sulphated ash, phosphorous and sulphur anti-wear additives for engine oils.* Lubrication Science, 2008. **20**: p. 103-136.
80. Jian-Huei Choo, Andrew K. Forrest, Hugh A. Spikes, *Influence of Organic Friction Modifier on Liquid Slip: A New Mechanism of Organic Friction Modifier Action.* Tribology Letters, 2007. **27**(2): p. 239-244.
81. Tobias Amann , Andreas Kailer, *Ultralow Friction of Mesogenic Fluid Mixtures in Tribological Reciprocating Systems.* Tribology Letters, 2009. **37**(2): p. 343-352.
82. Martin, J.M. and Ohmae, N., *Nanolubricants:* 2008, West Sussex, England: John Wiley & Sons.
83. Shin, S., Cusenza, A., and Shi, F., *Offset Crankshaft Effects on SI Engine Combustion and Friction Performance.* SAE Technical Paper 2004-01-0606, 2004.
84. Kim, K., Shah, P., Takiguchi, M., and Aoki, S., *Part 3: A Study of Friction and Lubrication Behavior for Gasoline Piston Skirt Profile Concepts.* SAE Technical Paper 2009-01-0193, 2009
85. Leong, D.K.W., Shayler, P. J., Pegg, I. G., Murphy, M., *Characterizing the effect of viscosity on friction in the piston assembly of internal combustion engines.* Proceedings of the Institution of Mechanical Engineers, Part J: Journal of Engineering Tribology, 2007. **221**(4): p. 469-478.
86. Kim, M., Dardalis, D., Matthews, R., and Kiehne, T., *Engine Friction Reduction Through Liner Rotation.* SAE Technical Paper 2005-01-1652, 2005.
87. Da Silveira, M., Gertz, L., Cervieri, A., Rodrigues, A., Senger, M.A., *Analysis of the Friction Losses in an Internal Combustion Engine.* SAE Technical Paper 2012-36-0303, 2012.
88. Bolander, N.W., Steenwyk, B. D., Sadeghi, F., Gerber, G. R., *Lubrication regime transitions at the piston ring-cylinder liner interface.* Proceedings of the Institution of Mechanical Engineers, Part J: Journal of Engineering Tribology, 2005. **219**(1): p. 19-31.
89. Carden, P., Bell, D., Priest, M., and Barrell, D., *Piston Assembly Friction Losses: Comparison of Measured and Predicted Data.* SAE Technical Paper 2006-01-0426, 2006.
90. Uras, H. and Patterson, D., *Measurement of Piston and Ring Assembly Friction Instantaneous IMEP Method.* SAE Technical Paper 830416, 1983.

91. Yun, J.E., Kim, S.S., *An Improved Approach to the Instantaneous IMEP Method for Piston-Ring Assembly Friction Force Measurement.* JSME international journal, Series II, 1992. **35, No 2**: p. 310-318.
92. Mufti, R.A. and Priest, M., *Experimental Evaluation of Piston-Assembly Friction Under Motored and Fired Conditions in a Gasoline Engine.* Journal of Tribology, 2004. **127**(4): p. 826-836.
93. Tishbein, H.W., *The Friction of Piston Rings.* NACA Technical Memorandum No. 1069, 1940.
94. Forbes, J.E. and Taylor, E.S., *A Method for Studying Piston Friction.* NACA Wartime Report, 1943.
95. Leary, W.A. and Jovellanos, J.U., *A Study of Piston and Ring Friction.* NACA Wartime Report 1944.
96. Livengood, J.C. and Wallour, C., *A Study of Piston-Ring Friction.* NACA Techincal Note 1249, 1947.
97. Rogowski, A.R., *Method of Measuring the Instantaneous Friction of Piston Rings in a Firing Engine* SAE Paper 610263, 1963.
98. Yun, J.E. and Kim, S.S., *New Device for Piston-Ring Assembly Friction Measurement in IDI Diesel Engine.* JSME International Journal, Series B, 1993. **36(4)**: p. 723-729.
99. Kikuchi, T., Ito, S. and Y. Nakayama,Y., *Piston friction analysis using a direct-injection single-cylinder gasoline engine.* JSAE Review, 2003. **24**(1): p. 53-58.
100. Madden, D., Kim, K., and Takiguchi, M., *Part 1: Piston Friction and Noise Study of Three Different Piston Architectures for an Automotive Gasoline Engine.* SAE Technical Paper 2006-01-0427, 2006.
101. Ha, K.P., *Liner mounting structure for measuring piston friction*. 2002, Patent US 20020083913 A1.
102. Nakayama, K., Yasutake, Y., Takiguti, M., and Furuhama, S., *Effect of Piston Motion on Piston Skirt Friction of a Gasoline Engine.* SAE Technical Paper 970839, 1997.
103. Urabe, M., Tomomatsu, T., Ishiki, K., Takiguchi, M., Someya, T., *Variation of Piston Friction Force and Ring Lubricating Condition in a Diesel Engine with EGR.* SAE Technical Paper 982660, 1998.
104. Teraguchi, S., Suzuki, W., Takiguchi, M., and Sato, D., *Effects of Lubricating Oil Supply on Reductions of Piston Slap Vibration and Piston Friction.* SAE Technical Paper 2001-01-0566, 2001.

105. Kim, K., Godward, T., Takiguchi, M., and Aoki, S., *Part 2: The Effects of Lubricating Oil Film Thickness Distribution on Gasoline Engine Piston Friction.* SAE Technical Paper 2007-01-1247, 2007.
106. Liao, K., Liu, Y., Kim, D., Urzua, P., Tian, T., *Practical challenges in determining piston ring friction.* Proceedings of the Institution of Mechanical Engineers, Part J: Journal of Engineering Tribology, 2012.
107. Wakuri, Y., Soejima, M., Ejima, Y., Hamatake, T., Kitahara, T., *Studies on Friction Characteristics of Reciprocating Engines.* SAE Technical Paper 952471, 1995.
108. Taylor, R.I., Evans, P.G., *In situ piston measurements.* Proc MechE Part J: J Eng Tribology 2004. **218**: p. 185–200.
109. Koch, F., Geiger, U., and Hermsen, F., *PIFFO - Piston Friction Force Measurements During Engine Operation* SAE Technical Paper 960306, 1996.
110. O'Rourke, B., Stanglmaier, R., and Radford, D., *Development of a Floating-Liner Engine for Improving the Mechanical Efficiency of High Performance Engines.* SAE Technical Paper 2006-01-3636, 2006.
111. Gore, M., Theaker, M., Howell-Smith, S., Rahnejat, H., King, P.D., *Direct measurement of piston friction of internal-combustion engines using the floating-liner principle.* Proceedings of the Institution of Mechanical Engineers, Part D: Journal of Automobile Engineering, 2013.
112. Kunkel, S., Werner, M., and Wachtmeister, G., *Setting Up a Measuring Device to Determine the Friction of the Piston Assembly.* SAE Int. J. Mater. Manuf., 2011. **4(1)** p. 340-351.
113. Kim, D., Ito, A., Ishikawa, Y., Osawa, K., Iwasaki, Y., *Friction Characteristics of Steel Pistons for Diesel Engines.* Journal of Materials Research and Technology, 2012. **1**(2): p. 96-102.
114. R. Alewijnse, A 21st Century friction correlation for Engine Performance Analysis , in *IMechE:Internal Combustion Engines*. 2015: Royal College of Physicians in London, United Kingdom.
115. Merkle, A., Kunkel, S., and Wachtmeister, G., *Analysis of the Mixed Friction in the Piston Assembly of a SI Engine.* SAE Int. J. Engines 2012. **5(3)**: p. 1487-1497.
116. *HBM measure and predict with confidence*. http://www.hbm.com/en/3215/strain-gauges-or-piezoelectric-sensors/ [cited 2016 10th of March].
117. T. Jaglinski, A.N., R. Schmitz, R. S. Lakes, *Study of Bolt Load Loss in Bolted Aluminum Joints.* J. Eng. Mater. T., 2007. **129 (1)**: p. 48–54

118. Munney, M.J., *Light and Heavy Vehicle Technology*. 1988: Heinemann Newnes.
119. Emiliano Pipitone, A.B., *Determination of TDC in internal combustion engines by a newly developed thermodynamic approach.* Applied Thermal Engineering, 2010. **30**: p. 1914-1926.
120. Rocco, V., *Dynamic T.D.C. and Thermodynamic Loss Angle Measurement in a D. I. Diesel Engine.* SAE Technical Paper 851546, 1985.
121. Sta, M., *Thermodynamic Determination of T.D.C. in Piston Combustion Engines.* SAE Technical Paper 960610, 1996.
122. Taraza, D., Henein, N., and Bryzik, W., *Friction Losses in Multi-Cylinder Diesel Engines.* SAE Technical Paper 2000-01-0921, 2000.
123. *System Comparison of Steel & Aluminium Pistons for PC Diesel Engines.* Auto Tech Review 2014. **3**(10): p. 24-29.
124. Allmaier, H., Knauder, C., Salhofer, S., Reich, F.M., Schalk, E., Ofner, H., Wagner, A., *An experimental study of the load and heat influence from combustion on engine friction.* International Journal of Engine Research, 2015.
125. Tian, T., *Dynamic behaviours of piston rings and their practical impact—Part ii: oil transport, friction, and wear of ring/liner interface and the effects of piston and ring dynamics.* Proc IMechE Part J: J Eng Tribology, 2002. **216** p. 229–247.
126. Victor Albert Walter Hillier, Peter Coombes, *Hillier's Fundamentals of Motor Vehicle Technology, Book 1*. 5th ed. 2004, Cheltenham: Nelson Thornes Ltd.
127. Sandoval, D. and Heywood, J., *An Improved Friction Model for Spark-Ignition Engines.* SAE Technical Paper 2003-01-0725, 2003.
128. Rakopoulos, C., Giakoumis, E., and Rakopoulos, D., *The Effect of Friction Modelling on the Prediction of Turbocharged Diesel Engine Transient Operation.* SAE Technical Paper 2004-01-0925, 2004.

Appendices

Appendix A Matlab script to convert raw data into friction force

```
close all;

clear all;

clc;

% First a loop to allow entering and/or saving of the input data:

%

data_entered = 0;

while data_entered ~= 1

   csv_or_mat = input('Load from a pre-saved .mat file, or from a new .csv file? (select m or c): ', 's');


   if strcmp(csv_or_mat, 'c') == 1 % User wants to open and save a new .csv file

      % Allow the user to pick the data files:

      cell_1_filename = uigetfile('*.csv', 'Select .csv file for load cell 1');

      cell_2_filename = uigetfile('*.csv', 'Select .csv file for load cell 2');

      temp_filename = uigetfile('*.csv', 'Select .csv file for Temperatures');

      accel_filename = uigetfile('*.csv', 'Select .csv file for Accelerometer');

       % Read the variables from the .csv files

      data = csvread(temp_filename);

      load_cell_1 = csvread(cell_1_filename);

      load_cell_2 = csvread(cell_2_filename);

      g_meter = csvread(accel_filename);

      disp(sprintf('*'));

      filename_check = input('Derive .mat filename from .csv file names, or enter your own? (select d or e): ', 's');

      if strcmp(filename_check, 'd') == 1
```

```
% User wants to save the csv data into a .mat file under the same filename as the
.csv files from which the data was derived


mat_filename =  cell_1_filename(1:37); % User wants to save the csv data into a
.mat file under their own filename
        elseif strcmp(filename_check, 'e') == 1
            disp(sprintf('*'));
            mat_filename = input('Enter filename:', 's');
        else
            disp(sprintf('*'));
            disp(sprintf('Error! Choose either d(erive) or e(nter)'));
            disp(sprintf('*'));


        end
save_string = ['save ' mat_filename ' data load_cell_1 load_cell_2 g_meter;'];
        eval(save_string);
        data_entered = 1;


    elseif strcmp(csv_or_mat, 'm') == 1 % User wants to load a pre-saved .mat file
        mat_filename = uigetfile('*.mat', 'Select .mat file for the test');
        load(mat_filename)
        data_entered = 1;
    else
        disp(sprintf('*'));
        disp(sprintf('Error! Choose either m(at) or c(sv)'));
        disp(sprintf('*'));
    end
end
 % Get rid of the first few rows of the data where the load cell signal traces
contain zeros -
```

```
 zero_check = sum(load_cell_1, 2);
zero_rows = find(zero_check == 0);


if isempty(zero_rows) == 1;
    start_row = 0;
else
    start_row = zero_rows(end);
end
load_cell_1 = load_cell_1(start_row + 1:end, :);
load_cell_2 = load_cell_2(start_row + 1:end, :);
pressure=g_meter(start_row + 1:end, :);
data = data(start_row + 1:end, :);
 stribeck_degrees_start = 90;
stribeck_degrees_end = 95;
pulses_per_degree = 2;
degs = (0:(1/pulses_per_degree):360-(1/pulses_per_degree));
bore = 86.009e-3;
stroke = 94.6e-3;
 TDC_pos = 354;


comp_temps=[80];
comp_pressure=[60];
temp_range =2;
press_range=1;
% Pull out every (grab_every)th row in the load cell raw data matrices, for
plotting
% to see how the offset and trace shape changes over the test duration:
grab_every = 20;
cell_1_low_res = load_cell_1(10:grab_every:end, :);
cell_2_low_res = load_cell_2(10:grab_every:end, :);
```

```
 liner_temp_midstroke_thrust = data(:, 16);
ambient_temp = data(:, 9);
jacket_inlet = data(:, 12);
sump_temp = data(:, 14);
gallery_temp = data(:, 10);
liner_temp_top_thrust = data(:, 15);
 liner_temp_top_antithrust = data(:, 17);
liner_temp_midstroke_antithrust = data(:, 18);
av_liner_temp = (1/2) * ( liner_temp_midstroke_thrust ...
    + liner_temp_midstroke_antithrust);

 % load cell calibration
  cell_1_sensitivity=(av_liner_temp.*.0789) + 641.15;
 cell_2_sensitivity=(av_liner_temp.*  -.9984) + 658.75;

 friction_1=(repmat(cell_1_sensitivity,1, 720)).*load_cell_1;
friction_2=(repmat(cell_2_sensitivity,1, 720)).*load_cell_2;

seal_ring_force_cell_1_sensitivity=(av_liner_temp.*.0268)+3.6706; %
force/pressure (N/bar) variation with temperature
seal_ring_force_cell_2_sensitivity=(av_liner_temp.*-0.0333)+4.6012;

seal_friction_1=(repmat(seal_ring_force_cell_1_sensitivity,1, 720)).*pressure;
seal_friction_2=(repmat(seal_ring_force_cell_2_sensitivity,1, 720)).*pressure;
rev_friction_1=friction_1+seal_friction_1;
rev_friction_2=friction_2+seal_friction_2;

 % Now realign the load cell and accelerometer traces so that TDC
% occurs at zero on the X axis, using the TDC index obtained with the AVL
% tool:
```

```
 TDC_index = round(1 + TDC_pos*pulses_per_degree); %Add 1 because pulse 1
= degree zero.

friction_1_aligned = [rev_friction_1(:,TDC_index:end) rev_friction_1(:,
1:(TDC_index-1))];

friction_2_aligned = [rev_friction_2(:,TDC_index:end) rev_friction_2(:,
1:(TDC_index-1))];

pressure_aligned= [pressure(:,TDC_index:end) pressure(:, 1:(TDC_index-1))];


 % ESTIMATE THE OFFSET OF THE FRICTION SIGNALS

%
**********************************************************************
********

   if TDC_pos >= 180

      BDC_index = TDC_index - 180*pulses_per_degree;

   elseif TDC_pos < 180

      BDC_index = TDC_index + 180*pulses_per_degree;

   end

   offset_cell_1 = mean(rev_friction_1(:, BDC_index-10:BDC_index+15), 2);

   offset_cell_2 = mean(rev_friction_2(:, BDC_index-10:BDC_index+15), 2);


 % APPLY THE OFFSETS TO THE FRICTION TRACES, CALCULATE

% Subtract the offsets from the TDC-aligned friction matrices to give

% the corrected/zeroed friction traces:

corrected_friction_cell_1 = friction_1_aligned - repmat(offset_cell_1, 1, 720);

corrected_friction_cell_2 = friction_2_aligned - repmat(offset_cell_2, 1, 720);

corrected_friction = corrected_friction_cell_1 + corrected_friction_cell_2;


friction = corrected_friction;% - liner_inertia;

% Pull out the important temperatures from the analogue data

%
**********************************************************************
********
```

```
%
**********************************************************************
********

 % Calculate the duty parameter, based upon liner average oil temperature,

% mean piston speed and total ring pack tan load per unit face area

rpm = data(:, 25);

mean_piston_speed = 2*stroke*(rpm/60); % m/sec


% Pick out the average friction traces at some pre-determined liner

% Define the values and indices of the comparison temperatures:


% Now pick out indices where the average liner temperature falls in the

% comparison ranges:


mean_friction = [];

mean_pressure=[];


for j = 1:size(comp_temps)


   temp_indices = find( av_liner_temp>= comp_temps(j)-temp_range
&av_liner_temp<= comp_temps(j)+temp_range);

   temp_press=pressure_aligned(temp_indices,:);

   temp_friction=friction(temp_indices,:);


   for t = 1:size(comp_pressure) %#ok<ALIGN>


   press_indices = find( temp_press(:,1)>= comp_pressure(t)-press_range
&temp_press(:,1) <= comp_pressure(t)+press_range);

   mean_friction = vertcat(mean_friction, mean(temp_friction(press_indices,
:),1));

   mean_pressure = vertcat(mean_pressure, mean(temp_press(press_indices,
:),1));
```

```
end

end

 pressure_comp=mean_pressure';


 % ASSUMING A CONSTANT SPEED TEST, define where the speed is below 99%
of

% the set point

set_point_speed = mean(rpm((end - 60):end));

speed_low = find(rpm<0.99*set_point_speed);

speed_ok_from = speed_low(end);


 % variables needed for plots of friction against crank angle

xd=degs;

data=mean_friction;

 % two cycles

degs_720=0:0.5:719.5;

data_720=[data,data];

 % load mean friction data

for t_c=1:size(comp_pressure)

    fr_d=mean_friction;

    fr_d_1=data_720;

end

 %% piston work and power calculations

% con rod length 160 mm

c_len=160e-3;

 c_rad=(stroke)/2;

% piston displacement

p_d=((c_rad.*2).*(((bore*1e-3./2).^2).*pi));

 % numerical integration to find total friction work
```

```
% calculate once only for all 6 sets

r_rad=(xd.*(pi))./180;

pist_pos=(c_rad.*(cos(r_rad)))+(((c_len.^2)-
(c_rad.^2).*(sin(r_rad).^2))).^0.5;


 for r3=1:size(comp_pressure)

        fmep_inter=fr_d(r3,:);

    work_tot=abs( trapz(pist_pos,fmep_inter) );

    power_pot=(work_tot/p_d)*2e-5;

      A_fmep_all(r3)=power_pot;

    end

 A_fric=fr_d';

 A_fmep=A_fmep_all';
```